Title: Hundreds of *Colobus* (Cercopithecidae: Primates) fossils from the later Pleistocene of Ethiopia's Middle Awash study area

Running title: New *Colobus* fossils from the Afar Rift, Ethiopia

Authors: Brasil, Marianne F.[1,2]; Monson, Tesla A.[3]; Taylor, Catherine E.[2,4]; Yohler, Ryan M.[2,4]; Hlusko, Leslea J.[2,4,5]

Affiliations: [1]Berkeley Geochronology Center, Berkeley, CA; [2]Human Evolution Research Center, University of California Berkeley, Berkeley, CA; [3]Department of Anthropology, Western Washington University, Bellingham, WA; [4]Department of Integrative Biology, University of California Berkeley, Berkeley, CA; [5]Centro Nacional de Investigación sobre la Evolución Humana (CENIEH), Burgos, Spain

Corresponding author: Brasil, Marianne F. (email: mbrasil@berkeley.edu)

Abstract

Objectives
The aim of this study is to introduce and systematically assess a new assemblage of colobine fossils (n=360) recovered from Late Pleistocene (ca. 100,000 years ago) sediments in the Middle Awash research area, Afar Rift, Ethiopia.

Materials and Methods
We describe the colobine fossils relative to extant colobine taxa and Middle Pleistocene fossil samples from "Andalee" and Asbole, Ethiopia using linear dental, cranial, and postcranial metrics, as well as qualitative features. We also document the ontogenetic and sex profiles of this sample.

Results
Based on morphological affinities to extant and fossil *Colobus*, we refer these 360 individuals to *Colobus* cf. *guereza*. The majority of the individuals (76%) fall into young- and middle-adult age categories. Females are slightly better represented than males, although the majority of individuals (84%) could not be assigned to sex.

Discussion
Details of the last half million years of *Colobus* morphological evolution have remained obscured by a sparse fossil record. The newly recovered, prepared, and curated fossils described herein add significantly to the record of this group. Several morphologies seen in these new fossils fall between the Asbole *Colobus* sample and extant *Colobus guereza*, suggesting an ancestral-descendant phyletic relationship among the three time-successive samples. The populational variation documented among these samples indicates that the distinctive pattern of sexual dimorphism observed in *C. guereza* had evolved by 100 ka.

Keywords: cercopithecid evolution, colobine fossil record, African colobines, *Colobus guereza*, sexual dimorphism

1 | Introduction

Subfamily Colobinae, within Family Cercopithecidae, is represented in Africa by three extant genera: *Colobus* (black and white colobus monkeys), *Piliocolobus* (red colobus monkeys), and *Procolobus* (olive colobus monkeys). Molecular evidence suggests that *Procolobus* and *Piliocolobus* shared a last common ancestor around 6.4-6.0 Ma and that this clade shared a last common ancestor with *Colobus* around 9.1-7.5 Ma (Perelman et al., 2011; Springer et al., 2012; Ting, 2008). Today, *Piliocolobus* is broadly distributed across western and central Africa, *Procolobus* is restricted to coastal western Africa, and *Colobus* spans western to eastern Africa (Groves, 2007). *Colobus* is the only colobine genus whose range extends into northeastern Africa, and is the only colobine present in modern-day Ethiopia (Oates, 1994; Oates & Trocco, 1983). In general, *Colobus*, *Piliocolobus*, and *Procolobus* are distinguishable by their pelage color (black, red, and olive, respectively) and their body size (large, medium, and small, respectively; Bruner, Pucci, & Jones, 2006), in addition to behavioral and hard and soft tissue differences (reviewed in Groves, 2007).

In contrast to the monotypic extant *Procolobus*, containing only the single species *Procolobus verus*, *Piliocolobus* contains multiple allopatric taxa that are variably categorized as subspecies of *Piliocolobus badius* (e.g., Ting, 2008) or as separate species (see reviews of red colobus classifications in Grubb et al., 2003, and Kingdon et al., 2013). Extant *Colobus* is comprised of four (*Colobus angolensis*, *Colobus guereza*, *Colobus polykomos*, and *Colobus satanus*; Hull, 1979; Schwarz, 1929) or five species (elevating *Colobus p. vellerosus* to the species rank; Groves, 2007; Kingdon et al., 2013; Oates & Trocco, 1983). These *Colobus* species are primarily distinguished on the basis of white markings on the body, the proportion of white fur on the tail, the size of the tail brush, and the acoustic structure of the loud calls of adult males (Groves, 2007; Oates, Bocian, & Terranova, 2000; Rahm, 1970), with some subtle craniometric differences (Hull, 1979). *Colobus guereza* is the most widely distributed of the *Colobus* species and is further divided into a variable number of recognized subspecies (Grubb et al., 2003; Zinner et al., 2019).

Although colobines today span a large swath of the African continent and encompass a wide breadth of morphological and behavioral diversity, the recent fossil record of these extant genera is nearly non-existent (Jablonski & Frost, 2010). Molecular evidence has clarified some details of the recent evolutionary history of this group (e.g., Ting, 2008; Wang et al., 2012; and see alternative interpretation in Roos et al., 2011), but the morphological evolution of African colobines in the Middle and Late Pleistocene remains poorly understood.

The earliest fossil record for colobines in Africa extends back to the Middle Miocene in Kenya (Tugen Hills, ca. 12.5 Ma; Rossie, Gilbert, & Hill, 2013). Multiple colobine taxa are known from Middle and Late Miocene deposits in the Tugen Hills, including fossils of *Microcolobus* that were until recently the earliest known colobine fossils (ca. 9.5-9.0 Ma; Benefit & Pickford, 1986; Gilbert, Goble, & Hill, 2010; Rossie et al., 2013). Also known from the Late Miocene of Kenya are colobines from the Nakali Formation (arboreally-adapted *Microcolobus* at ca. 9.9-9.8 Ma; Nakatsukasa et al., 2010) and Lemudong'o (*Paracolobus* at ca. 6 Ma; Hlusko, 2007). Colobines are also known from the Late Miocene of Algeria (Menacer; Arambourg, 1959), Chad (partially terrestrial *Cercopithecoides* at ca. 7 Ma; Pallas et al., 2019), Egypt (*Libypithecus*, latest Miocene; Stromer, 1913), Ethiopia (Chorora Formation, ca. 8.5-7.0 Ma, and Middle Awash, ca. 5.7 and 5.3 Ma; Frost et al., 2009; Suwa et al., 2015), Libya (As Sahabi;

Meikle, 1987), and tentatively Uganda (Nkondo Formation; Senut, 1994). Multiple colobine taxa are also known from the Late Miocene and Early Pliocene of Lothagam (including *Cercopithecoides* from ca. 5.0-4.2 Ma; Leakey, Teaford, & Ward, 2003).

The fossil record for colobines in Africa improves in the Pliocene and suggests that they diversified during this time (reviewed in Frost, Gilbert, & Nakatsukasa, 2022 and Jablonski & Frost, 2010, and summarized below). Multiple genera are recognized from Pliocene deposits, including *Cercopithecoides*, *Paracolobus*, *Kuseracolobus,* and *Rhinocolobus*. Most of the Pliocene forms are large-bodied. Some later Pliocene taxa may have been partially terrestrial (e.g., *Cercopithecoides williamsi* and *Cercopithecoides kimeui*; Jablonski, Leakey, Ward, & Antón, 2008), but most are inferred to have been primarily arboreal (Hlusko, 2006; Jablonski & Frost, 2010). Most of these forms are morphologically distinct, and their phylogenetic relations with extant colobines remains uncertain. It is not until the Early Pleistocene that fossils more similar to extant taxa appear more frequently in the record (Jablonski & Leakey, 2008). Of these later taxa, *Cercopithecoides* has been linked to extant African colobines based on shared pollical reduction (Frost, Gilbert, Pugh, Guthrie, & Delson, 2015). Furthermore, this genus has been hypothesized as ancestral to *Colobus* on the basis of similarities in mandibular, humeral, and femoral morphology (Jablonski & Frost, 2010).

With the exception of a single mandible from Pliocene sediments of Kanam East referred to *Colobus* sp., fossils that are clearly assignable to *Colobus* are not observed until the Middle Pleistocene (Frost & Alemseged, 2007; Harrison & Harris, 1996; Jablonski & Frost, 2010; Kalb, Jaegar, Jolly, & Kana, 1982). Middle Pleistocene colobine samples include a few fossils from Kapthurin, isolated teeth from Taung, and two samples from the Afar Rift of Ethiopia: "Andalee" in the Middle Awash study area, and Asbole (Frost, 2001a; Frost & Alemseged, 2007; Kalb et al., 1982; Szalay & Delson, 1979). Of these, the Asbole area has yielded the largest colobine sample, with 69 individuals attributed to *Colobus* sp. from ca. 600 ka (Frost & Alemseged, 2007). Also from Ethiopia is a partial skull identified as *Colobus* sp. from the Omo Kibish, although its provenience within the formation is uncertain and a description has yet to be published (Assefa, Yirga, & Reed, 2008). Only one fossil has been attributed to an extant colobine species, *Colobus guereza*, from presumed Pleistocene sediments at Wad Medani, Sudan (Frost & Alemseged, 2007; Simons, 1967).

The evidence from the Middle Pleistocene at "Andalee" and Asbole suggests that *Colobus* has undergone significant evolutionary changes during the last half million years, hinting at a shift toward a smaller degree of sexual dimorphism in extant *Colobus* (Frost & Alemseged, 2007). This suggestive fossil evidence makes the last half million years of *Colobus* evolution particularly intriguing, and any fossils from this time period are particularly valuable.

Here we describe a large sample of colobine fossils (n=360) recovered from Late Pleistocene sediments in the Middle Awash study area. This colobine assemblage is a subset of an assemblage of nearly one thousand cercopithecid specimens recovered from the Halibee member, the cercopithecin and papionin constituents of which are described in Taylor, Brasil, Monson, Yohler, & Hlusko (*submitted*) and Brasil, Monson, Taylor, Yohler, & Hlusko (*submitted*), respectively. The colobine sample described herein fills the gap between the Middle Pleistocene fossils known from "Andalee" and Asbole, and the modern taxa living in the Afar Rift of Ethiopia today. Taking into account the geographic and chronological position of this assemblage, we pose two hypotheses:

(1) The 100,000-year-old Faro Daba fossils, chronologically intermediate to the Asbole fossils and living *C. guereza*, sample a segment of an evolving species lineage in Ethiopia.
(2) The Faro Daba and Asbole fossils sample two distinct colobine lineages. In this scenario, the Faro Daba fossils are ancestral to modern *C. guereza.*

These hypotheses guide our comparative assessments, by which we document the morphological affinities of this fossil assemblage and consider the insights it provides into the last half million years of colobine evolution in the region. Considering the young geological age of the Faro Daba colobines and their geographic position, we predict that this sample will align most closely with *C. guereza* among the extant samples. We also predict that the Faro Daba sample will align with the Asbole fossils in some features, particularly those that the Asbole fossils share with *C. guereza,* but that some features will yield significant differences between these two fossil samples.

1.1 | Geological context

The colobine fossils described herein are part of an exceptionally large cercopithecid assemblage recovered from the Halibee member of the Dawaitoli Formation. This cercopithecid assemblage is drawn from two chronostratigraphic units within the Halibee member: the Faro Daba and Chai Baro beds (Brasil et al., *submitted*; Niespolo et al., 2021; Taylor et al., *submitted*).

The colobine fossils were collected exclusively from the Faro Daba beds. These fossils were eroded from sediments either above or below a widespread marker horizon of basaltic tuff (the AFBT), which is not datable by Ar/Ar. However, obsidian just below the AFBT has proven susceptible to Ar/Ar and yielded a maximum age of 106 ka (Morgan, Renne, Taylor, & WoldeGabriel, 2009). Overlying ostrich eggshell susceptible to U-Th methods provides a minimum age of 96 ka (Niespolo et al., 2021). Additional details about the geological contexts of the cercopithecid fossils recovered from the Halibee member, as well as field collection protocols, are reported in Taylor et al. (*submitted*) and Niespolo et al. (2021).

2 | Materials

2.1 | The fossil assemblage

We describe a large sample (n=360 individually numbered specimens) of colobine fossils from Late Pleistocene sediments in the Middle Awash study area of the Afar Rift of Ethiopia. The Faro Daba sample includes only colobines and cercopithecins, while the older Chai Baro sample includes only papionins and cercopithecins, and lacks colobines. The colobine sample described here was recovered from a single chronostratigraphic interval, the Faro Daba beds, and can be considered to be geologically contemporaneous. All of the Faro Daba fossils are housed at the National Museum of Ethiopia in Addis Ababa and are under the control and care of the Authority for Research and Conservation of Cultural Heritage.

We describe the Faro Daba colobine fossils comparatively, with reference to extant colobines and to two geographically and chronologically proximate fossil assemblages from "Andalee" and Asbole, Ethiopia (Table 1). We refer to "Andalee" here in quotation marks because this locality name derives from the original fieldwork by the Rift Valley Research

Mission in Ethiopia (RVRME; Frost, 2001a; Kalb et al., 1982). As fieldwork has continued, the Afar names originally applied, and the geological placement originally inferred, have been updated. We therefore place this name in quotation marks to indicate that these are historical terms, while still maintaining continuity with the older literature.

2.2 | Extant comparative samples

We comparatively assess the Faro Daba colobine sample relative to a large sample of extant colobines, representing 308 individuals and nine species (Table 1). We focus our assessment on extant African colobines, and particularly with species of *Colobus,* because they are geographically proximate to the Faro Daba sample, are similar in body size, and have been previously noted as relevant comparisons (Frost, 2001a; Frost & Alemseged, 2007). We supplement our comparative data with measurements downloaded from the PRImate Morphology Online database (PRIMO); data sources are detailed in Table 1 and the dataset associated with this manuscript ([*reference online location in data repository here*]).

Our comparative dental analyses include eight extant colobine taxa: *Colobus angolensis, Colobus guereza*, *Piliocolobus badius*, *Piliocolobus oustaleti*, *Piliocolobus tholloni*, *Procolobus verus*, *Nasalis larvatus*, and *Presbytis rubicunda* (see Table 1). The latter two Asian taxa are included to provide a broader comparison within colobines.

The cranial analyses include *C. guereza*, *Pi. badius*, *Pi. oustaleti*, and *Pr. verus*. The mandibular analyses include the same taxa as the cranial analyses with the addition of *C. polykomos.* The analyses of limb indices include *C. guereza*. We rely on published data from Frost et al. (2020) for additional postcranial comparisons with *C. guereza*, *Piliocolobus* spp., *Presbytis* spp., and *Nasalis larvatus*.

2.3 | Comparative fossils

Colobines are poorly represented in the African Middle and Late Pleistocene fossil records with the exception of an assemblage identified as *Colobus* sp. from Asbole in the Afar Region of Ethiopia at ca. 600 ka (Frost & Alemseged, 2007) and another slightly smaller sample from "Andalee" in the Afar Rift, from Middle Pleistocene sediments (Frost, 2001a; Kalb et al., 1982). These two samples are thought likely to belong to the same taxon (Frost, 2001a; Frost & Alemseged, 2007), and they are particularly appropriate comparative samples for the Halibee member fossils given their geographic and chronological proximity. We examined the original fossils from Asbole and include in our analyses published dental metric data for 47 individuals from the *Colobus* sp. Asbole sample, taken from Frost and Alemseged (2007). We also include published dental metric data from Frost (2001a) for the "Andalee" fossils, both from Middle Pleistocene sediments (n=31, here referred to as "Andalee") and Middle Stone Age deposits (n=4, here referred to as "Upper Andalee" following Frost, 2001a).

2.4 | Data collection methods

Our approach to data collection was guided by two aims. First, we targeted features that have previously been identified as taxonomically and systematically informative among African colobines (e.g., molar crown shape, projection of the lower face, mandibular corpus depth; Frost, 2001b; Napier, 1985; Szalay & Delson, 1979). Second, we collected standard measurements

across the cranium, mandible, dentition, and postcranium with the goal of documenting variation in the assemblage, testing phylogenetic and functional hypotheses, and making these data available for downstream study by other researchers.

In addition to focusing our data collection from the Faro Daba fossils on taxonomically diagnostic craniodental traits within colobines, we made quantitative and qualitative observations of postcranial traits interpreted to correlate with variation in cercopithecid locomotion. Additionally, we collected data on sex and age to characterize the demographic constitution of the assemblage. All data collection from the Middle Awash fossils was completed on the original fossils housed at the National Museum of Ethiopia. All fossil-derived data presented herein are published in the dataset associated with this manuscript and its counterparts ([*reference online location in data repository here*]; Brasil et al., *submitted*; Taylor et al., *submitted*).

Data collection protocols are consistent with those of Taylor et al. (*submitted*) and Brasil et al. (*submitted*). We provide brief overviews of our methods below; more detailed descriptions of our data collection protocols are reported in Taylor et al. (*submitted*).

2.4.1 | Cranial

We collected standard cranial linear metrics to document variation in the Faro Daba colobine sample and assess cranial size and shape affinities with extant and fossil colobines. We compared linear metrics that reflect size differences (e.g., calvarial width, interorbital breadth). We also calculated ratios to assess muzzle and facial shape, which are reported to vary between extant colobine taxa (Frost, 2001b; Groves, 2007). We present analyses of those linear metrics and ratios for which a relatively large number of individuals is now available in the Faro Daba sample, and that were found to be most diagnostic. We also qualitatively assessed the crania for taxonomically informative features, as detailed in the Results section below.

Cranial measurements were taken from the Faro Daba fossils by a single observer (TAM) following standard protocols (see Monson, 2020; Monson, Brasil, Stratford, & Hlusko, 2017). The following 17 cranial measurements were collected: calvarial length, facial length, facial width, interorbital breadth, maximum cranial breadth, maximum calvarial width, maximum cranial length, maximum width at the upper canines, muzzle width at *ectomolare*, muzzle width at the maxillary fossae, nasal height, nasal width, orbital height, orbital width, palatal length, palatal width at the third molars, and palatal width at the upper canines. We supplemented our extant comparative data with measurements downloaded from the PRIMO database (see Table 1).

2.4.2 | Mandibular

Mandibular depth (height) is known to vary across extant colobine taxa (Frost, 2001b; Frost & Alemseged, 2007). In order to compare the Faro Daba colobines with extant and fossil samples, we collected three standard mandibular metrics from the Faro Daba fossils: mandibular corpus depth at the midpoints of the mandibular first, second, and third molars. These measurements were collected by CET from standardized photographs using ImageJ (Schneider, Rasband, Eliceiri, 2012) following Gilbert et al. (2021). We supplemented these data with measurements downloaded from the PRIMO database (see Table 1).

2.4.3 | Dental

Dental measurements were collected from the Faro Daba fossils following standard protocols (e.g., Grieco, Rizk, & Hlusko, 2013). Maxillary dental measurements were taken by TAM and mandibular dental measurements were taken by MFB. Additional details on measurement protocols applicable to all the Halibee cercopithecids are reported in Taylor et al. (*submitted*). Among the colobine sample, specifically, there is a mesial flange on the buccal side of the mandibular fourth premolar, which was measured as part of the mesiodistal length.

Measurements were not adjusted for interproximal wear, and it should be noted that the measurement methods employed for the Asbole fossils by Frost & Alemseged (2007) do not specify whether they adjusted for interproximal wear, which may affect the comparability of measurements between the two samples. Additionally, we did not measure canine crown height because this measurement is affected by wear, and complete canine crowns (i.e., with an unbroken cusp tip) are rare in the Faro Daba colobine assemblage. We note this here because we instead rely on basal crown diameters in our comparative analyses of canine sexual dimorphism in the Asbole and Faro Daba colobines, and even slight differences in orientation between different observers can have a large impact on these measurements.

To assess sexual dimorphism and the distribution of canine size, we rely on frequency plots. The weakly bimodal distribution of canine size indicates that male and female morphology overlaps considerably. As a result, sex could not be reliably estimated for the majority of the Faro Daba colobine fossils. Consequently, the individuals for which sex could be estimated are at the lower and upper ends of the size range, and calculating a sexual dimorphism index based on measurements for these individuals would artificially inflate the estimate. We therefore compare the distribution of canine metrics across the Faro Daba colobines, *C. guereza*, and the samples from "Andalee" and Asbole.

Our extant comparative data were collected following the same standard protocols as for the fossils (Grieco et al., 2013). We supplemented our comparative data with measurements for extant taxa downloaded from the PRIMO database (see Table 1).

We assessed molar crown shape using ratios of standard linear metrics. For both the maxillary and mandibular second molars, we assessed buccolingual width relative to mesiodistal length because this crown shape ratio for the maxillary second molar was previously shown to discriminate between colobine taxa (Pallas et al., 2019). We also compared the ratio of mesial versus distal buccolingual width of the lophs for the mandibular third molar, which has previously been reported to distinguish extant *Colobus* from other colobines (i.e., wider distal than mesial lophs in *Colobus*; Szalay & Delson, 1979).

In addition to these standard dental ratios, we also assessed two dental ratios that describe the relative sizes of the postcanine teeth, calculated from mesiodistal length measurements. The premolar-molar module (PMM), defined as the ratio of the mesiodistal length of the second mandibular molar to the fourth mandibular premolar (M2L/P4L), describes the relative size of the molars to the premolars (Hlusko et al., 2016). The molar module component (MMC), defined as the ratio of the mesiodistal length of the third mandibular molar to first mandibular molar (M3L/M1L), describes the relative sizes of the molars (Hlusko et al., 2016). We employ these ratios here because they have been shown to be highly heritable and independent of body size (Hlusko et al., 2016), taxonomically useful at the generic level within primates (Hlusko et al., 2016; Monson, Armitage, & Hlusko, 2018), and phylogenetically conserved across mammals (Monson et al., 2019; Zuercher, Monson, Dvoretzky, Ravindramurthy, & Hlusko, 2020). Furthermore, these ratios have been shown to vary at the species level in hominids (Brasil,

Monson, Schmitt, & Hlusko, 2020). As such, they are taxonomically and phylogenetically informative traits, and we employ them to assess the affinities of the Faro Daba fossil assemblage to extant and fossil colobine taxa.

2.4.4 | Postcranial

Measurement of postcranial elements was guided by previous studies assessing morphological correlates of locomotion (e.g., Elton et al., 2016; Frost & Delson, 2002; Harrison, 1989; Strasser, 1992; see Taylor et al., *submitted* section 4.1.3). The following three postcranial features were compared: epicondyle ratio of the distal humerus, relative medial trochlear flange length of the distal humerus, and relative greater trochanter projection of the proximal femur. CET collected the linear postcranial measurements used to calculate these ratios, following previously published methodologies (Elton et al., 2016; Frost & Delson, 2002). We compared these data to those published by Frost et al. (2020) for extant colobines.

We also collected humeral epicondyle angle and femoral neck-shaft angle measurements. However, we do not compare these to data reported in Frost et al. (2020) because we found interobserver measurement error rates to be high for these two angular measurements (see Taylor et al., *submitted*, for discussion). We report these measurements here because they are commonly assessed in studies of cercopithecid postcranial anatomy. However, we caution against relying too heavily on these measurements, particularly as they compare to measurements collected by other researchers, because our intra- and interobserver error rates indicate that these data may not be reliably replicated or compared across researchers.

To document variation among the fossils and to make additional data available for future research, we also collected standard linear measurements across the postcranium. We employ maximum length measurements of the humerus, radius, femur, and tibia in our calculations of intra-and inter-membral indices. The additional metrics were not found to be diagnostically or functionally informative for this initial taxonomic description, but we report them in the dataset associated with this manuscript ([*reference online location in data repository here*]). We rely on published comparative extant data for limb indices, collated from Arenson et al. (2020).

2.4.5 | Sex

Sex was estimated independently by two observers (LJH and MFB) based on the morphology of the canine-premolar honing complex. Sex assessments made by each observer were compared, and when in disagreement, the sex was assessed again and discussed. If concurrence was not easily reached, the sex was marked as "uncertain".

2.4.6 | Ontogenetic age

We conducted a broad-scale survey to characterize the distribution of age-at-death. We recorded ontogenetic age on a scale of one to six for all craniodental specimens for which postcanine tooth position could be ascertained with absolute confidence, and that were readily identified to genus (see Supporting Information Table S1 for scoring criteria). We employ age scores based on tooth eruption and wear rather than specific estimates of chronological age because of the considerable variation in timing and sequence of tooth eruption in colobines (Harvati, 2000; Monson & Hlusko, 2018).

2.5 | Analytical methods

2.5.1 | A population-based approach to taxonomy

The large size and notable preservation of the Faro Daba colobine fossil assemblage makes a traditional specimen-by-specimen description impractical (see Figures 1-3, and Taylor et al., *submitted*, for a more in-depth justification). Accordingly, we take a population-based approach to the taxonomic description of this sample by comparatively describing the cranial, dental, and postcranial anatomies relative to our extant and fossil samples. We outline our taxonomic criteria and differential diagnosis procedures, and we describe the morphologies observed in the sample in a broader populational sense than in traditional descriptive practice (specimen-by-specimen, anatomical element-by-element) most often applied to much smaller assemblages of fossils. Because this sample is essentially modern in its skeletal morphology (as detailed below), our description focuses on quantitative comparisons and photographic illustration. For readers who prefer written descriptions over photographs, we refer to character matrices and descriptions published elsewhere that detail modern *Colobus* morphology (e.g., Groves, 2007; Strasser & Delson, 1987). A full inventory of elements for each individual specimen in the sample is included in Appendix 1.

2.5.2 | Statistical analyses

To quantitatively assess morphological similarities between the Faro Daba fossils and the comparative samples, we employed the Kruskal-Wallis test with a Dunn's *post hoc* test. Considering the small and unevenly distributed sample sizes, we employed these more statistically stringent non-parametric rather than parametric tests to test for sample mean differences. We ran the Dunn's *post hoc* tests with and without a Bonferroni correction for multiple comparisons but report only the uncorrected significance results since the correction overwhelmed nearly all of the statistical signal. For all tests, significance was set at $p<0.05$. All statistical analyses were performed using base R functions and the *FSA* package (for the Dunn's *post hoc* test; Ogle, Doll, Wheeler, & Dinno, 2021) in the R statistical environment v3.6.1 (R Core Team, 2019).

For each variable, the Faro Daba fossils were compared to the extant and fossil samples to test the null hypothesis that there is no difference in group means. Failure to reject the null hypothesis is consistent with the interpretation that the samples are not significantly different. Rejection of the null hypothesis is consistent with the interpretation that the samples are significantly different, and that they may represent different taxa. We tested for statistical differences between samples for all of the following cranial and mandibular variables, for which the largest sample sizes were available for the Faro Daba fossils: facial length, interorbital breadth, palatal width at the level of the maxillary canines, and mandibular corpus height at the first, second, and third molars, respectively. The following dental variables were also tested for differences: maxillary canine length, maxillary second molar mesiodistal length, ratio of the maxillary second molar anterior crown width to mesiodistal crown length, ratio of the mandibular fourth premolar mesiodistal length to first molar mesiodistal length, ratio of mesial to distal buccolingual width of the mandibular third molar, mandibular Molar Module Component

(MMC), and mandibular Premolar-Molar Module (PMM). Three postcranial indices were also assessed: brachial, crural, and humerofemoral.

Descriptive statistics were calculated in Microsoft Excel, and bivariate plots, boxplots, and histograms were produced using *ggplot2* (v3.3.0, Wickham, 2016) in the R statistical environment v3.6.1 (R Core Team, 2019) and compiled in Adobe Illustrator CC 2019 (Adobe, Inc.). Boxplots for postcranial metrics of comparative samples were adapted from Frost et al. (2020) using Adobe Illustrator CC 2019 (Adobe, Inc.).

2.5.3 | Approach to taxonomic identification

Our approach to the taxonomic designation of this sample included three main steps:

Step 1: For each fossil cataloged as belonging to Family Cercopithecidae, we first determined whether it belonged to Subfamily Colobinae. This assessment was made based on craniodental morphology – the diagnostic criteria employed included the presence of a broad interorbital pillar, a mandibular corpus that deepens posteriorly, and postcanine crown morphology typical of colobines (Verheyen, 1962; Vogel, 1966). Colobines are characterized by tall tooth crowns with deep notches and high occlusal relief, defined as a high ratio of notch height/crown height below the notch (NH/NR ratio; Benefit, 1993; Benefit, 2000; Delson, 1975; Groves, 2007). Individuals with lingual enamel on the lower incisors, lingual cingula on the upper incisors, and a small caniniform maxillary second incisor relative to the maxillary first incisor were also classified as colobines (following, for example, Frost & Alemseged, 2007; Szalay & Delson, 1979). Additionally, the presence of a flange on the mesiobuccal side of the mandibular fourth premolar, a paraconid on the mandibular third premolar, and cuspids on the distal margins of the mandibular lateral incisors were employed as diagnostic colobine features (Delson, 1975; Hlusko, 2006, 2007; Szalay & Delson, 1979). Colobines were also distinguished from cercopithecins by the presence of a hypoconulid on the lower third molar, by larger maxillary premolars (with the third premolar having a triangular crown shape and the fourth premolar a round or oval shape), by incisors with a twisted morphology along the long axis of the tooth, by a more robust mandibular symphysis, and by a taller and thicker mandibular corpus (e.g., Szalay & Delson, 1979; Jablonski & Frost, 2010).

For individuals preserving only postcranial anatomy, colobines were distinguished from cercopithecins based on the following diagnostic features: a round and symmetrical humeral head, straight humeral shaft, dull trochlear keel on the distal humerus, round and spherical capitulum, curved ulnar shaft, long olecranon process, proximally flattened greater trochanter, larger lateral than medial epicondyle on the distal femur, wide distal femur, and wide femoral patellar groove (following Frost & Alemseged, 2007; Gebo & Sargis, 1994; Nakatsukasa et al., 2010; Sargis, Terranova, & Gebo, 2008). Although colobines are larger on average than cercopithecins (Frost & Alemseged, 2007; Nakatsukasa et al., 2010), the considerable overlap in size observed in this assemblage made postcranial size alone an unreliable feature for diagnostic use.

Step 2: All individuals identified as colobines on the basis of the features described above were then considered together to test the null hypothesis that the Faro Daba colobine sample includes a range of variation comparable to what is usually observed in a single colobine species. The results of our metric and qualitative assessments relative to our comparative samples (detailed below) fail to reject this hypothesis. Having failed to reject the hypothesis that the sample encompasses a single species, we then moved to assessing the taxonomic affinities of the

sample relative to extant and fossil taxa (features employed to make our taxonomic attribution are detailed below). Many descriptive studies of fossils present metric data but rely heavily on qualitative morphology. Here we rely more heavily on metric data for our assessments of craniodental and postcranial affinities, for which we have a good sense of the range of variation in this sample because of the large number of individuals.

Step 3: Based on the results of these comparative analyses, we then refined our taxonomic identifications. In the following Results sections, we detail the diagnostic morphological features that served as criteria for our referrals to genus and species (following descriptions from Frost & Alemseged, 2007, Groves, 2007, and Napier, 1985, except where otherwise noted).

3 | Results

3.1 | Organization of the results

Below we describe the morphological affinities of the Faro Daba colobine sample through craniodental, mandibular, and postcranial metric comparisons. In so doing, we detail the criteria used to refer individual specimens to genus and species. We follow this taxonomic description with a presentation of the results of our age and sex assessments.

3.2 | Systematic paleontology

Family Cercopithecidae Gray, 1821
Subfamily Colobinae Jerdon, 1867
Genus *Colobus* Illiger, 1811
Colobus* cf. *guereza Rüppell, 1835

3.2.1 | Cranial and mandibular results

The Faro Daba crania are moderately prognathic, more similar to *Colobus* and *Piliocolobus* than to the weakly prognathic *Procolobus* (Figures 4 & 5). The orientation of the premaxillae, a feature likely correlated with prognathism, is more similar to *Colobus* than *Procolobus* in being sloped rather than more vertical (Figures 4 & 5). The supraorbital arches are similar to *Colobus* in being thin and lacking notches/foramina, unlike the thick arches of *Procolobus* (Figure 4; Verheyen, 1962). They differ from the straight and robust supraorbital arches of *Piliocolobus*, the latter often punctuated by notches or foramina. Like *Colobus* and *Piliocolobus*, the borders of the piriform aperture are rounded and there is no anterior nasal spine; this is unlike *Procolobus* in which an incipient nasal spine is common and the aperture margins are sharp. Despite the good preservation of the Faro Daba fossils, very few crania preserve enough of the vault to permit observation of the posterior temporal line morphology. A sagittal crest is present in one individual (Figure 4, right column), and although this feature is more common in adult males of *Procolobus* and *Piliocolobus*, it does occur occasionally in *Colobus*, and therefore is not taxonomically conclusive when observed on an individual specimen.

In both cranial size and shape comparisons, the Faro Daba fossils overlap most consistently with *Colobus* among the extant colobine samples (Figure 6). This overlap is most apparent in measurements of palatal width, calvarial width, and the relative widths of the face

and calvarium (Figure 6c, d, & f). Relative to extant *Colobus*, the fossil ranges and means are most offset for facial length, facial width, and the proportion between facial length and palatal width (Figure 6a, b, & e).

For facial length, the fossils are significantly different from *C. guereza* in the Kruskal-Wallis comparison (at $p<0.05$; Table 2). The interorbital breadth is also significantly different from *C. guereza*, whereas the palatal width at the level of the maxillary canines is not (Table 2). Descriptive statistics for cranial measurements of the Faro Daba fossils are reported in Table 3.

The ascending ramus of the Faro Daba colobine mandibles is vertical as in *Colobus* and unlike the posteriorly sloping ramus of *Procolobus*. The lower margin of the mandible curves upward at the anterior end as in *Colobus*. The corpus varies in depth along its length, with an undulating lower margin, as is often seen in *Colobus* but unlike the mandibles of *Procolobus*, in which the upper and lower margins of the mandible are straight and parallel (Figures 5, 7, & 8). The gonial angle is expanded, and there is a distinct mylohyoid line on the medial surface of the ascending ramus, as in *Colobus*. The height of the mandibular corpus is similar to extant and fossil *Colobus* and also overlaps *Piliocolobus* and *Procolobus* (Figure 9 and Table 4). No significant differences were returned for any of the pairwise comparisons of mandibular corpus height, at any of the three molar positions (Table 2).

Although the Faro Daba fossils match *Procolobus* and *Piliocolobus* in some cranial features, as detailed above, each of these features is also shared with *Colobus.* The signal across the cranial and mandibular anatomy is a clear and consistent affinity to *Colobus*.

3.2.2 | Dental results

The Faro Daba fossils are similar to *Colobus* in having lateral maxillary incisors that angle medially at their incisal tips (Figures 5g & 10). They are also similar to *Colobus* in having weakly sexually dimorphic canines, differing from the more sexually dimorphic canines of *Procolobus* and *Piliocolobus* (Hayes, Freedman, & Oxnard, 1996). The distal edge of the mandibular third molar exhibits considerable variation in this fossil sample, with some individuals presenting a tuberculum sextum (as is common in *Procolobus*), while others have a reduced or even absent hypoconulid. The mandibular first and second molars of some individuals have a small fifth cusp at their distal edge. The maxillary third molars mirror this variation in cusp number and size, with some individuals presenting a small fifth cusp at the distal edge of the crown.

Procolobus is the smallest of the African colobines (average body mass of 3.8 kg and 4.3 kg for females and males, respectively), *Piliocolobus* is intermediate (7.1 kg and 9.9 kg), and *Colobus* is the largest (8.5 kg and 10.4 kg; Bruner et al., 2006; Hayes et al., 1996; Ledevin & Koyabu, 2019). The Faro Daba fossils are most similar in dental size to *Colobus* (Figures 11 & 12). The maxillary and mandibular dental metrics capturing size, crown shape, and postcanine proportions align the fossils most closely with extant *C. guereza* and are distinct from extant *C. angolensis* and the Asbole colobine sample (Figures 11 & 12; see Figures 5, 8, and 10 for views of the dentition and Tables 5 and 6 for dental metrics).

In maxillary postcanine dental size, the Faro Daba fossils are nearly indistinguishable from modern *C. guereza* and are larger than *Procolobus*, *Piliocolobus*, *C. angolensis*, and the "Andalee" and Asbole fossils (Figure 11a, b). These differences are significant for all pairwise comparisons to the Faro Daba fossils, with the exception of *C. guereza*, *Pi. oustaleti,* and *Pi. tholloni* for the Kruskal-Wallis comparison of maxillary second molar mesiodistal length (Table

7). The "Andalee" and Asbole fossils are not significantly different from one another for maxillary second molar mesiodistal length (Kruskal-Wallis, p=0.356), nor are they different from *C. angolensis* (Kruskal-Wallis, p=0.807 and p=0.347, respectively), but they are both different from *C. guereza* (Kruskal-Wallis, p=0.017 and p<0.001).

In maxillary second molar crown shape, the Faro Daba sample is similar to all extant and fossil *Colobus* samples (Figure 11c). Among the comparative samples with more than two individuals, the Faro Daba fossils are significantly different from *C. angolensis* and *Pi. oustaleti*, but not from *C. guereza*, "Andalee," Asbole, or *Pi. badius* (Table 7).

The mandibular dental metrics are also most like extant *Colobus*, specifically *C. guereza* (Figure 12). This affinity is most apparent in postcanine dental proportions (Figure 12b, d). The ratio of the mandibular fourth premolar to the first molar mesiodistal length (Figure 12d) among the Faro Daba fossils is significantly different from all extant and fossil African colobine samples with more than two individuals (i.e., not including *Pi. tholloni* or *Pr. verus*; Table 7). The "Andalee" and Asbole samples are both different from *C. guereza* (Kruskal-Wallis, p<0.001 for both pairwise comparisons), but not from *C. angolensis* (Kruskal-Wallis, p=0.761 and p=0.939, respectively) or each other (Kruskal-Wallis, p=0.804).

One of the largest deviations from modern *C. guereza* is in the mandibular PMM and MMC values, for which the Faro Daba sample provides overlap between the modern *C. guereza* and Asbole samples (Figure 12c). The results of statistical comparisons for the PMM are the same as for the ratio of the mandibular fourth premolar to the first molar mesiodistal length, above (with the only exception that the "Andalee" sample is not significantly different from the Faro Daba sample; Table 7). For the MMC, the Faro Daba sample is significantly different from extant *C. guereza, Pi. badius*, and *Pi. oustaleti*, but not *C. angolensis* or the "Andalee" or Asbole fossils (for the comparisons of samples with more than two individuals; Table 7).

Despite previous indications that crown shape of the mandibular third molar distinguishes extant *Colobus* from other colobines (i.e., wider distal than mesial lophs in *Colobus*; Szalay & Delson, 1979), the ratio of mesial versus distal buccolingual width does not differ significantly between the Faro Daba sample and any of the extant and fossil *Colobus*, *Piliocolobus*, and *Procolobus* samples (Table 7).

One of the most distinctive morphologies of the Faro Daba colobines is the presence of large canines in females, which also characterizes extant *C. guereza*. In contrast, the fossils from "Andalee" and Asbole are described as exhibiting greater sexual dimorphism in the canines relative to extant *C. guereza*, with females having small canines relative to males. The range and distribution of maxillary and mandibular canine metrics in the Faro Daba fossils align closely with extant *C. guereza* and plainly differ from those of the earlier "Andalee" and Asbole fossils (Figure 13). These patterns are statistically supported because maxillary canine mesiodistal length in the Faro Daba sample is not significantly different from extant *C. guereza*, but is different from the "Andalee" and Asbole fossil samples (Table 7). Additionally, the "Andalee" and Asbole samples are not significantly different from each other (Kruskal-Wallis, p=0.808), but both are different from extant *C. guereza* (Kruskal-Wallis, p=0.039 and p<0.001, respectively).

3.2.3 | Postcranial results

The postcranial morphology is generally consistent with extant *C. guereza* (Figure 14). The Faro Daba sample values for epicondyle ratio and relative greater trochanter projection closely

overlap the range of modern *C. guereza* (Figure 14a, c). The relative flange length range overlaps and exceeds the upper end of the modern *C. guereza* range (Figure 14b). A low humeral medial epicondyle angle, high neck-shaft angle of the femur, high epicondyle ratio, small relative flange length, and smaller relative projection of the greater trochanter are all features exhibited by the Faro Daba fossils (Table 8). We reiterate our caution against relying too heavily on these measurements, as our intra- and inter-observer rates indicate that they may not be reliably replicated (see Methods for more details). Regardless, all of these features have been used to infer arboreality in colobine taxa (Frost & Delson, 2002; Harrison, 1989). The metapodials and phalanges are also typical of arboreal colobine taxa in being long and curved (Szalay & Delson, 1979).

The limb indices are also similar to extant *C. guereza*, although the crural index is slightly greater in the fossils (Figure 15). Neither the brachial nor the humerofemoral index are significantly different from extant *C. guereza* (Kruskal-Wallis, p=0.999 and p=0.644, respectively), in contrast to the crural index (Kruskal-Wallis, p=0.012). See Figures 16 and 17 for views of the humeral remains, Figures 18 and 19 for ulnar remains, Figure 19 for radial remains, and Figures 20 and 21 for femoral remains. Descriptive statistics for postcranial metrics are reported in Table 8 (and see the associated dataset for a complete list of metrics and individual measurements).

3.2.4 | Referred material

The lines of anatomical evidence described above indicate that the Faro Daba fossils are most similar to *C. guereza* among the extant African colobines, supporting attribution to this taxon. A stronger affinity to *C. guereza* than to other extant colobines is particularly evident in the dental morphology.

However, the fossils deviate from *C. guereza* in a few morphological features. In mandibular postcanine proportions (i.e., fourth premolar relative to first molar mesiodistal length), the fossils are most similar to *C. guereza* among the comparative samples and are clearly different from *C. angolensis*, but their range is slightly offset (Figure 12b, d). For other measures of postcanine dental proportions (the mandibular PMM and MMC) the Faro Daba fossils fall between extant *C. guereza* and the *Colobus* fossils from "Andalee" and Asbole in PMM vs. MMC morphospace (Figure 12c). In postcranial anatomy, the Faro Daba colobines similarly overlap with extant *C. guereza* in all metrics, but slightly exceed the extant range in their relative humeral flange lengths and crural indices (Figure 14b and Supporting Information Figure S1).

Taking these subtle deviations into account and considering that modern *Colobus* species are primarily distinguished by data inaccessible in the fossil record (i.e., behavior and pelage, Groves, 2007), we conservatively refer all 360 individuals to *Colobus* cf. *guereza* (see Appendix 1 for a full list of referred specimens). Of these 360 individuals, 153 have less well-preserved taxonomically diagnostic anatomy (e.g., edentulous maxillae and mandibles, isolated postcranial fragments). Considering that there is no evidence of multiple colobine species in the Faro Daba sample, and that the 153 more fragmentary individuals fall within the morphological range encapsulated by the more securely referred *Colobus* cf. *guereza* fossils, it is likely that these individuals belong to the same taxon. We therefore refer these 153 individuals to *Colobus* cf. *guereza*, but we note the uncertainty introduced by their more fragmentary condition (indicated in Appendix 1).

3.3 | Sample characteristics: sex and age profiles

3.3.1 | Sex

Sex estimation based on the canine honing complex was possible for 178 specimens and results are reported in Table 9. In contrast to the results reported by Taylor et al. (*submitted*) for the cf. *Chlorocebus* specimens from the same sedimentary unit, we were only able to estimate sex for a small proportion (17%) of *Colobus* specimens. Whereas the cf. *Chlorocebus* fossils have relatively little overlap between males and females in the canine honing complex morphology, the variation observed in the *Colobus* fossils is more continuous, with most individuals falling in the middle of the morphological range (see Figure 13). The difficulty of estimating sex in this sample is interpreted to reflect a low level of sexual dimorphism comparable to what is observed in extant *C. guereza*.

3.3.2 | Ontogenetic age

We were able to score age for 160 of the 360 *Colobus* cf. *guereza* specimens, using the criteria listed in Supporting Information Table S1. The results of the age estimation are reported in Table 10. Nearly half of the sample was assigned an age score of four, which corresponds to a young adult age. The majority of the sample falls within the young- and middle-aged adult categories with scores of four and five (see Supporting Information Figures S1 and S2 for views of juvenile individuals).

4 | Discussion

The Faro Daba fossils have clear morphological affinities to extant *C. guereza,* albeit with a few morphological differences such as postcanine dental proportions (Figure 12b-d). Today, *C. guereza* is the only colobine species present in Ethiopia, represented by two subspecies: *C. g. guereza* and *C. g. gallarum* (Ibrahim, Bekele, & Yazezew, 2017; Oates, 1994; Oates & Trocco, 1983; Zinner et al., 2019). The subspecific taxonomy of *C. guereza* is not well-resolved, and the subspecies that are recognized appear to intergrade geographically and morphologically (Groves, 2007; Zinner et al., 2019). In light of this, and considering that subspecies distinctions are mostly rooted in pelage variation that does not preserve in the fossil record, we do not attempt a subspecific identification for the Faro Daba fossils (Groves, 2007).

4.1 | Relationship to Middle Pleistocene colobine fossils from the Afar Rift

In most morphological features, the Faro Daba colobine fossils are similar to the *Colobus* sp. fossil sample from Asbole, but they differ in two ways: they are larger than the Asbole fossils and more similar in size to modern *C. guereza*, and the females exhibit the large "male-type" canines typical of modern *C. guereza*, whereas the Asbole females have smaller, "female-type" canines (Frost & Alemseged, 2007; Hull, 1979). These differences return to the question of how these two samples may be related, for which we have posed two hypotheses: (1) the Faro Daba fossils sample a 100,000-year-old snapshot of a single evolving species lineage in Ethiopia, or (2) the Faro Daba and Asbole fossils sample two distinct colobine species lineages and the Faro Daba fossils are ancestral to modern *C. guereza.*

Considering the biogeographical implications of the second hypothesis, in which a second colobine species would have been present in Ethiopia ca. 100 ka if the Faro Daba and Asbole fossils sample two distinct lineages, the first hypothesis is more parsimonious. The dental evidence also lends support to the first hypothesis. The mandibular postcanine proportions (i.e., molar module component and premolar-molar module, see Methods) reflect a shift from higher to lower PMM values (larger to smaller second molars relative to fourth premolars), seriated from Asbole to Faro Daba to modern *C. guereza*, respectively (Figure 12c). MMC reflects a phylogenetically conserved and slowly evolving aspect of the mammalian dentition, whereas PMM reflects evolutionary change over shorter time-frames, which accords with the pattern observed for the colobines from Asbole, Faro Daba, and extant *C. guereza* (Brasil et al., 2020; Hlusko et al., 2016; Monson et al., 2019; Zuercher et al., 2020). This morphological gradient in PMM values across these three time-successive *Colobus* samples suggests a potential phyletic relationship between them, lending support to the first hypothesis.

However, the PMM values for the Asbole fossils are also intermediate to the Faro Daba fossils and extant *C. angolensis* (Figure 12c). In dental size and other measures of postcanine proportions, the Asbole fossils are more similar to *C. angolensis* than to *C. guereza* or the Faro Daba fossils (Figure 11a, b and Figure 12b, d). These results recall Frost's (2001a) suggestion that the "Andalee" and Asbole fossils have the strongest affinity to *C. angolensis* among the extant colobines. If the "Andalee" and Asbole fossils are indeed more closely related to *C. angolensis* than *C. guereza*, this would reflect a considerable range expansion for the former and would mean that the geographic range of *C. angolensis* has changed notably over the last half million years (Frost & Alemseged, 2007). An alternative hypothesis consistent with our first hypothesis above is that the "Andalee" and Asbole fossils are morphologically similar to *C. angolensis* but are part of the *C. guereza* lineage, and ancestral to the Faro Daba fossils. In their description of the Asbole fossils, Frost and Alemseged (2007) note that it is not clear whether these older colobines are ancestral to *C. guereza* or another extant species, or whether they represent an extinct species. Additional fossils from the half million years between Asbole (ca. 600 ka) and Faro Daba (ca. 100 ka) are necessary to parse out the finer details of these phylogenetic relationships and biogeographic patterns.

Whatever their relationship with the "Andalee" and Asbole fossils, the younger Faro Daba fossils are indistinguishable from modern *C. guereza* in nearly all measurements, suggesting this species has occupied the Awash Valley for at least 100 ka. The age profile, with a relatively large portion of the sample composed of young and middle-aged adults, suggests that the Faro Daba *Colobus* were subject to at least some of the same predatory pressures as extant *C. guereza* (Dunbar & Dunbar, 1974). Their association with cf. *Chlorocebus* (see Taylor et al., *submitted*) further suggests that their ecology was similar to their modern counterpart, as these two genera co-occur today (Dunbar & Dunbar, 1974; Frost & Alemseged, 2007; Napier, 1981; 1985).

4.2 | Implications for sexual dimorphism evolution

As noted previously, a distinctive feature of the Faro Daba colobine assemblage is the sample size and preservation (Figures 1-3). The large sample size of this assemblage makes it possible to characterize the range of variation for population-level traits, such as the degree of sexual dimorphism. This is rare in paleontology because of the constraints of sample size.

One noted difference between the Faro Daba and Asbole colobine samples is the amount of sexual dimorphism in the canines and lower third premolars (Frost & Alemseged, 2007). The Asbole females are described as lacking the "male-type" canines typical of modern *C. guereza* females and present in the Faro Daba fossils. Frost and Alemseged (2007) do not assign the Asbole *Colobus* fossils to the extant species *C. guereza* because of this perceived difference in sexual dimorphism. For the Faro Daba fossils, the range of variation and the lack of a strongly bimodal distribution for canine size are not consistent with strong sexual dimorphism. The Faro Daba canine size distribution overlaps with modern *C. guereza* and reflects a relatively low level of sexual dimorphism in the honing complex, a phenomenon that appears to be the result of large female canine size (Figure 13). This relatively low level of sexual dimorphism makes sex estimation for these fossils challenging compared to other cercopithecid taxa (see Taylor et al., *submitted*).

The distribution of canine metrics suggests that the high degree of sexual dimorphism described for the Asbole fossils may be, at least in part, an artifact of the relatively small sample size (Figure 13). The range of values, although shifted because of the smaller dental size of the Asbole fossils relative to Faro Daba or modern *C. guereza,* is actually slightly narrower compared to the latter two groups. This is also true of the "Andalee" fossils, an even smaller sample. This similarity in range suggests that the apparently greater sexual dimorphism in the "Andalee" and Asbole samples may simply be the result of incomplete sampling in the central part of the size range, and that samples of four to eleven individuals do not provide enough information about population-level variation. It should also be noted that we did not assess canine crown height (see Methods), and that greater crown height is part of what gives female *C. guereza* a "male-type" appearance. Nonetheless, the possible uneven sampling of the distribution, in combination with the smaller overall size of the "Andalee" and Asbole fossils, may contribute to the interpretation that the female canines are not of the "male-type," particularly if the extant *C. guereza* size range is used as a frame of reference.

If the degree of canine size sexual dimorphism in the "Andalee" and Asbole samples is similar to extant *C. guereza*, and is ancestral along this modern species' lineage, then this feature evolved earlier than previous estimates (e.g., Frost & Alemseged, 2007). Alternatively, if the Asbole fossils are indeed characterized by a greater degree of canine sexual dimorphism, and they sample an earlier segment of the *C. guereza* lineage than the Faro Daba fossils, this would mean that a shift in dimorphism occurred in the intervening half million years. It is also possible, as noted above, that the "Andalee" and Asbole fossils sample another lineage entirely (e.g., *C. angolensis*), in which case they would not bear on *C. guereza* sexual dimorphism evolution, but could provide valuable data for interpreting the evolutionary history of sexual dimorphism within *Colobus* more broadly.

Although the significance of the "male-type" canines typical of *C. guereza* females remains unclear, previous studies have suggested that this morphology may have evolved in response to predation pressure, changes in social organization (i.e., female-female competition), or most likely, some combination of these selection pressures (Hayes, Freedman, & Oxnard, 1995; Hayes et al., 1996). Across primates more generally, canine sexual dimorphism is associated with social structure (e.g., mating systems and intrasexual competition), body size, and/or developmental variation (Harvey, Kavanagh, & Clutton-Brock, 1978; Leutenegger, 1982; Leutenegger & Cheverud, 1982; Leutenegger & Kelly, 1977; Plavcan, 2001). As additional data for extant *C. guereza* morphology, behavior, social organization, and ecology become available, they may well shed light on the significance of the low degree of canine dimorphism. These

insights can, in turn, be leveraged to make inferences about the evolutionary history of *Colobus*, particularly with regard to aspects such as behavior and social structure that are often difficult to interpret from fossil evidence.

We are not suggesting that the Middle Pleistocene Asbole fossils should be more specifically referred to *C. guereza*, particularly since Frost and Alemseged (2007) note other differences, such as mandibular depth and corpus shape, as well as clear differences in overall size (Figures 11-13). However, comparison of distributions between the earlier "Andalee" and Asbole samples, and the later Faro Daba sample suggest that the inferred changes in sexual dimorphism in *Colobus* between 600 ka and today could represent a sampling artifact. Ongoing analyses of large and newly acquired and curated colobine samples from the Andalto member of the Dawaitoli Formation will further clarify colobine evolution during the Middle Pleistocene.

5 | Conclusion

The large new sample of later Pleistocene colobine fossils from the Faro Daba beds of the Halibee member, Dawaitoli Formation, Middle Awash study area is a valuable addition to the colobine fossil record of eastern Africa. These fossils match extant *C. guereza* in nearly all craniodental and postcranial metrics and morphologies, but because of a few subtle differences from the extant representatives of the species, we conservatively refer them to *Colobus* cf. *guereza*. The large size of this sample permits assessment of population-level variation at ca. 100 ka in the Awash Valley: insights never before afforded for African colobine fossils. The range of variation observed bears directly on the interpretation of the colobine fossil record and highlights the difficulty of drawing interpretations from small or single-individual samples.

Acknowledgements

We are grateful to the members of the Middle Awash research team without whose efforts this research would not exist. We especially thank the project co-directors B. Asfaw, Y. Beyene, G. WoldeGabriel, and T. White for their support. We thank the Human Evolution Research Center at UC Berkeley and its donors for funding travel to the National Museum of Ethiopia. We are also grateful to the Afar Regional Government and to the Afar people of the Middle Awash, for their collaboration, contributions, and sacrifices made to advance the fieldwork that yielded this fossil assemblage. We thank the Authority for Research and Conservation of Cultural Heritage and the National Museum of Ethiopia for permission to study fossils in their care. We thank W. Amerga, Y. Assefa, M. Endalamaw, T. Gebremedhin, T. Getachew, and G. Tekle for laboratory and/or field assistance.

We also thank the following repositories, and their personnel who provided access to extant specimens included in this study: the American Museum of Natural History, the Cleveland Museum of Natural History, the Smithsonian Institution's National Museum of Natural History, and the Anthropology Department at the University of Zurich. We thank Dr. Eric Delson and colleagues for access to data downloaded from PRIMO, the NYCEP PRImate Morphology Online database (http://primo.nycep.org).

Collection of the comparative dental and cranial data was supported by NSF grants 0500179, 0616308, 1025263, 0327208, 0130277, 1720128 awarded to LJH. MFB, TAM, CET, and RMY were partially supported by Desmond Clark Graduate Fellowships from the Human Evolution Research Center at UC Berkeley for the portion of this study that was completed at the

National Museum of Ethiopia. MFB was partially supported by a Chancellor's Fellowship and the Portuguese Studies Program at UC Berkeley, and the John Templeton Foundation. During the course of this study, TAM was partially supported by the National Science Foundation in Switzerland, and UC Berkeley's Human Evolution Research Center, Museum of Vertebrate Zoology, Department of Integrative Biology, and Museum of Paleontology. CET was supported by NSF DGE 1752814 for a portion of this study. We thank J. Carlson, M. Krouse, A. Peck, A. Weitz, and T. White for helpful feedback, support, and discussion.

Data Availability Statement

The data that support the findings of this study are openly available in *figshare* at http://doi.org/[doi to be specified immediately prior to publication], reference number [reference number to be specified immediately prior to publication].

References

Arenson, J. L., Sargis, E. J., Hart, J. A., Hart, T. B., Detwiler, K. M., & Gilbert, C. C. (2020). Skeletal morphology of the lesula (*Cercopithecus lomamiensis*) and the evolution of guenon locomotor behavior. *American Journal of Physical Anthropology*, *172*(1), 3-24. doi:10.1002/ajpa.24025

Arambourg, C. (1959). Vertébrés continentaux du Miocène supérieur de l'Afrique du Nord. *Paléontologie 4*, 5-159.

Assefa, Z., Yirga, S., & Reed, K. E. (2008). The large-mammal fauna from the Kibish Formation. *Journal of Human Evolution*, *55*(3), 501-512. doi:10.1016/j.jhevol.2008.05.015

Benefit, B. K. (1993). The permanent dentition and phylogenetic position of *Victoriapithecus* from Maboko Island, Kenya. *Journal of Human Evolution*, *25*(2), 83-172.

Benefit, B. R. (2000). Old World monkey origins and diversification: An evolutionary study of diet and dentition. In P. F. Whitehead & C. J. Jolly (Eds.), *Old World Monkeys* (pp. 133-179). Cambridge: Cambridge University Press.

Benefit, B. R., & Pickford, M. (1986). Miocene fossil cercopithecoids from Kenya. *American Journal of Physical Anthropology, 69*(4), 441-464. doi:10.1002/ajpa.1330690404

Brasil, M. F., Monson, T. A., Schmitt, C. A., & Hlusko, L. J. (2020). A genotype: phenotype approach to testing taxonomic hypotheses in hominids. *The Science of Nature, 107*, 40. doi:10.1007/s00114-020-01696-9

Brasil, M. F., Monson, T. A., Taylor, C. E., Yohler, R. M., & Hlusko, L. J. (*submitted*). A fossil assemblage of near-modern *Papio hamadryas* from the Afar Depression of Ethiopia. Submitted to *American Journal of Physical Anthropology*.

[dataset] Brasil, M. F., Monson, T. A., Taylor, C. E., Yohler, R. M., & Hlusko, L. J. To be made available on *figshare* immediately prior to the publication of this manuscript.

Bruner, E., Pucci, A., & Jones, T. (2006). Cranial morphology and anatomy of two adult females of *Piliocolobus gordonorum* (Udzungwa Red Colobus) (Mammalia, Primates: Colobinae). *Aldrovandia, 2*, 73-78.

Delson, E. (1975). Evolutionary history of the Cercopithecidae. In F. S. Szalay (Ed.), *Approaches to Primate Paleontology* (pp. 167-217). Basel: Karger.

Dunbar, R. I. M., & Dunbar, E. P. (1974). Ecology and population dynamics of *Colobus guereza* in Ethiopia. *Folia Primatologica, 21*, 188-208. doi:10.1159/000155600

Elton, S., Jansson, A. U., Meloro, C., Louys, J., Plummer, T., & Bishop, L. C. (2016). Exploring morphological generality in the Old World monkey postcranium using an ecomorphological framework. *Journal of Anatomy, 228*(4), 534-560. doi:10.1111/joa.12428

Frost, S. R. (2001a). Fossil Cercopithecidae from the Afar depression, Ethiopia: Species systematics and comparison to the Turkana Basin (Doctoral dissertation). City University of New York, New York.

Frost, S. R. (2001b). New Early Pliocene Cercopithecidae (Mammalia: Primates) from Aramis, Middle Awash Valley, Ethiopia. *American Museum Novitates*, *3350*, 1-36.

Frost, S. R., & Alemseged, Z. (2007). Middle Pleistocene fossil Cercopithecidae from Asbole, Afar Region, Ethiopia. *Journal of Human Evolution, 53*(3), 227-259. doi:10.1016/j.jhevol.2007.02.003

Frost, S. R., & Delson, E. (2002). Fossil Cercopithecidae from the Hadar Formation and surrounding areas of the Afar Depression, Ethiopia. *Journal of Human Evolution, 43*(5), 687-748. doi:10.1053/jhev.2002.0603

Frost, S. R., Gilbert, C. C., & Nakatsukasa, M. (2022). The Colobine Fossil Record. In I. Matsuda, C. Grueter, & J. Teichroeb (Eds.), *The Colobines: Natural History, Behaviour and Ecological Diversity* (pp. 13-31). Cambridge: Cambridge University Press. doi:10.1017/9781108347150.004

Frost, S. R., Gilbert, C. C., Pugh, K. D., Guthrie, E. H., & Delson, E. (2015). The hand of *Cercopithecoides williamsi* (Mammalia, Primates): earliest evidence for thumb reduction among colobine monkeys. *PLoS ONE*, *10*(5), e0125030. doi:10.1371/journal.pone.0125030

Frost, S. R., Haile-Selassie, Y., & Hlusko, J. (2009). Cercopithecidae. In Y. Haile-Selassie & G. WoldeGabriel (Eds.), *Ardipithecus kadabba: Late Miocene evidence from the Middle Awash, Ethiopia* (pp. 135-158). Berkeley and Los Angeles, CA: University of California Press.

Frost, S. R., Simpson, S. W., Levin, N. E., Quade, J., Rogers, M. J., & Semaw, S. (2020). Fossil Cercopithecidae from the Early Pliocene Sagantole Formation at Gona, Ethiopia. *Journal of Human Evolution, 144*, 102789. doi:10.1016/j.jhevol.2020.102789

Gebo, D. L., & Sargis, E. J. (1994). Terrestrial adaptations in the postcranial skeletons of guenons. *American Journal of Physical Anthropology, 93*(3), 341-371. doi:10.1002/ajpa.1330930306

Gilbert, C. C., Gilissen, E., Arenson, J. L., Patel, B. A., Nakatsukasa, M., Hart, T. B., ... & Sargis, E. J. (2021). Morphological analysis of new Dryas Monkey specimens from the Central Congo Basin: Taxonomic considerations and an emended diagnosis. *American Journal of Physical Anthropology, 176(3)*, 361-389. doi:10.1002/ajpa.24278

Gilbert, C. C., Goble, E. D., & Hill, A. (2010). Miocene Cercopithecoidea from the Tugen Hills, Kenya. *Journal of Human Evolution*, *59*(5), 465-483. doi:10.1016/j.jhevol.2010.05.005

Gray, J. E. (1821). On the natural arrangement of vertebrose animals. *London Medical Repository, 15*, 296-310.

Grieco, T. M., Rizk, O. T., & Hlusko, L. J. (2013). A modular framework characterizes micro- and macroevolution of Old World monkey dentitions. *Evolution, 67*(1), 241-259. doi:10.1111/j.1558-5646.2012.01757.x

Groves, C. P. (2007). The taxonomic diversity of the Colobinae of Africa. *Journal of Anthropological Sciences, 85*, 7-34.
Grubb, P., Butynski, T. M., Oates, J. F., Bearder, S. K., Disotell, T. R., Groves, C. P., & Struhsaker, T. T. (2003). Assessment of the diversity of African primates. *International Journal of Primatology, 24*(6), 1301-1357. doi:10.1023/B:IJOP.0000005994.86792.b9
Harrison, T. (1989). New postcranial remains of *Victoriapithecus* from the middle Miocene of Kenya. *Journal of Human Evolution*, *18*(1), 3-54. doi:10.1016/0047-2484(89)90022-5
Harrison, T., & Harris, E. E. (1996). Plio-Pleistocene cercopithecids from Kanam East, western Kenya. *Journal of Human Evolution, 30*(6), 539-561. doi:10.1006/jhev.1996.0042
Harvati, K. (2000). Dental eruption sequence among colobine primates. *American Journal of Physical Anthropology, 112*(1), 69-85. doi:10.1002/(SICI)1096-8644(200005)112:1<69::AID-AJPA8>3.0.CO;2-I
Harvey, P. H., Kavanagh, M., & Clutton-Brock, T. H. (1978). Canine tooth size in female primates. *Nature, 276*, 817-818. doi:10.1038/276817a0
Hayes, V. J., Freedman, L., & Oxnard, C. E. (1995). The differential expression of dental sexual dimorphism in subspecies of *Colobus guereza*. *International Journal of Primatology, 16*(6), 971-996. doi:10.1007/BF02696112
Hayes, V. J., Freedman, L., & Oxnard, C. E. (1996). Dental sexual dimorphism and morphology in African colobus monkeys as related to diet. *International Journal of Primatology, 17*(5), 725-757. doi:10.1007/BF02735262
Hlusko, L. J. (2006). A new large Pliocene colobine species (Mammalia: Primates) from Asa Issie, Ethiopia. *Geobios, 39*(1), 57-69. doi:10.1016/j.geobios.2004.09.001
Hlusko, L. J. (2007). A new late Miocene species of *Paracolobus* and other Cercopithecoidea (Mammalia: Primates) fossils from Lemudong'o, Kenya. *Kirtlandia, 56*, 72-85.
Hlusko, L. J., Schmitt, C. A., Monson, T. A., Brasil, M. F., & Mahaney, M. C. (2016). The integration of quantitative genetics, paleontology, and neontology reveals genetic underpinnings of primate dental evolution. *Proceedings of the National Academy of Sciences, 113*(33), 9262-9267. doi:10.1073/pnas.1605901113
Hull, D. B. (1979). A craniometric study of the black and white *Colobus* Illiger 1811 (Primates: Cercopithecoidea). *American Journal of Physical Anthropology, 51*(2), 163-181. doi:10.1002/ajpa.1330510204
Ibrahim, H., Bekele, A., & Yazezew, D. (2017). Population structure and feeding ecology of Guereza (*Colobus guereza*) in Borena-Sayint National Park, northern Ethiopia. *International Journal of Biodiversity and Conservation, 9*(11), 323-333. doi:10.5897/IJBC2017.1114
Illiger, C. (1811). *Prodromus systematis mammalium et avium additis terminus zoographics utriudque classis.* Berlin: C. Salfeld.
Jablonski, N., & Leakey, M. (2008). Systematic paleontology of the small colobines. In N. G. Jablonski & M. G. Leakey (Eds.), *Koobi Fora Research Project: Volume 6. The Fossil Monkeys* (pp. 12-30). San Francisco: California Academy of Sciences.
Jablonski, N. G., & Frost, S. R. (2010). Cercopithecoidea. In L. Werdelin & W. J. Sanders (Eds.), *Cenozoic Mammals of Africa* (pp. 393-428). Berkeley: University of California Press.
Jablonski, N. G., Leakey, M. G., Ward, C. V., & Antón, M. (2008). Systematic paleontology of the large colobines. In N. G. Jablonski & M. G. Leakey (Eds.), *Koobi Fora Research*

Project: Volume 6. The Fossil Monkeys (pp. 31-102). San Francisco: California Academy of Sciences.
Jerdon, T. C. (1867). *The Mammals of India: A Natural History of All the Animals Known to Inhabit Continental India*. Rourkee: Thompson College.
Kalb, J. E., Jaegar, M., Jolly, C. J., & Kana, B. (1982). Preliminary geology, paleontology and paleoecology of a Sangoan site at Andalee, Middle Awash Valley, Ethiopia. *Journal of Archaeological Science, 9*(4), 349-363. doi:10.1016/0305-4403(82)90040-1
Kingdon, J., Happold, D., Butynski, T., Hoffmann, M., Happold, M., & Kalina, J. (2013). *Mammals of Africa. Volume II: Primates*. London: Bloomsbury.
Leakey, M. G., Teaford, M. F., & Ward, C. V. (2003). Cercopithecidae from Lothagam. In M. G. Leakey & J. M. Harris (Eds.), *Lothagam: the Dawn of Humanity in Eastern Africa* (pp. 201-248). New York: Columbia University Press. doi:10.7312/leak11870-011
Ledevin, R., & Koyabu, D. (2019). Patterns and constraints of craniofacial variation in colobine monkeys: disentangling the effects of phylogeny, allometry and diet. *Evolutionary Biology, 46*(1), 14-34. doi:10.1007/s11692-019-09469-7
Leutenegger, W. (1982). Scaling of sexual dimorphism in body weight and canine size in primates. *Folia Primatologica, 37*, 163-176. doi:10.1159/000156031
Leutenegger, W., & Cheverud, J. (1982). Correlates of sexual dimorphism in primates: ecological and size variables. *International Journal of Primatology, 3*(4), 387-402. doi:10.1007/BF02693740
Leutenegger, W., & Kelly, J. T. (1977). Relationship of sexual dimorphism in canine size and body size to social, behavioral, and ecological correlates in anthropoid primates. *Primates, 18*(1), 117-136. doi:10.1007/BF02382954
Meikle, W. E. (1987). Fossil Cercopithecidae from the Sahabi Formation. In N. T. Boaz, A. El-Arnauti, A. W. Gaziry, J. de Heinzelin, & D. D. Boaz (Eds.), *Neogene Paleontology and Geology of Sahabi* (pp. 119–127). New York: Liss.
Monson, T. A. (2020). Patterns and magnitudes of craniofacial covariation in extant cercopithecids. *The Anatomical Record, 303*(12), 3068-3084. doi:10.1002/ar.24398
Monson, T. A., Armitage, D. W., & Hlusko, L. J. (2018). Using machine learning to classify extant apes and interpret the dental morphology of the chimpanzee-human last common ancestor. *PaleoBios, 35*, ucmp_paleobios_40776.
Monson, T. A., Boisserie, J. R., Brasil, M. F., Clay, S. M., Dvoretzky, R., Ravindramurthy, S., . . . Hlusko, L. J. (2019). Evidence of strong stabilizing effects on the evolution of boreoeutherian (Mammalia) dental proportions. *Ecology and Evolution, 9*(13), 7597-7612. doi:10.1002/ece3.5309
Monson, T. A., Brasil, M. F., Stratford, D. J., & Hlusko, L. J. (2017). Patterns of craniofacial variation and taxonomic diversity in the South African Cercopithecidae fossil record. *Palaeontologia Electronica, 20.1.7A*, 1-20. doi:10.26879/690
Monson, T. A., & Hlusko, L. J. (2018). Breaking the rules: Phylogeny, not life history, explains dental eruption sequence in primates. *American Journal of Physical Anthropology*, *167*(2), 217-233. doi: 10.1002/ajpa.23618
Morgan, L. E., Renne, P. R., Taylor, R., & WoldeGabriel, G. (2009). Archaeological age constraints from extrusion ages of obsidian: Examples from the Middle Awash, Ethiopia. *Quaternary Geochronology, 4*(3), 193-203. doi:10.1016/j.quageo.2009.01.001

Nakatsukasa, M., Mbua, E., Sawada, Y., Sakai, T., Nakaya, H., Yano, W., & Kunimatsu, Y. (2010). Earliest colobine skeletons from Nakali, Kenya. *American Journal of Physical Anthropology, 143*(3), 365-382. doi:10.1002/ajpa.21327

Napier, P. H. (1981). *Catalog of Primates in the British Museum (Natural History) and elsewhere in the British Isles, Part II: Family Cercopithecidae, Subfamily Cercopithecinae*. London: British Museum (Natural History).

Napier, P. H. (1985). *Catalog of Primates in the British Museum (Natural History) and elsewhere in the British Isles, Part III: Family Cercopithecidae, Subfamily Colobinae*. London: British Museum (Natural History).

Niespolo, E. M., WoldeGabriel, G., Hart, W. K., Renne, P. R., Sharpe, W. D, Shackley, S. M., … White, T. D. (2021). Integrative geochronology calibrates the Middle and Late Stone Ages of Ethiopia's Afar Rift. *Proceedings of the National Academy of Sciences, 118(50),* e2116329118. doi:10.1073/pnas.2116329118

Oates, J. F. (1994). The natural history of African colobines. In A. G. Davies & J. F. Oates (Eds.), *Colobine monkeys: Their ecology, behaviour and evolution* (pp. 75-128). Cambridge: University Press.

Oates, J. F., Bocian, C. M., & Terranova, C. J. (2000). The loud calls of black and white colobus monkeys: their adaptive and taxonomic significance in light of new data. In P. F. Whitehead & C. J. Jolly (Eds.), *Old World Monkeys* (pp. 431-452). Cambridge: Cambridge University Press.

Oates, J. F., & Trocco, T. F. (1983). Taxonomy and phylogeny of black-and-white colobus monkeys. *Folia Primatologica, 40*, 83-113. doi:10.1159/000156092

Ogle, D. H., Doll, J. C., Wheeler, P., & Dinno, A. (2021). *FSA: Fisheries Stock Analysis*. R package version 0.9.1, https://github.com/droglenc/FSA

Pallas, L., Daver, G., Mackaye, H. T., Likius, A., Vignaud, P., & Guy, F. (2019). A window into the early evolutionary history of Cercopithecidae: Late Miocene evidence from Chad, Central Africa. *Journal of Human Evolution*, *132*, 61-79. doi:10.1016/j.jhevol.2019.03.013

Perelman, P., Johnson, W. E., Roos, C., Seuánez, H. N., Horvath, J. E., Moreira, M. A., ... & Pecon-Slattery, J. (2011). A molecular phylogeny of living primates. *PLoS Genetics*, *7*(3), e1001342. doi:10.1371/journal.pgen.1001342

Plavcan, J. M. (2001). Sexual dimorphism in primate evolution. *Yearbook of Physical Anthropology, 116*(S33), 25-53. doi:10.1002/ajpa.10011

R Core Team. (2019). *R: A language and environment for statistical computing*. Retrieved from https://www.R-project.org/

Rahm, U. (1970). Ecology, zoogeography and systematics of some African forest monkeys. In J. R. Napier & P. H. Napier (Eds.), *Old World Monkeys* (pp. 591-626). London and New York: Academic Press.

Roos, C., Zinner, D., Kubatko, L. S., Schwarz, C., Yang, M., Meyer, D., . . . Osterholz, M. (2011). Nuclear versus mitochondrial DNA: evidence for hybridization in colobine monkeys. *BMC Evolutionary Biology, 11*, 77. doi:10.1186/1471-2148-11-77

Rossie, J. B., Gilbert, C. C., & Hill, A. (2013). Early cercopithecid monkeys from the Tugen Hills, Kenya. *Proceedings of the National Academy of Sciences*, *110*(15), 5818-5822. doi:10.1073/pnas.1213691110

Rüppell, E. (1835). Neue Wirbelthiere zu der Fauna von Abbyssinien gehörig. In *Säugethiere* (Vol. 1, pp. 1-16). Frankfurt am Main: Siegmund Schmerber.

Sargis, E. J., Terranova, C. J., & Gebo, D. L. (2008). Evolutionary morphology of the guenon postcranium and its taxonomic implications. In E. J. Sargis & M. Dagosto (Eds.), *Mammalian Evolutionary Morphology* (pp. 361-372). Dordrecht: Springer.

Schneider, C. A., Rasband, W. S., & Eliceiri, K. W. (2012). NIH Image to ImageJ: 25 years of image analysis. *Nature methods, 9*, 671-675. doi:10.1038/nmeth.2089

Schwarz, E. (1929). On the local races and distribution of the black and white colobus monkeys. *Proceedings of the Zoological Society of London, 99*(3), 585-598. doi:10.1111/j.1469-7998.1929.tb07707.x

Senut, B. (1994). Cercopithecoidea néogènes et quaternaires du rift occidental (Ouganda). In B. Senut & M. Pickford (Eds). *Geology and Palaeobiology of the Albertine Rift Valley, Uganda-Zaire. Volume II: Palaeobiology* (pp. 195–205). Orléans: CIFEG.

Simons, E. L. (1967). A fossil *Colobus* skull from the Sudan (Primates, Cercopithecidae). *Postilla, 111*, 1-12.

Springer, M. S., Meredith, R. W., Gatesy, J., Emerling, C. A., Park, J., Rabosky, D. L., ... & Murphy, W. J. (2012). Macroevolutionary dynamics and historical biogeography of primate diversification inferred from a species supermatrix. *PLoS ONE*, *7*(11), e49521. doi:10.1371/journal.pone.0049521

Strasser, E. (1992). Hindlimb proportions, allometry, and biomechanics in Old World monkeys (Primates, Cercopithecidae). *American Journal of Physical Anthropology*, *87*(2), 187-213.

Strasser, E., & Delson, E. (1987). Cladistic analysis of cercopithecid relationships. *Journal of Human Evolution, 16*(1), 81-99. doi:10.1016/0047-2484(87)90061-3

Stromer, E. (1913). Mitteilungen über Wirbeltierreste aus dem Mittelpliocän des Natrontales (Ägypten). *Zeitschrift der Deutschen Geologischen Gesellschaft, 65*, 350-372.

Suwa, G., Beyene, Y., Nakaya, H., Bernor, R. L., Boisserie, J. R., Bibi, F., ... & Asfaw, B. (2015). Newly discovered cercopithecid, equid and other mammalian fossils from the Chorora Formation, Ethiopia. *Anthropological Science*, *123*, 19-39. doi:10.1537/ase.150206

Szalay, F. S., & Delson, E. (1979). *Evolutionary History of the Primates*. New York: Academic Press.

Taylor, C. E., Brasil, M. F., Monson, T. A., Yohler, R. M., & Hlusko, L. J. (*submitted*). Halibee fossil assemblages reveal later Pleistocene cercopithecins (Cercopithecidae: Primates) in the Middle Awash of Ethiopia. Submitted to *American Journal of Biological Anthropology*.

Ting, N. (2008). Mitochondrial relationships and divergence dates of the African colobines: evidence of Miocene origins for the living colobus monkeys. *Journal of Human Evolution, 55*(2), 312-325. doi:10.1016/j.jhevol.2008.02.011

Verheyen, W. N. (1962). Contribution à la craniologie comparée des primates: les genres *Colobus* Illiger 1811 et *Cercopithecus* Linné 1758. *Musee Royal de l'Afrique Centrale, Tervuren, Annales, 105*, 1-255.

Vogel, C. (1966). Morphologische studien am gesichtsschadel catarrhiner Primaten. *Bibliotheca Primatol*ogica, *4*, 1-226.

Wang, X. P., Yu, L., Roos, C., Ting, N., Chen, C. P., Wang, J., & Zhang, Y. P. (2012). Phylogenetic relationships among the colobine monkeys revisited: new insights from analyses of complete mt genomes and 44 nuclear non-coding markers. *PLoS ONE, 7*(4), e36274. doi:10.1371/journal.pone.0036274

Wickham, H. (2016). *ggplot2: elegant graphics for data analysis*. New York: Springer.
Zinner, D., Tesfaye, D., Stenseth, N. C., Bekele, A., Mekonnen, A., Doeschner, S., . . . Roos, C. (2019). Is *Colobus guereza gallarum* a valid endemic Ethiopian taxon? *Primate Biology, 6*, 7-16. doi:10.5194/pb-6-7-2019
Zuercher, M. E., Monson, T. A., Dvoretzky, R. R., Ravindramurthy, S., & Hlusko, L. J. (2020). Dental variation in megabats (Chiroptera: Pteropodidae): Tooth metrics correlate with body size and tooth proportions reflect phylogeny. *Journal of Mammalian Evolution*, 1-16. doi:10.1007/s10914-020-09508-7

Figure Legends

Figure 1 Crania of Faro Daba *Colobus* cf. *guereza* in anterior view. Clockwise from top left: HAL-VP-9/730, HAL-VP-9/319, HAL-VP-9/723, HAL-VP-9/332, HAL-VP-9/5, HAL-VP-9/489, HAL-VP-9/1572, and HAL-VP-9/779. The individuals at the far left and right are a probable female and male, respectively; sex is uncertain for the six individuals in the center. Crania are aesthetically arranged to provide a sense of preservation and variation in the assemblage. See subsequent figures for more traditional views. Scale is approximate.

Figure 2 Distribution of anatomical regions represented in the Faro Daba *Colobus* cf. *guereza* sample. (a) Number of cataloged specimens with cranial, dental, and/or mandibular remains, postcranial remains, and both types of remains. (b) Number of cataloged specimens preserving elements from nine anatomical regions. Note that cataloged specimens are counted in multiple categories (e.g., the 43 individuals with both types of remains in (a) are also counted in the two categories above). Elements classified as belonging to the "shoulder" include the clavicle and the scapula; the "pelvis" includes the os coxae and the sacrum. See Appendix 1 for a full list of specimens and element inventory.

Figure 3 Faro Daba *Colobus* cf. *guereza* skeleton, HAL-VP-9/1102. Sex is uncertain. Phalanges are arranged along the right side from proximal (top group) to intermediate (middle group) to distal (bottom group). This is one of the most complete single individuals recovered, but it should be noted that there are more than a dozen relatively complete partial skeletons in the Faro Daba colobine assemblage (see Appendix 1 for inventory).

Figure 4 Faro Daba *Colobus* cf. *guereza* and extant colobine adult crania. *Top panel*: Faro Daba *Colobus* cf. *guereza* in anterior (top row), superior (center row), and lateral (bottom row) views. Sex is uncertain for all fossil individuals. From left to right: HAL-VP-9/723, HAL-VP-9/779, and HAL-VP-9/1572. HAL-VP-9/723 (left) and HAL-VP-9/1572 (right) are pictured in left lateral view; anterior is to the left. HAL-VP-9/779 (center) is pictured in right lateral view; anterior is to the right. HAL-VP-9/723 includes associated vault fragments, dental remains, and a partial postcranial skeleton that are not pictured here. HAL-VP-9/779 does not preserve any additional associated elements beyond the cranium pictured here. HAL-VP-9/1572 includes mandibular, dental, and postcranial remains that are not pictured here; see Figure 10 for an occlusal view of the maxillary dentition of this individual. *Bottom panel*: Extant colobines in superior (top row) and left lateral (bottom row) views. Anterior is to the left. From left to right: *C. guereza* male (FMNH 31163), *C. angolensis* female (FMNH 27276), and *Pi. badius* female

(FMNH 15519). Images of extant specimens by Rebecca A. Banasiak, licensed under a Creative Commons Attribution-Noncommercial 4.0 International License. Scale is the same for both panels.

Figure 5 Maxillary and mandibular morphology of Faro Daba *Colobus* cf. *guereza* and maxillary morphology of Asbole *Colobus* sp. specimens prior to matrix cleaning (see Figure 7 for mandibular comparisons). *Left panel*: Two Faro Daba *Colobus* cf. *guereza* adult individuals preserving both maxillary and mandibular anatomy. HAL-VP-9/1101 (female) is pictured on the left and HAL-VP-9/488 (male) on the right. (a) HAL-VP-9/1101 maxilla in inferior view; anterior is up. (b) HAL-VP-9/1101 mandible in superior view; anterior is up. (c) HAL-VP-9/1101 mandible in right lateral view; anterior is to the right. (d) HAL-VP-9/488 mandible in right lateral view; anterior is to the right. (e) HAL-VP-9/488 maxilla in right lateral view; anterior is to the right. (f) HAL-VP-9/488 maxilla in superior view; anterior is down. (g) HAL-VP-9/488 maxilla in anterior view; superior is up. *Right panel*: Four Asbole individuals preserving maxillary anatomy. (h) ASB-254-6, male left maxilla in anterior view. (i) ASB-90, female left maxilla in anterior view. (j) ASB-90, female left maxilla in left lateral view; anterior is to the left. (k) ASB-90, female left maxilla in occlusal view; anterior is up. (l) ASB-214, male right maxilla in right lateral view; anterior is to the right. (m) ASB-214, male right maxilla in occlusal view; anterior is up. (n) ASB-87, female right maxilla in right lateral view; anterior is to the right. (o) ASB-87, female right maxilla in occlusal view; anterior is up. Images of the Asbole fossils are from Frost and Alemseged (2007). Scale is the same for both panels.

Figure 6 Cranial metrics for the Faro Daba *Colobus* cf. *guereza* fossils and comparative samples. (a) Facial length. (b) Facial width. (c) Palatal width at the level of the maxillary canines. (d) Maximum calvarial width. (e) Ratio of facial length to palatal width at the level of the maxillary canines. (f) Ratio of facial width to maximum calvarial width. Abbreviations: mm, millimeters.

Figure 7 Mandibular morphology of Faro Daba *Colobus* cf. *guereza*, Asbole *Colobus* sp., and extant *C. guereza. Left panel*: Faro Daba *Colobus* cf. *guereza* adult mandibles in right lateral view, demonstrating the preservation and variation in the assemblage. Mandibles are seriated from smallest (top) to largest (bottom) in general size. From top to bottom: HAL-VP-9/627 (probable female), HAL-VP-9/338, HAL-VP-9/590, HAL-VP-9/739 (female), HAL-VP-9/316, HAL-VP-2/59, and HAL-VP-9/488 (male). Sex is uncertain unless otherwise indicated above. *Right panel*: Asbole *Colobus* sp. and extant *C. guereza.* From top to bottom: ASB-215-2 (female), ASB-80 (female), ASB-254-13 (male), and extant *C. guereza* specimens HTB 0801 (female) and HTB 1504 (male). Mandibles are in right lateral view, except for ASB-254-13, which is in left lateral view. Images of the Asbole fossils are from Frost and Alemseged (2007). Scale is the same for both panels.

Figure 8 Faro Daba *Colobus* cf. *guereza* and Asbole *Colobus* sp. mandibles. *Top panel*: Faro Daba *Colobus* cf. *guereza* adult mandibles in superior (left) and left lateral (right) views. Top row: HAL-VP-9/733 (probable female). Bottom row: HAL-VP-9/556 (male). *Bottom panel*: Asbole *Colobus* sp. adult mandibles in superior (left) and right lateral (right) views. Top row: ASB-78 (male). Center row: ASB-100 (male). Bottom row: ASB-76 (female). Images of the Asbole fossils are from Frost and Alemseged (2007). Scale is the same for both panels.

Figure 9 Mandibular metrics for the Faro Daba *Colobus* cf. *guereza* fossils and comparative samples. (a) Height of the mandibular corpus at the midpoint of the mandibular first molar. (b) Height of the mandibular corpus at the midpoint of the mandibular third molar. Abbreviations: mm, millimeters; M1, first molar; M2, second molar.

Figure 10 Nearly complete adult maxillary dentitions of *Colobus* cf. *guereza* individuals HAL-VP-9/1572 (left) and HAL-VP-9/384 (right) in inferior view; anterior is up. Sex is uncertain for both individuals. See Figure 4 for additional views of the HAL-VP-9/1572 cranium.

Figure 11 Maxillary dental metrics for the Faro Daba *Colobus* cf. *guereza* fossils and comparative samples. (a) Mesiodistal crown length of the maxillary fourth premolar vs. maxillary first molar. (b) Mesiodistal crown length vs. anterior crown width of the maxillary second molar. (c) Ratio of the maxillary second molar anterior crown width to mesiodistal crown length. Abbreviations: mm, millimeters; L, mesiodistal crown length; AW, buccolingual width of the anterior loph; P4, M1, and M2 refer to the fourth premolar and first and second molars, respectively.

Figure 12 Mandibular dental metrics for the Faro Daba *Colobus* cf. *guereza* fossils and comparative samples. (a) Mesiodistal crown length vs. anterior crown width of the mandibular second molar. (b) Mesiodistal crown length of the mandibular fourth premolar vs. mandibular first molar. (c) Molar module component (MMC) vs. premolar-molar module (PMM); see Methods section for details on these dental ratios. Note that although three *Colobus* cf. *guereza* individuals at the low end of the MMC axis appear here as outliers, there are additional individuals that span the perceived gap in MMC values; they are not included here because they do not preserve the PMM. (d) Ratio of the mandibular fourth premolar mesiodistal crown length to mandibular first molar mesiodistal crown length. Abbreviations: mm, millimeters; L, mesiodistal crown length; AW, buccolingual width of the anterior loph; P4, M1, and M2 refer to the fourth premolar and first and second molars, respectively.

Figure 13 Frequency distributions of maxillary canine crown mesiodistal length (left) and buccolingual width (right) for the Faro Daba *Colobus* cf. *guereza* fossils and comparative *Colobus* samples. Measurements are in millimeters. The Faro Daba *Colobus* cf. *guereza* align closely with the extant *Colobus guereza* sample. The Middle Pleistocene *Colobus* sp. samples from “Andalee” and Asbole, Ethiopia, are smaller on average than both more recent samples. See text for a discussion of the implications of this size difference.

Figure 14 Boxplots of three postcranial metrics for the Faro Daba *Colobus* cf. *guereza* fossils and extant comparative samples. Sample sizes are indicated in parentheses. These metrics have been interpreted to reflect locomotory habitus in cercopithecids (see text for discussion). (a) Epicondyle ratio of the distal humerus. (b) Relative flange length of the distal humerus. (c) Relative greater trochanter projection of the proximal femur. Comparative plots for extant colobines are adapted from Frost et al. (2020).

Figure 15 Postcranial indices for the Faro Daba *Colobus* cf. *guereza* fossils and extant *Colobus guereza*. (a) Brachial index: (maximum radial length / maximum humeral length) * 100. (b) Crural index: (maximum tibial length / maximum femoral length) * 100. (c) Humerofemoral

index: (maximum humeral length / maximum femoral length) * 100. (d) Intermembral index: (maximum humeral + radial length) / (maximum femoral + tibial length)) * 100.

Figure 16 Faro Daba *Colobus* cf. *guereza* humeri in anterior view, demonstrating size variation in the assemblage. Humeri are seriated by distal end size from largest (left) to smallest (right). From left to right: HAL-VP-9/5, HAL-VP-9/1102, HAL-VP-9/1572, HAL-VP-9/1615, HAL-VP-9/1075, HAL-VP-9/1077, HAL-VP-2/32, HAL-VP-9/284, HAL-VP-9/1537, and HAL-VP-9/1444. See Figure 16 for additional humeral remains; note that some specimens pictured here have associated elements pictured in other figures.

Figure 17 Humeral morphology of Faro Daba *Colobus* cf. *guereza*, Asbole *Colobus* sp., and extant *C. guereza*. *Left panel*: (a) HAL-VP-9/1102 left humerus in anterior (left) and posterior (right) views. (b) HAL-VP-9/594 right proximal humerus in medial (left) and posterior (right) views. (c) HAL-VP-9/640 left proximal humerus in medial (left) and posterior (right) views. (d) HAL-VP-9/730 right proximal humerus in medial (left) and posterior (right) views. (e) HAL-VP-9/7 right distal humerus in anterior (left) and posterior (right) views. (f) HAL-VP-9/730 left proximal and distal humerus. Proximal portion is shown in medial (left) and posterior (right) views. Distal portion in shown in anterior (left) and posterior (right) views. (g) HAL-VP-9/1615 right proximal humerus in medial (left) and posterior (right) views. (h) HAL-VP-9/284 right proximal humerus in medial (left) and posterior (right) views. (i) HAL-VP-9/1077 right distal humerus in anterior (left) and posterior (right) views. (j) HAL-VP-9/632 left distal humerus in anterior (left) and posterior (right) views. (k) Extant *C. guereza* right male humerus (HTB 2140) in anterior (left) and posterior (right) views. (l) Asbole *Colobus* sp. distal humeri in anterior view. All are from the right side. Clockwise from left: ASB-210, ASB-250-2, ASB-91, ASB-233-18, ASB-204, and ASB-158. *Right panel*: Distal humeri in distal view, anterior is up. Scale is approximate. Left column, from top to bottom: HAL-VP-9/284 (left side), HAL-VP-9/632 (left side), HAL-VP-9/1077 (left side), HAL-VP-9/730 (left side), HAL-VP-9/1077 (right side), HAL-VP-9/1615 (right side), HAL-VP-9/1444 (right side). Right column, from top to bottom: HTB 2140 (right side), ASB-254-25 (left side), ASB-91 (right side), ASB-158 (right side), ASB-210 (right side), ASB-204 (right side), and ASB-233-18 (right side). See Figure 15 for additional humeral remains; note that some specimens pictured here have associated elements pictured in other figures. Images of the Asbole fossils are from Frost and Alemseged (2007).

Figure 18 Faro Daba *Colobus* cf. *guereza* ulnae in right lateral view, demonstrating size variation in the assemblage. Ulnae are seriated by proximal end size from largest (left) to smallest (right). From left to right: HAL-VP-9/1615, HAL-VP-2/59, HAL-VP-9/1572, HAL-VP-9/1102, HAL-VP-9/419, HAL-VP-9/284, HAL-VP-9/1048, HAL-VP-9/1537, and HAL-VP-9/989. See Figure 18 for additional ulnar remains; note that some specimens pictured here have associated elements pictured in other figures.

Figure 19 Faro Daba *Colobus* cf. *guereza* ulnae and radii with extant and fossil comparisons. *Top panel, from left to right*: HAL-VP-9/1102 left ulna, HAL-VP-9/640 left partial proximal ulna, extant *C. guereza* male right ulna (HTB 2140), and Asbole *Colobus* sp. left proximal ulna (ASB-42-A). Each ulna is shown in lateral (left) and anterior (right) views, except for ASB-42-A, which is only shown in lateral view. *Bottom panel, from left to right*: HAL-VP-9/284 right radius, HAL-VP-9/284 left partial radius, and extant *C. guereza* male right radius (HTB 2140).

Each radius is shown in approximately medial (left) and anterior (right) views. See Figure 17 for additional ulnar remains; note that some specimens pictured here have associated elements pictured in other figures. Images of the Asbole fossils are from Frost and Alemseged (2007). Scale is the same for both panels.

Figure 20 Faro Daba *Colobus* cf. *guereza* femora in anterior view, demonstrating size variation in the assemblage. Femora are seriated from largest (left) to smallest (right). From left to right: HAL-VP-2/88, HAL-VP-9/594, HAL-VP-9/730, HAL-VP-9/5, HAL-VP-9/1102, HAL-VP-9/284, and HAL-VP-9/1537. See Figure 20 for additional femoral remains; note that some specimens pictured here have associated elements pictured in other figures.

Figure 21 Faro Daba *Colobus* cf. *guereza* femora with extant and fossil comparisons. *Left panel*: Faro Daba *Colobus* cf. *guereza* femora. Each individual is shown in anterior (left) and posterior (right) views. Top row, from left to right: HAL-VP-9/1102 (left side), HAL-VP-9/1077 (right side), and HAL-VP-9/5 (right side, proximal and distal portions). Bottom row, from left to right: HAL-VP-9/284 (left side), HAL-VP-9/730 (left side), HAL-VP-9/811 (left proximal end, right distal end), and HAL-VP-9/732 (right side). *Right panel*: Extant *C. guereza* and Asbole *Colobus* sp. femora. Clockwise, from left: *C. guereza* right femur (HTB 2140) in anterior (left) and posterior (right) views, and three Asbole *Colobus* sp. left proximal femora in posterior view prior to matrix removal (ASB-210, ASB-250-1, and ASB-254-27). See Figure 19 for additional femoral remains; note that some specimens pictured here have associated elements pictured in other figures. Images of the Asbole fossils are from Frost and Alemseged (2007). Scale is the same for both panels.

Table 1 Comparative samples employed in this study

Taxon	*n*	Repository/Reference
Extant		
Colobus angolensis	22	PRIMO
Colobus guereza	136	AMNH; CMNH; NMNH; PRIMO; Arenson et al., 2020
Colobus polykomos	1	CMNH
Nasalis larvatus	30	AMNH; CMNH
Piliocolobus badius	17	ADZ; PRIMO
Piliocolobus oustaleti	18	PRIMO
Piliocolobus tholloni	2	PRIMO
Presbytis rubicunda	80	AMNH; NMNH
Procolobus verus	2	PRIMO
Fossil		
Colobus sp. (Asbole)	47	Frost & Alemseged, 2007
Colobus sp. ("Andalee")	31	Frost, 2001a
Colobus sp. ("Upper Andalee")	4	Frost, 2001a
Total	**390**	

Note: Samples reported here include cranial, dental, and/or postcranial data. These counts do not include individuals represented in the comparative plots adapted from Frost et al. (2020) in Figure 14.
Abbreviations: *n,* sample size; ADZ, Anthropology Department, University of Zurich; AMNH, American Museum of Natural History; CMNH, Cleveland Museum of Natural History; NMNH, Smithsonian's National Museum of Natural History; PRIMO, PRImate Morphometrics Online database.

Table 2 Results of statistical analyses for cranial and mandibular variables. Results of the Kruskal-Wallis tests are reported in the first column. Subsequent columns present the results of the Dunn's *post hoc* test for pairwise comparisons with Faro Daba *Colobus* cf. *guereza*. P-values are reported and bolded when significant (at $p<0.05$).

	Kruskal-Wallis	*C. guereza*	*C. polykomos*	*Colobus* sp. (Asbole)	*Pi. badius*	*Pi. oustaleti*	*Pr. verus*
Facial length							
	0.005	**0.030**	–	–	0.457	**0.024**	0.380
Interorbital breadth							
	0.005	**0.005**	–	–	0.071	0.994	**0.005**
Palatal width (at C^1)							
	0.018	0.119	–	–	0.069	0.102	0.422
Mandibular corpus height at M_1							
	0.093	0.718	0.342	0.172	0.059	0.610	0.101
Mandibular corpus height at M_2							
	0.115	0.760	0.519	0.279	0.056	0.549	0.097
Mandibular corpus height at M_3							
	0.166	0.211	0.150	0.532	0.670	0.115	0.585

Abbreviations: C^1, maxillary canine; M_1, mandibular first molar; M_2, mandibular second molar; M_3, mandibular third molar.

Table 3 Descriptive statistics for cranial measurements of Faro Daba *Colobus* cf. *guereza* fossils. Means and ranges are reported in millimeters.

Measurement	*n*	Mean	Range
Maximum length	1	111.9	–
Maximum breadth	1	66.9	–
Orbital width	10	23.2	20.6–26.4
Orbital height	7	20.7	18.0–23.4
Interorbital breadth	19	11.6	9.2–14.3
Nasal width	11	11.0	9.5–12.6
Nasal height	7	18.9	15.8–23.2
Muzzle width (at ectomolare)	12	37.2	33–43.9
Muzzle width (at max. fossae)[a]	9	29.1	24.9–32
Maximum width (at C^1)	9	32.0	25.4–37.0
Facial width	2	69.4	67.1–71.7
Maximum calvarial width[b]	4	44.0	40.5–46.8
Calvarial length	1	65.4	–
Palatal width (at M^3)	10	18.0	15.1–25.8
Palatal width (at C^1)	12	19.1	16.7–25.6
Palatal length	13	42.0	34.9–49.8
Facial length	6	43.4	38.5–53.5

Note: Measurement definitions are reported in Monson et al. (2017).
Abbreviations: *n*, sample size; C^1, maxillary canine; M^3, maxillary third molar.
[a]Maximum width of the muzzle, measured at the superior border of the maxillary fossae.
[b]Measured at the post-orbital constriction.

Table 4 Descriptive statistics for mandibular measurements of Faro Daba *Colobus* cf. *guereza* fossils. Means and ranges are reported in millimeters.

Measurement	*n*	Mean	Range
Mandibular corpus height at M_1	3	22.5	21.4–23.3
Mandibular corpus height at M_2	3	21.9	20.8–22.7
Mandibular corpus height at M_3	2	20.0	17.5–22.5

Abbreviations: *n*, sample size; M_1, mandibular first molar; M_2, mandibular second molar; M_3, mandibular third molar.

Table 5 Descriptive statistics for maxillary dental metrics of Faro Daba *Colobus* cf. *guereza* fossils and comparative *Colobus* samples. Means and ranges are reported in millimeters. Sample sizes are in parentheses, adjacent to the mean for each measurement.

		Colobus cf. *guereza*	*Colobus* sp. (Asbole)	*Colobus* sp. ("Andalee")	*Colobus angolensis*	*Colobus guereza*
M3L	*Mean*	7.4 (47)	6.5 (10)	7.4 (5)	6.9 (22)	7.4 (118)
	Range	6.6–8.8	5.6–7.2	6.7–8.1	6.1–7.8	6.3–9.1
M3AW	*Mean*	6.8 (46)	6.0 (9)	6.6 (6)	6.5 (20)	7.0 (106)
	Range	5.9–7.6	5.7–6.2	6.4–6.8	6.0–7.0	5.7–7.9
M3PW	*Mean*	6.2 (47)	5.4 (8)	5.8 (5)	5.4 (21)	6.4 (110)
	Range	4.8–7.6	5.0–5.7	5.5–6.0	4.6–6.2	5.3–7.5
M2L	*Mean*	7.5 (60)	6.4 (14)	6.9 (7)	6.8 (22)	7.5 (123)
	Range	6.8–8.1	6.0–6.9	6.4–7.4	6.1–7.2	6.1–8.5
M2AW	*Mean*	7.4 (57)	6.1 (13)	6.7 (5)	6.9 (22)	7.4 (119)
	Range	6.3–9.5	5.7–6.6	6.4–7.1	6.3–7.3	6.0–8.4
M2PW	*Mean*	6.7 (57)	5.7 (12)	6.0 (4)	6.3 (22)	6.8 (120)
	Range	5.9–7.4	5.3–5.9	5.7–6.2	5.1–6.9	5.8–8.2
M1L	*Mean*	7.1 (79)	6.0 (14)	6.7 (7)	6.3 (22)	6.9 (123)
	Range	6.5–7.9	4.7–6.5	6.0–7.3	5.8–6.8	5.8–7.8
M1AW	*Mean*	6.5 (65)	5.7 (13)	6.0 (6)	6.1 (22)	6.5 (109)
	Range	5.7–7.3	5.2–6.4	5.7–6.3	5.7–6.7	5.2–7.8
M1PW	*Mean*	6.2 (67)	5.5 (14)	5.7 (6)	5.8 (22)	6.2 (114)
	Range	5.3–7.1	5.0–6.1	5.2–6.0	5.3–6.3	5.2–7.2
P4L	*Mean*	5.2 (69)	4.5 (16)	4.6 (4)	4.7 (22)	5.1 (120)
	Range	4.6–5.9	4.0–5.1	4.4–4.8	4.1–5.5	4.2–6.4
P4W	*Mean*	6.7 (64)	5.9 (16)	5.9 (3)	6.1 (22)	6.8 (119)
	Range	5.5–8.0	5.3–6.3	5.9–6.0	5.5–6.9	5.5–8.2
P3L	*Mean*	5.3 (60)	4.6 (17)	4.9 (3)	–	5.1 (116)
	Range	4.5–6.6	3.7–5.2	4.8–5.1	–	4.0–6.2
P3W	*Mean*	5.8 (53)	5.0 (15)	5.5 (2)	–	5.9 (116)
	Range	4.4–6.9	4.3–5.5	5.4–5.5	–	4.8–6.9
CL	*Mean*	8.4 (40)	6.2 (11)	6.3 (4)	–	8.3 (66)
	Range	6.2–10.6	4.6–8.4	4.7–9.2	–	6.1–11.0
CW	*Mean*	6.8 (40)	4.6 (10)	5.0 (4)	–	6.3 (66)
	Range	5.4–8.4	3.7–6.1	3.5–7.2	–	4.5–7.7
I2L	*Mean*	4.4 (18)	2.8 (5)	3.7 (4)	–	–
	Range	3.8–5.3	1.8–3.8	3.2–4.4	–	–
I2W	*Mean*	3.4 (20)	3.3 (5)	4.1 (4)	–	–
	Range	2.2–4.1	3.0–3.5	3.8–4.3	–	–
I1L	*Mean*	5.2 (15)	–	4.7 (5)	4.9 (17)	–
	Range	4.4–5.8	–	4.2–5.2	4.1–5.5	–
I1W	*Mean*	3.8 (15)	–	4.3 (5)	4.6 (17)	–
	Range	3.0–4.6	–	3.7–4.7	3.9–5.3	–

Note: Mesiodistal lengths of the incisors reported here were measured at the incisal edge; lengths measured at the cementoenamel junction are reported in the associated dataset ([*reference online data archival location*]). Abbreviations: M, P, C, and I refer to molars, premolars, canines, and incisors, respectively, and numbers denote tooth position; L, mesiodistal length of the crown; W, buccolingual width of the crown; AW, buccolingual width across the anterior (mesial) loph of the crown; PW, buccolingual width across the posterior (distal) loph of the crown.

Table 6 Descriptive statistics for mandibular dental metrics of Faro Daba *Colobus* cf. *guereza* fossils and comparative *Colobus* samples. Means and ranges are reported in millimeters. Sample sizes are in parentheses, adjacent to the mean for each measurement.

		Colobus cf. *guereza*	*Colobus* sp. (Asbole)	*Colobus* sp. ("Andalee")	*Colobus angolensis*	*Colobus guereza*
M3L	*Mean*	9.3 (75)	8.2 (14)	9.6 (8)	8.6 (22)	9.6 (119)
	Range	6.6–10.5	7.3–9.0	9.1–10.1	8.0–9.5	7.9–11.3
M3AW	*Mean*	6.3 (66)	5.2 (13)	6.0 (5)	5.8 (21)	6.4 (114)
	Range	5.4–7.0	4.6–6.0	5.7–6.4	5.2–6.3	5.3–7.7
M3PW	*Mean*	6.2 (75)	5.1 (11)	6.1 (6)	5.8 (20)	6.4 (104)
	Range	5.3–6.8	4.8–5.7	5.6–6.4	5.3–6.1	5.4–7.4
M2L	*Mean*	8.0 (94)	6.5 (22)	7.3 (10)	7.1 (22)	7.7 (124)
	Range	6.9–8.8	5.8–7.2	6.7–7.6	6.3–7.7	6.5–8.9
M2AW	*Mean*	6.5 (86)	5.3 (19)	5.7 (8)	5.9 (22)	6.2 (111)
	Range	5.7–7.1	4.8–5.7	4.9–6.3	5.4–6.4	5.0–7.2
M2PW	*Mean*	6.7 (83)	5.6 (18)	5.8 (7)	6.1 (21)	6.4 (112)
	Range	6.0–7.3	5.3–6.6	5.4–6.1	5.6–6.6	5.1–7.5
M1L	*Mean*	7.4 (89)	6.3 (22)	6.9 (11)	6.5 (22)	7.1 (124)
	Range	6.7–8.1	5.7–7.1	6.1–7.5	4.8–7.0	6.0–7.9
M1AW	*Mean*	5.5 (76)	4.4 (19)	4.8 (9)	5.1 (21)	5.2 (96)
	Range	5.0–6.3	3.9–5.0	4.4–5.1	4.7–5.5	4.1–6.0
M1PW	*Mean*	5.9 (72)	5.0 (19)	5.4 (10)	5.3 (21)	5.5 (95)
	Range	5.5–6.6	4.6–5.4	5.0–5.8	4.5–5.7	4.5–6.4
P4L	*Mean*	7.0 (64)	4.9 (18)	5.5 (6)	5.2 (22)	7.3 (119)
	Range	5.6–9.1	4.2–5.7	4.2–6.4	4.3–6.0	5.3–8.9
P4W	*Mean*	4.9 (57)	3.9 (18)	4.3 (6)	4.6 (22)	4.9 (115)
	Range	4.3–5.7	3.6–4.2	4.1–4.5	4.0–6.6	3.9–6.0
P3L	*Mean*	7.9 (33)	5.7 (16)	6.6 (5)	–	–
	Range	6.2–9.9	4.2–6.7	6.0–7.9	–	–
P3W	*Mean*	5.3 (41)	3.5 (15)	4.4 (5)	–	–
	Range	4.2–6.5	2.8–3.9	3.7–5.6	–	–
P3FL	*Mean*	8.0 (36)	–	–	–	–
	Range	6.3–9.5	–	–	–	–
CL	*Mean*	5.1 (23)	4.5 (10)	6.0 (1)	–	7.4 (70)
	Range	4.2–6.0	3.4–5.5	–	–	5.7–8.8
CW	*Mean*	7.3 (19)	5.6 (10)	3.9 (1)	–	5.0 (70)
	Range	6.4–8.2	3.8–6.6	–	–	3.5–6.3
I2L	*Mean*	3.9 (18)	3.4 (8)	–	–	–
	Range	3.2–4.6	3.0–3.7	–	–	–
I2W	*Mean*	4.6 (19)	4.2 (10)	4.1 (1)	–	–
	Range	4.3–5.2	3.6–4.9	–	–	–
I1L	*Mean*	3.9 (20)	3.2 (6)	–	–	–
	Range	3.1–5.2	2.5–4.8	–	–	–
I1W	*Mean*	4.4 (16)	4.0 (7)	–	–	–
	Range	4.0–5.0	3.6–4.3	–	–	–

Note: Mesiodistal lengths of the incisors reported here were measured at the incisal edge; lengths measured at the cementoenamel junction are reported in the associated dataset ([*reference online data archival location*]). Abbreviations: M, P, C, and I refer to molars, premolars, canines, and incisors, respectively, and numbers denote tooth position; L, mesiodistal length of the crown; W, buccolingual width of the crown; AW, buccolingual width across the anterior (mesial) loph of the crown; PW, buccolingual width across the posterior (distal) loph of the crown; FL, mesiodistal length of the crown, taken in lateral view and including the mesial extension of the flange on the buccal side.

Table 7 Results of statistical analyses for dental variables. Results of the Kruskal-Wallis tests are reported in the first column. Subsequent columns present the results of the Dunn's *post hoc* test for pairwise comparisons with Faro Daba *Colobus* cf. *guereza*. P-values are reported and bolded when significant (at $p<0.05$).

	Kruskal-Wallis	*C. angolensis*	*C. guereza*	*Colobus* sp. ("Andalee")	*Colobus* sp. (Asbole)	*Pi. badius*	*Pi. oustaleti*	*Pi. tholloni*	*Pr. verus*
Max. CL									
	<0.001	–	0.983	**0.043**	**<0.001**	0.282	**0.103**	0.254	**0.033**
Max. M2L									
	<0.001	**<0.001**	0.718	**0.013**	**<0.001**	**<0.001**	0.327	0.294	**0.004**
Max. M2AW/M2L									
	<0.001	**0.019**	0.377	0.909	0.161	0.093	**<0.001**	0.515	0.728
Man. P4L/M1L									
	<0.001	**<0.001**	**<0.001**	**0.026**	**<0.001**	**0.004**	**0.002**	0.294	0.239
Man. M3AW/M3PW									
	<0.001	0.409	0.930	0.715	0.714	0.210	0.550	0.387	0.713
Man. MMC									
	<0.001	0.113	**<0.001**	0.079	0.115	**0.001**	**0.042**	0.793	0.478
Man. PMM									
	<0.001	**<0.001**	**<0.001**	0.065	**<0.001**	**0.020**	**0.013**	0.729	0.482

Abbreviations: Max., maxillary; Man., mandibular.; M, P, and C refer to molars, premolars, and canines, respectively, and numbers denote tooth position; L, mesiodistal length of the crown; AW, buccolingual width across the anterior (mesial) loph of the crown; PW, buccolingual width across the posterior (distal) loph of the crown; MMC, molar module component; PMM, premolar-molar module.

Table 8 Descriptive statistics for postcranial metrics of Faro Daba *Colobus* cf. *guereza* fossils

Measurement	*n*	Mean	Range
Humeral maximum length	5	152.7 mm	146.0–156.2 mm
Humeral head diameter	12	17.3 mm	15.9–18.9 mm
Humeral epicondyle angle	11	37.4º	31.7–43.8º
Humeral epicondyle ratio[a]	12	18.5	13.1–23.1
Humeral relative flange length[a]	13	67.1	56.8–77.3
Radial maximum length	3	146.1 mm	144.9–147.7 mm
Ulnar maximum length	3	164.1 mm	159.3–167.8 mm
Femoral maximum length	7	200.5 mm	193.5–208.8 mm
Femoral head diameter	15	17.1 mm	15.3–18.3 mm
Femoral neck-shaft angle	10	121.8º	114.9–127.0º
Femoral relative greater trochanter projection[a]	14	40.1	26.0–48.8
Tibial maximum length	6	189.2 mm	181.6–207.1 mm
Fibular maximum length	1	170.1 mm	–
Brachial index[b]	2	94.5	94.4–94.6
Crural index[b]	5	93.9	92.2–96.4
Humerofemoral index[b]	3	77.4	75.6–79.7
Intermembral index[b]	1	78.9	–

Note: Additional postcranial measurements and measurement definitions are provided in the dataset associated with this manuscript ([*reference online location in data repository here*]).
Abbreviations: *n*, sample size.
[a]See Figure 14 and for comparison with extant samples.
[b]See Figure 15 for index definition and comparison with extant *C. guereza*.

Table 9 Sex estimation results for Faro Daba *Colobus* cf. *guereza* fossils

Sex category	Number of individuals	Frequency (%)
F	7	4
F?	10	6
M	7	4
M?	5	3
Uncertain	149	84
Total	**178**	**-**

Table 10 Age assessment results for Faro Daba *Colobus* cf. *guereza* fossils

Age score	Number of individuals	Frequency (%)
1	1	<1
2	9	6
3	10	6
4	75	47
5	47	29
6	18	11
Total	**160**	**-**

Appendix 1 Inventory of specimens referred to *Colobus* cf. *guereza*

Specimen ID	Sex	Element(s)
HAL-VP-2/2 *	M	L. MAN (P3-M3); VER (caud.)
HAL-VP-2/3	–	R. LM2
HAL-VP-2/13 *	–	R. MAN w/ symph. (partial R. C, partial R. M2)
HAL-VP-2/22 *	–	Skeletal frags. + dentition
HAL-VP-2/28 *	–	HUM (prox. shaft)
HAL-VP-2/32	U	R. MAX (partial M1 or 2); isolated partial upper C; R. FRO frag.; CRA frag.; L. MAN w/ symph. (L. I1-2 roots, partial C, partial P3, P4-M2); R. MAN (P4, M3, partial M1-M2); partial SAC; L. SCA frag.; several VER; R. & L. prox. TIB; L. CAL; dist. FEM; R. prox. FEM; L. partial OCX; R. dist. HUM; L. HUM; prox. FEM shaft frag.; associated frags
HAL-VP-2/34	U	L. MAN (P4-M2)
HAL-VP-2/40 *	–	R. HUM (prox. + shaft)
HAL-VP-2/42 *	–	R. UdM2
HAL-VP-2/59	U	MAX (L. I1-2, R. I1-2, partial R. C, R. P3-M3); FRO frag.; OCC frag.; 2 CRA frags.; R. MAN w/ symph. (R. I1-2 roots, partial R. C-M1, R. M2-M3, L. I1-2, partial L. C, roots of L. P3-P4); L. MAN frag. (L. M1-M2, roots of L. M3); MTP; 2 prox. MTP frags.; dist. MTP frag.; several prox. and intermediate PHX; R. dist. ULN; R. prox. FIB; FEM (condyle); R. CAL; L. TAL; R. & L. prox. ULN; L. dist. RAD; prox. HUM; L. dist. HUM; HUM dist. shaft; R. prox. TIB; L. partial prox. TIB; R. & L. dist. TIB; L. FEM prox. shaft; R. OCX (acetabular frag.); OCX frag.; 5 VER; 1 axis; 6 partial VER; VER frags.; RIB frags.; associated long bone frags.
HAL-VP-2/77 *	–	R. LdM2
HAL-VP-2/88	U	L. MAX (P3-M1); isolated R. UM1; R. FEM; partial L. SCA; RIB & VER frags.; L. dist. HUM; R. & L. dist. TIB; prox. TIB; L. OCX frag.; L. CAL; R. TAL; partial L. TAL; 2 podials; CRA & long bone frags.
HAL-VP-2/91	M	R. MAX (C, P3); L. MAX (C); CRA frags.; R. FEM prox. shaft; shaft frags.
HAL-VP-2/109 *	–	R. MAN (edent.)
HAL-VP-2/115 *	–	FRO
HAL-VP-2/116 *	–	FRO
HAL-VP-2/117 *	–	R. ULN (prox.) + RAD (prox.)
HAL-VP-2/126 *	–	FEM (prox. and dist. w/ shaft frag.); L. TIB (dist.); R. glenoid fossa of SCA; 4 partial VER; associated long bone frags.
HAL-VP-2/127	U	L. MAN w/ symph. (R. I1-2, L. I1-M2); isolated L. LM3 and R. LP3; R. + L. MAX (L. I1-M2, R. I2-M3 (erupting))
HAL-VP-2/128 *	–	L. HUM (dist.); L. ULN (prox.); partial VER (caud.); 2 shaft frags.
HAL-VP-2/131	U	R. MAN (P3, M1-M3)
HAL-VP-2/148	–	L. LM2

HAL-VP-2/152	U	L. MAN (M2-M3)
HAL-VP-2/159 *	–	R. ULN (prox.)
HAL-VP-2/167	–	L. UM; R. UI2
HAL-VP-2/170 *	–	R. FEM (dist.)
HAL-VP-2/193 *	–	R. MAX (R. UI1-I2)
HAL-VP-2/196 *	–	UM
HAL-VP-3/11	U	R. MAX (P3-M3)
HAL-VP-3/22	U	MAX (P3-M2, all partial)
HAL-VP-3/32 *	–	L. MAN (P4, M3 unerupted)
HAL-VP-3/35 *	–	R. OCX frag. (w/ acetabulum); R. + L. FEM (prox.)
HAL-VP-3/43	U	R. + L. MAN (R. + L. I1-2, dC-dM1, P4-M2)
HAL-VP-3/48 *	–	R. ULN (prox.)
HAL-VP-3/55 *	–	L. UM
HAL-VP-3/61 *	–	R. ULN (prox.)
HAL-VP-3/67 *	–	L. HUM (dist.)
HAL-VP-3/76	U	L. MAX (P3-M2)
HAL-VP-3/98	–	L. LM3
HAL-VP-3/107 *	–	R. FEM (prox.)
HAL-VP-3/121 *	–	L. UP3-4
HAL-VP-3/126	–	L. UM
HAL-VP-3/138 *	–	L. RAD (prox.); L. ULN (prox.); 2 shaft frags.
HAL-VP-3/140 *	–	R. FEM (prox.)
HAL-VP-3/144	–	L. MAX (C-P4)
HAL-VP-3/147 *	–	R. ULN (prox.)
HAL-VP-3/153 *	–	FEM (dist.)
HAL-VP-3/156 *	–	L. FEM (prox.)
HAL-VP-3/160 *	–	R. FEM (prox.)
HAL-VP-3/164	–	R. LM3
HAL-VP-3/166	U	L. MAN (M2)
HAL-VP-3/178	–	R. M1 or 2
HAL-VP-3/182	U	R. MAX (P4-M2)
HAL-VP-3/187 *	–	FEM (dist.)
HAL-VP-3/203 *	–	L. FEM (prox.)
HAL-VP-3/208	–	L. LM3
HAL-VP-3/220	U	R. LM2-M3
HAL-VP-3/221 *	–	MAN (symph., edent.)
HAL-VP-3/252 *	–	R. LM1 or 2

HAL-VP-9/2	F?	L. MAN (P3-M3, partial C and I2); R. MAN (C-P3); R. MAN (M1-M2); L. MAX (P3-M3)
HAL-VP-9/5	M?	CRA (missing calvarium and R. ZYG), MAX includes L. I1-I2 roots, L. P3-M3, R. I1-I2 roots, partial R. C, R. P4-M3; L. MAN (P4-M3); R. MAN (I2, C roots, P3-P4, M1-M2, M3 roots); R. TEM frag.; R. + L. FEM; L. TIB; R. TIB (in frags.); FIB (dist.); R. HUM; R. + L. ULN; R. + L. RAD; pelvic frags.; R. + L. CAL; TAL; 2 podials; MTP frags.; multiple PHX; misc. frags.
HAL-VP-9/6 *	–	R. + L. TIB (dist.); R. FEM (prox.); MTC1; MTC4; partial L. OCX; 3 partial VER; R. CAL; long bone frag.; RIB frag.
HAL-VP-9/7	M	MAN (L. I1, I2 root, P3-P4 roots, partial M1, M2-3; R. I1, I2 root, P3, P4-M1 roots, M2-M3); L. MAX w/ ZYG (M1-M2, I1-P4 roots, M3 roots); SAC; TAL; L. FEM (dist. w/ shaft); R. HUM (dist. w/ shaft); FEM (prox.); PHX; ULN (prox.); CRA frags.; long bone frags.
HAL-VP-9/8	U	R. + L. MAX (R. P4-M3)
HAL-VP-9/15	U	MAN w/ symph. (R. P4-M2); L. MAN frag. (P4); L. MAN frag. (M3)
HAL-VP-9/221 *	–	R. MAN (M1 frag.)
HAL-VP-9/243	U	L. MAX (C-M2)
HAL-VP-9/244	U	R. MAX (P3-M3)
HAL-VP-9/245 *	–	L. RAD (prox.); L. ULN (prox.); L. HUM (dist.); shaft frag.
HAL-VP-9/248	U	R. MAX (C-P4)
HAL-VP-9/249	U	L. MAX (P3-M2)
HAL-VP-9/250 *	–	L. HUM (dist. w/ shaft)
HAL-VP-9/256	U	L. MAN (M2-M3)
HAL-VP-9/267 *	–	L. UI1 frag.
HAL-VP-9/275 *	–	R. MAX (I1-C roots); TIB (prox.); L. OCX frag.; L. TAL; R. CAL; R. FEM (prox.); 2 shaft frags.; 2 misc. frags.
HAL-VP-9/276 *	–	L. FEM (prox.); L. TAL
HAL-VP-9/279 *	–	R. + L. MAN (symph. w/ L. I1-P3 roots; L. P4)
HAL-VP-9/280	M?	R. MAN (I2-C roots, P3-M3); L. MAN (P3-M3); L. MAX (M1-M3); R. MAX (partial RI1, RI2, RC root); isolated L. UC; isolated L. UI1; isolated R. UM3
HAL-VP-9/283	U	R. MAX (C-M3); L. MAX (M1-M2); L. MAN (P4-M3); R. MAN (M2-M3)
HAL-VP-9/284	M?	L. MAN (M1-M3); R. MAN (C-M3); L. MAX (P3-M3, partial C); R. MAX (I1-I2, partial C, P4-M3); isolated L. UI2; FRO (w/ glabella); R. TEM (auditory meatus w/ partial mastoid process); R. + L. TIB; L. FEM; R. FEM (prox. and dist.); R. + L. HUM; R. + L. RAD (L. missing dist. end); R. + L. ULN; FIB shaft; FIB (dist., fused to CAL); R. + L. CAL; multiple podials; MTP (including 2 fused sets and 2 complete isolated MTPs); MTP frags.; several PHX (incl. complete and frags.); VER bodies; multiple VER (caud.); CRA frags; long bone frags.; pelvic frags.; SCA frags
HAL-VP-9/285 *	–	R. + L. FEM (dist.)

HAL-VP-9/287 *	–	R. HUM (dist.)
HAL-VP-9/289 *	–	Imm. L. TIB (dist.); L. RAD (prox.); L. FEM (prox. and dist.); long bone frags.
HAL-VP-9/290	U	FRO; R. + L. NAS
HAL-VP-9/292	U	L. LM3
HAL-VP-9/293 *	–	2 R. OCX frags.; 3 L. OCX frags; 1. OCX frag. (side unknown); L. FEM (prox.); R. FEM (prox.); FEM (dist.); R. TIB (dist.); shaft frags.
HAL-VP-9/295	U	L. MAN (M3)
HAL-VP-9/297	–	L. LM1
HAL-VP-9/298	U	R. MAX (P3-M2); R. TEM; L. ZYG
HAL-VP-9/303	U	R. + L. MAN (L. C-P4 erupting, L. M1-M2, R. C-P3 erupting, R. dM2-M2)
HAL-VP-9/304	U	R. MAX (P3-M3); L. MAX (C-M3)
HAL-VP-9/305	U	R. MAN (P4-M3)
HAL-VP-9/309	U	R MAN. (P4-M1 roots, M2, M3 roots); L. UM1 or 2; R. HUM (partial dist.); R. RAD (prox.); HUM (dist. shaft); misc. frags.
HAL-VP-9/310	U	L. MAN (P4-M2)
HAL-VP-9/312 *	–	R. HUM; L. HUM (prox.); L. HUM (dist.); R. + L. partial SCA; R. + L. partial OCX; R. TIB; FEM (dist.); FIB (prox. and dist.); partial SAC; VER and misc. frags.
HAL-VP-9/315	U	L. MAN (M2-M3)
HAL-VP-9/316	U	MAN (L. P3-P4; R. P3-M2)
HAL-VP-9/319	U	Skull w/ R. FRO and orbit, R. + L. MAX (only tooth roots preserved); MAN w/ symph. (L. M3-M1, L. + R. I1, R. P4, R. I2-P3 roots); HUM (dist.); partial pelvis; CRA and long bone frags.
HAL-VP-9/325	U	MAN w/ symph. (L. P4-M1)
HAL-VP-9/327 *	–	L. HUM (prox.); L. ULN (prox. w/ shaft); L. SCA (w/ glenoid); L. RAD (prox. w/ shaft); L. HUM (dist.); R. TIB (prox. w/ shaft); L. partial OCX; 2 partial VER; RIB and misc. frags.
HAL-VP-9/331	U	L. MAX (P3-M3)
HAL-VP-9/332	U	Skull w/ MAX (R. M1-M3, L. P3-M3), FRO, CRA frags., MAN (R. C-M3)
HAL-VP-9/338	U	L. MAN (P3, M2-M3); R. MAN (P3-M3)
HAL-VP-9/340	U	L. MAN (dM2-M2)
HAL-VP-9/348 *	–	R. HUM (dist.); HUM (prox. shaft); shaft frags.
HAL-VP-9/350	F?	R. MAN (P4-M3)
HAL-VP-9/352	U	R. MAX (P3-M3)
HAL-VP-9/355	U	Partial CRA w/ R. MAX (M1, M3); L. FEM (lesser trochanter); 2 CRA vault frags.
HAL-VP-9/359	U	R. + L. MAN (L. P4-M1)
HAL-VP-9/361	U	R. MAX (M1); R. MAN (P4-M3)
HAL-VP-9/363	F?	MAN (R. C-P4; L. P3-M3)

HAL-VP-9/365	F?	L. MAX (P3-M3); R. MAX frag. (M1-M3); R. MAX frag. (partial C-P4)
HAL-VP-9/368	F	L. MAN (P3-P4)
HAL-VP-9/370	F?	R. MAN w/ symph. (partial L. I1, L. I2-P4, partial R. C, R. P3-M1, partial R. M2-M3); isolated L. M3; isolated R. I1; isolated R. C; isolated R. I2; isolated L. P4; L. MAN (M1-M3); CRA frags.
HAL-VP-9/371 *	–	MAN symph. (partial L. I1-C, partial R. I2-C, partial R. P4)
HAL-VP-9/382 *	–	L. MAX (M1); L. FEM (prox.); R. ULN (prox.)
HAL-VP-9/384	U	R. MAX (I1, C-M3); L. MAX (I1-M3); L. MAN (P4-M3); isolated L. LP3; R. MAN (P4-M1); CRA and long bone frags.
HAL-VP-9/386	U	L. MAN (P4-M3); L. MAX (edent.)
HAL-VP-9/388 *	–	R. HUM (dist.)
HAL-VP-9/390 *	–	L. HUM (dist.)
HAL-VP-9/391 *	–	MAN symph. (L. C)
HAL-VP-9/395	U	L. MAX (M1, M3)
HAL-VP-9/404 *	–	R. HUM (prox.)
HAL-VP-9/406	U	L. MAN (P4-M2)
HAL-VP-9/411	U	L. MAN (P3-P4)
HAL-VP-9/414 *	–	L. HUM (prox.)
HAL-VP-9/419	U	R. MAX (P3-M3); L. TEM frag.; ULN (prox.); RAD (prox.); OCX frag.; 1 VER frag.; 1 RIB frag.; 4 MTP frags.; 1 PHX frag.; misc. frags.
HAL-VP-9/425	U	L. MAN (M3)
HAL-VP-9/426	U	MAX (L. P4-M2); L. MAN (M1-M3); MAN symph. (L. P3)
HAL-VP-9/427	U	R. MAX (M1-M3)
HAL-VP-9/428 *	–	L. MAX (M1-M2)
HAL-VP-9/429 *	–	FEM (dist.); 2 SES
HAL-VP-9/435 *	–	L. ULN (prox.); 2 shaft frags.
HAL-VP-9/437	U	Skull frags.; isolated R. UM2; isolated L. LM3 (dist. part)
HAL-VP-9/453	U	R. MAX (P3-M2)
HAL-VP-9/458	U	MAN (L. P3; R. + L. M1-M3)
HAL-VP-9/459	U	L. MAX (P3-M1); L. MAX (C erupting); isolated L. UI1; isolated R. + L. LM1
HAL-VP-9/464	U	L. MAN (M1-M3)
HAL-VP-9/467 *	–	L. MAN (P4, M1 roots); 2 FEM (prox.); R. + L. FEM (dist.); TIB (prox.); L. SCA frag.; 1 VER frag.; 1 shaft frag.; misc. frags.
HAL-VP-9/481	U	L. MAX (C-P4, partial I1 and I2, partial M1-M3)
HAL-VP-9/484 *	–	R. HUM (prox.); RAD (partial prox.); R. HUM (dist.); R. RAD (dist.); R. ULN (prox.); L. ULN (partial prox.); R. FEM (prox.); L. FEM (prox.); FEM (dist.); 2 L. OCX frags.; R. OCX frag.; 2 MTC (partial prox.); 3 partial PHX; 13 partial VER; misc. frags.
HAL-VP-9/485	U	R. MAN (M2-M3)

HAL-VP-9/488	M	L. MAN (M1-M3); R. MAN w/ symph. (L. I1-I2; R. I1-I2, P3-M3); MAX (R. + L. I1-M3 w/ partial C's); R. HUM (dist.)
HAL-VP-9/489	U	CRA w/ R. MAX (P3-M2), L. MAX (P3-M3)
HAL-VP-9/492	U	R. MAN (dM1-M1); R. MAX (dM2-M2; P4 erupting); isolated R. UI2 and L. LM2
HAL-VP-9/493	U	L. MAN (dM2-M1)
HAL-VP-9/495	U	R. MAX (partial C, P3-P4); L. MAX (partial C)
HAL-VP-9/497	U	L. MAN (M1-M3)
HAL-VP-9/520 *	–	L. FEM (prox.)
HAL-VP-9/525	U	R. MAN (dM1-dM2)
HAL-VP-9/526 *	–	R. FEM (prox.)
HAL-VP-9/527 *	–	L. FEM (prox.)
HAL-VP-9/536 *	–	L. ULN (prox.)
HAL-VP-9/537 *	–	R. HUM (dist.)
HAL-VP-9/548 *	–	R. HUM (dist.)
HAL-VP-9/551 *	–	L. MAN (edent.)
HAL-VP-9/552 *	–	L. HUM (dist.); ULN (prox.); R. FEM (prox.); misc. frags.
HAL-VP-9/553 *	–	R. FEM (prox.); R. OCX frag.; L. OCX frag.; several VER frags.; ULN (prox.); shaft frags.
HAL-VP-9/554	U	R. + L. MAN w/ symph. (L. C root, P4-M1 roots, M2, M3 erupting; R. P3 root, P4-M2); isolated L. LP3; isolated L. LI2; isolated R. LC; MAN (condyle); L. MAX (I1, C erupting, P3-P4); R. MAX (C in crypt, partial P3); isolated R. UdC; isolated R. UI2; tooth frags.; R. + L. FRO; 3 pelvic frags.; R. + L. TIB shaft; R. + L. FEM shaft; RAD shaft; R. + L. ULN shaft; 5 VER (caud.); misc. frags.
HAL-VP-9/556	M	MAN (L. I2, P3-M3; R. P4-M1, partial M2, M3); 2 long bone shafts
HAL-VP-9/557	M?	R. MAX (P3-M2); L. MAX (P3-M3); R. MAN (M1-M2); MAN frag. w/ symph. (R. P3-P4); L. MAN (M3); TIB (dist.); HUM shaft; CRA frags.; long bone frags.
HAL-VP-9/558 *	–	MAN (R. + L. dI1-dM2)
HAL-VP-9/559	U	L. MAN (M1-M2)
HAL-VP-9/561 *	–	L. HUM (dist.); L. FEM (prox.); R. HUM (dist. shaft); L. OCX frag.; shaft frags.
HAL-VP-9/563	U	L. MAN (M2-M3); isolated partial C
HAL-VP-9/564 *	–	R. + L. TIB (prox.); FEM (dist.)
HAL-VP-9/565 *	–	R. HUM (dist.)
HAL-VP-9/568	U	L. MAN (M1-M3)
HAL-VP-9/570 *	–	MAX (L. I1, P4-M2; R. P3)
HAL-VP-9/573 *	–	L. MAN w/ symph. (partial C-P3); L. MAX (partial M1-M2); CRA frag.
HAL-VP-9/574	U	R. MAN (partial M1-M3)

HAL-VP-9/576 *	–	R. HUM (prox.)
HAL-VP-9/578	–	R. MAX (M1); L. MAN (mesial half of M1 or 2); TEM frag. (w/ TMJ)
HAL-VP-9/590	U	MAN w/ symph. (R. P3-M3)
HAL-VP-9/592	U	FRO frag.; R. ULN (prox.); R. RAD (dist.); R. TIB (dist.); shaft frags.
HAL-VP-9/594	U	L. MAX frag. (M1-M3); L. MAX frag. (C); R. MAX frag. (partial C-P3, P4); isolated L. UI1; L. FEM; L. HUM (dist.); R. HUM (prox. w/ shaft); R. + L. RAD (prox.); ULN (partial prox.); CLA; CAL; partial FRO w/ glabella; partial L. ZYG; 9 VER; RIB frags.; CRA frags.; long bone shaft frags.
HAL-VP-9/597	U	L. LM3
HAL-VP-9/601	U	R. MAX (C-M3); isolated L. UM3; R. MAN (M1-M2); L. MAN (M3); CRA frags.
HAL-VP-9/604 *	–	R. ULN (prox.); R. HUM (dist.); shaft frag.
HAL-VP-9/606	U	R. MAX (partial P3, P4-M3)
HAL-VP-9/608	U	L. MAN (M1-M2)
HAL-VP-9/611	–	R. MAN (M1-M2)
HAL-VP-9/617	U	R. MAX (P3-P4); L. MAX frag. (P3-P4), L. MAX frag. (M2-M3); R. MAN (P4-M3); L. MAN (M3); isolated partial LC; CRA frags.
HAL-VP-9/627	F?	R. MAN (C-M3)
HAL-VP-9/628	U	R. MAN (partial M1-M3)
HAL-VP-9/632	U	R. MAN (C-P3, M1-M2); FRO frag. w/ NAS; L. HUM (dist.); R. HUM (dist. shaft); L. ULN (partial prox.); L. FEM (partial prox.); partial L. OCX; long bone shaft frags.
HAL-VP-9/640	U	R. MAN (M1-M3); ULN (prox.); R. + L. FEM (prox.); pelvis; HUM (prox.); RAD (prox.); SCA (spine); misc. postcranial frags.
HAL-VP-9/642	M	MAN w/ symph. (R. I1, C-P3, partial P4; partial L. I1-P3, P4, partial M1-M2)
HAL-VP-9/647 *	–	HUM (prox.)
HAL-VP-9/653	U	R. MAX (P4-M3)
HAL-VP-9/656	F	MAN (R. I1-P3; L. I1, C-P3)
HAL-VP-9/657	U	L. MAN (P4-M3)
HAL-VP-9/665 *	–	R. RAD (dist.); RAD (head); R. ULN (prox.); ULN (shaft frag.); R. HUM (dist. w/ shaft); partial L. OCX; R. RAD (shaft frag.)
HAL-VP-9/672	U	L. MAN (P3-M3)
HAL-VP-9/687 *	–	L. ULN (prox. w/ shaft)
HAL-VP-9/693	F?	L. MAX (partial C, P3-M3)
HAL-VP-9/703 *	–	Partial R. OCX; FEM (dist.); TIB (prox.); partial L. TIB (dist.); 1 podial; shaft frags.
HAL-VP-9/704 *	–	L. MAN (C-P4)
HAL-VP-9/705	U	L. MAN (M2-M3)

HAL-VP-9/706	M?	MAN (R. + L. I1-C)
HAL-VP-9/707	–	R. UP3
HAL-VP-9/708 *	–	MAN (R. P3)
HAL-VP-9/713	U	R. MAN (M2-partial M3); M3
HAL-VP-9/718 *	–	R. RAD (prox.)
HAL-VP-9/720	U	Partial FRO; UC; R. MAX (M1-M2); L. MAX (M1-M3); partial VER body; pelvic frag. (acetabular region); CRA and postcranial frags.
HAL-VP-9/723	U	Skull with facial skeleton, vault bones, and R. + L. TEM frags.; R. UP4; R. UM2-3; L. UP3-M3; isolated L. UC; R. UC frag.; partial axis; 1 VER; multiple partial VER and ribs; 3 STE segments; partial SAC; 5 OCX frags.; R. FEM (prox.); TIB (prox.); R. TIB (dist.); R. CAL; R. TAL; L. FIB (prox.); FEM (dist.); assorted hand and foot bones; limb bone frags.
HAL-VP-9/726 *	–	L. HUM (dist.)
HAL-VP-9/730	F?	Partial CRA missing most of posterior vault and base; MAX (R. I1-I2 roots, partial C, P3-M3; L. I1-C roots, partial P3, P4-M3; note possible supernumerary incisor (there are 5 roots between the canines)); R. MAN w/ symph. (L. I1-C, partial P3-P4; partial R. C-P3, P4-M3); L. MAN (M2-M3); isolated L. LM1 (in matrix); MAN (condyle); CRA frags.; R. + L. TEM frags; R. FEM; L. FEM (prox., dist., 2 shaft frags.); R. + L. HUM (prox. and dist.); PAT; L. TIB; R. TIB (nearly complete); R. + L. FIB (prox.); FIB (dist.); R. + L. RAD (prox. and dist.); R. + L. ULN (prox. and dist.); partial L. OCX, R. OCX (nearly complete, w/ frags.); R. SCA frag.; STE (manubrium); SAC; nearly complete RIB; many RIB frags.; R. + L. CAL; R. TAL; many podials; 2 complete and many partial MTP; prox., int., and dist. PHX and frags.; many VER and VER frags.
HAL-VP-9/732	U	R. MAX (partial P4, M1-M3); L. MAX (P3-M1); R. UC frag.; MAN (R. P3); L. LM1 or M2; C tip; R. TIB; L. OCX; partial R. OCX; SAC; L. PAT; R. FEM (prox. and dist.); L. FEM shaft; FIB (dist.); CAL; TAL; multiple MTP (two cemented together); several PHX frags.; 2 VER (caud.); VER frags.; RIB frags.; misc. frags.
HAL-VP-9/733	F?	MAN (R. + L. C-M3)
HAL-VP-9/737 *	–	L. HUM (prox.)
HAL-VP-9/739	F	R. MAN (I1, P3-M3)
HAL-VP-9/743	U	L. MAX (P4-M2)
HAL-VP-9/744 *	–	R. HUM (dist.)
HAL-VP-9/745	–	R. MAN (edent.)
HAL-VP-9/746	–	R. MAN (I1, M2-M3); postcranial frags.
HAL-VP-9/747 *	–	R. FEM (prox.)
HAL-VP-9/750	U	R. MAN (M1, M2-M3 roots)
HAL-VP-9/753 *	–	R. MAX (partial M2)
HAL-VP-9/755	U	L. MAN (partial M1, M2-M3); R. MAN (partial M1-M2); L. LP4 and R. LP3-P4 in concretion; CRA frag.

HAL-VP-9/757	U	L. MAN (partial M1, M2-M3); isolated LP3
HAL-VP-9/758 *	–	L. HUM (dist. w/ shaft)
HAL-VP-9/759	–	L. MAN (P3-M2); isolated L. LC
HAL-VP-9/761	U	R. MAX (M1-M3)
HAL-VP-9/764	U	R. MAX (P3, partial P4-M2)
HAL-VP-9/769 *	–	L. RAD (prox.)
HAL-VP-9/778	U	MAN (R. + L. I1-I2, dC-dM2, M1-M2, M3 germ)
HAL-VP-9/779	U	Partial CRA
HAL-VP-9/785 *	–	R. RAD (prox.)
HAL-VP-9/788 *	–	L. MAN w/ symph. (edent.)
HAL-VP-9/797	–	Partial MAX (P4-M2); SAC; TIB (dist.); TAL; VER body; pelvic frag. (acetabular region); long bone frags.
HAL-VP-9/811	F?	L. MAN w/ symph. (I1-I2 roots, partial C, P3-M3); R. MAN (I1-P3, P4 roots); MAN (condyle); R. HUM (prox.); HUM (dist. shaft); L. RAD (dist.); L. RAD (prox.); R. RAD (prox. shaft.); L. FEM (prox.); R. FEM (prox.); R. FEM (dist.); R. + L. TIB (prox.); R. + L. TIB (dist.); R. + L. FIB (prox.); L. FIB (dist.); L. CAL; R. TAL; R. + L. NAV; multiple MTP, PHX, and podials; 4 OCX frags.; multiple partial VER; limb bone and misc. frags.
HAL-VP-9/817	F	MAN (L. P3, M1-M3; R. M1-M2, partial M3)
HAL-VP-9/822 *	–	R. FEM (prox.); partial VER (caud.); 2 shaft frags.
HAL-VP-9/826 *	–	L. MAX (partial I1, I2-P4)
HAL-VP-9/841	U	L. MAN (partial P3, P4)
HAL-VP-9/844 *	–	L. HUM (prox.)
HAL-VP-9/845 *	–	R. HUM (dist.); FEM (dist.); FEM (head); RAD (prox.); partial L. CAL; limb bone frags.
HAL-VP-9/849 *	–	R. FEM (prox. and shaft frags.)
HAL-VP-9/858	U	R. UM3
HAL-VP-9/866 *	–	Partial R. OCX; 2 L. OCX frags.; SAC; TIB (dist.); L. CAL; R. FEM (prox.); 2 FEM (dist.); 14 partial VER; misc. frags.
HAL-VP-9/867	U	MAN w/ symph. (L. I1-I2, C root, P3-P4, M1 roots, M2-M3; R. I1-I2, C root, P3, P4 root, M1-M2, M3 roots); L. MAX (partial I1, I2, partial C, P3-M2, M3 roots); R. MAX (P3-M2, partial M3); MAN (condyle)
HAL-VP-9/877 *	–	R. ULN (prox. and dist.)
HAL-VP-9/880	U	R. MAN (P4-M3)
HAL-VP-9/886	–	R. UP3
HAL-VP-9/895 *	U	R. MAN (P3-M2, partial M3)
HAL-VP-9/900	U	R. + L. MAN (dI1-I2; R. dM1-M1; L. dM2-M1)
HAL-VP-9/901	U	L. MAN (partial M2, M3); R. MAN (I2 root, C); isolated L. LC; isolated L. UM1 or 2; L. FRO; CRA frags.

HAL-VP-9/909 *	–	MAN symph. (edent.)
HAL-VP-9/910	–	L. MAX (M1)
HAL-VP-9/912	U	R. MAX (partial P3, partial M1)
HAL-VP-9/924 *	–	R. HUM (dist.)
HAL-VP-9/928	U	R. MAX (M3)
HAL-VP-9/931	U	L. MAN (edent.)
HAL-VP-9/960	–	L. MAX (I1-C)
HAL-VP-9/968	–	L. MAN (M2)
HAL-VP-9/977 *	–	R. MAX (partial I1-2, C-P3 roots, partial P4-M3); L. MAN (M2-M3 roots); R. MAN (P4-M2 roots, partial M3); FRO (w/ glabella); L. TEM; CAL; MAN (condyle); FEM (prox. and dist.); 2 pelvic frags.; R. + L. ULN (prox.); HUM (head); RAD (dist.); 4 partial VER; skull frag.; misc. frags.
HAL-VP-9/980	U	R. MAN (M1-M2, M3 roots)
HAL-VP-9/983	U	R. MAN (P3-M3); L. MAN (M2)
HAL-VP-9/985 *	–	R. HUM (prox.); R. + L. HUM (dist.); L. ULN (prox.); R. + L. FEM (prox.); R. TIB (dist.); MTP (prox.); VER frag. (caud.); FEM (condyle); partial VER body; misc. frag.
HAL-VP-9/988	U	MAN (L. I1-P4; R. P3-P4)
HAL-VP-9/989	F	R. MAN w/ symph. (L. C-R. P4 roots, R. M1-M3); L. MAN (M1-M3); FEM (dist.); partial SAC; SCA frag. (w/ glenoid); RAD (prox.); CAL; HUM (head); TIB (dist.); VER frags.; postcranial frags.
HAL-VP-9/992 *	–	L. MAN (edent.); FRO
HAL-VP-9/999	–	R. MAX (P3)
HAL-VP-9/1003 *	–	L. + R. TIB; L. + R. FEM (dist.); R. FEM (prox.); R. ULN (prox.); 14 VER; R. + L. HUM (shafts); L. CAL; R. TAL; PAT; 3 podials; 13 MTP; 2 RIB frags.; 2 SCA frags.; partial L. OCX; partial SAC
HAL-VP-9/1012 *	–	L. FEM (prox.)
HAL-VP-9/1020	U	R. MAN (M2-M3); L. MAN (M1); MAN symph.
HAL-VP-9/1022	U	R. MAN (M1-M3)
HAL-VP-9/1024 *	–	R. HUM (prox.)
HAL-VP-9/1029	M	L. MAX (P4-M3 frag.)
HAL-VP-9/1030 *	–	R. MAX (P3-M3)
HAL-VP-9/1032 *	–	FEM (dist.)
HAL-VP-9/1035	U	L. MAX (M1, M3, partial M2); R. MAX (M2-M3); L. MAX (P3-P4); isolated R. UP3 and R. + L. UC
HAL-VP-9/1042 *	–	L. HUM (prox.)
HAL-VP-9/1048	U	R. MAN (M1-M2); intermediate PHX; R. ULN (prox.)
HAL-VP-9/1061 *	–	L. SCA (w/ glenoid); L. HUM (dist.)

HAL-VP-9/1068 *	–	L. HUM (dist.)
HAL-VP-9/1070	U	L. MAX (C-M2); R. UP4
HAL-VP-9/1071	U	L. MAN (I1-P4)
HAL-VP-9/1073	U	R. MAN (M2-M3)
HAL-VP-9/1074 *	–	L. FEM (prox.)
HAL-VP-9/1075	U	R. MAN (M1-M3 roots); L. MAX (P3-P4); MAN (condyle); TIB (prox. w/ shaft); HUM (dist.); TIB (dist.); CRA frags.; VER (caud.); RIB frags.
HAL-VP-9/1077	U	L. MAX (P3, partial P4, M1); isolated R. UP3; isolated L. LM1-2; isolated R. LP3-M1; R. MAN (M2-M3); MAN (condyle); R. + L. FEM (w/ dist. frags.); partial L. OCX; partial R. OCX (2 frags.); L. TIB (prox. w/ shaft, dist. frag.); R. TIB (dist. w/ shaft, prox. frag.); R. HUM (dist. w/ shaft, prox. w/ shaft); L. HUM (dist.); CAL; 2 TAL; 4 podials; SCA (glenoid fossa); R. RAD (prox. w/ shaft); L. RAD (tuberosity); ULN shaft; 9 intermediate and prox. PHX; 3 distal PHX; 5 VER (caud.); VER frags; PAT; CRA frags (incl. a piece of orbit); FIB (dist. w/ shaft); misc. frags.
HAL-VP-9/1097	U	R. + L. MAN (M1-M3)
HAL-VP-9/1099	U	R. MAX (I1-M1); CRA frag.
HAL-VP-9/1101	F	L. MAX (I2, P3-M3); R. MAX (C-M3); MAN (L. I1-I2, P3-M3; R. C-M3); CRA frags.
HAL-VP-9/1102	U	Partial CRA w/ SPH, FRO, L. MAX (R. I2, partial L. C, P3-M3); R. LI2; R. LP3; R. MAN (w/ condyle, M3); 2 CRA frags.; R. + L. CLA; 1st rib; RIB frags.; R. + L. HUM; R. + L. ULN; L. RAD (prox.); R. RAD (dist.); R. SCA (3 frags.); L. SCA frag.; R. + L. partial OCX; R. + L. PAT; R. + L. TIB; R. + L. FEM; R. FIB; L. FIB (prox., dist., shaft frag.); multiple VER and VER frags.; SAC; two STE segments incl. manubrium; 8 prox. PHX; 7 int. PHX; 7 terminal PHX; 4 dist. MTP; 5 prox. ends of prox. PHX; 1 prox. end of int. PHX; 3 dist. ends of PHX; R. CAL; R. + L. TAL; R. + L. CUB; R. + L. NAV; 4 cuneiforms; LUN; CAP; 1 scaphoid; 3 podials; L. MTT 1-5; R. MTT 1-5; L. MTC 2 and 5; R. MTC 2-5; misc. frags.
HAL-VP-9/1108	U	R. MAN (L. I2-R. P3 roots, P4-M3); R. MAX (partial C-P4, complete M1-M3); RAD (prox.); CRA frags.
HAL-VP-9/1109 *	–	R. FEM (prox.)
HAL-VP-9/1113	U	L. MAX (M1)
HAL-VP-9/1115	U	L. MAX (P3-M1)
HAL-VP-9/1117 *	–	R. RAD (prox.)
HAL-VP-9/1119 *	–	L. MAN (edent.); MAN symph.
HAL-VP-9/1124 *	–	L. HUM (dist.)
HAL-VP-9/1127	U	R. MAN (I1-P3 roots, partial P4-M2, M3 roots)
HAL-VP-9/1128	–	R. LdM2
HAL-VP-9/1145 *	–	R. HUM (dist.)
HAL-VP-9/1150 *	–	R. FEM (prox.)
HAL-VP-9/1156 *	–	L. MAX (edent.)

HAL-VP-9/1170	–	L. UI1
HAL-VP-9/1172	U	MAN (R. dM1-dM2)
HAL-VP-9/1176 *	–	R. MAX (I2 erupting, dM1-M1)
HAL-VP-9/1401	–	L. LM2
HAL-VP-9/1403 *	–	L. ULN (prox.)
HAL-VP-9/1404 *	–	L. MAN (edent.)
HAL-VP-9/1416 *	–	MAN symph. (edent.)
HAL-VP-9/1417 *	–	R. + L. MAN (L.dM1-M1, R.dM1-2)
HAL-VP-9/1428	–	L. LM3
HAL-VP-9/1434	U	R. LP4-M1; R. LM3; L. LC; L. LM1-3
HAL-VP-9/1441	–	R. LM2
HAL-VP-9/1442	–	LM3
HAL-VP-9/1444	U	LM3; R. HUM (dist., shaft)
HAL-VP-9/1445 *	–	L. MAN (edent.)
HAL-VP-9/1453 *	–	R. MAX (C-M3 roots, M1 frag.)
HAL-VP-9/1457	U	R. MAX (P3-M2); FRO frag.
HAL-VP-9/1459 *	–	R. MAX (P4, partial M1); R. MAN (M1-M3 roots); isolated R. LM; R. MAN (condyle); L. HUM (prox.); L. + R. HUM (dist.); R. + L. RAD (prox.); R. RAD (partial dist.); L. SCA frag; PAT; R. + L. ULN (prox.); R. FEM (prox.); TIB (prox.); R. TIB (dist.); R. + L. FEM (prox.); assorted hand and foot bones; many VER and RIB frags.; partial SAC; 3 STE segments; R. OCX frag.; misc. frags.
HAL-VP-9/1460	U	L. MAX (C-M3)
HAL-VP-9/1461	U	MAN (L. I1-I2, M1-M2; R. I1, P4-M2; P3's and C's erupting)
HAL-VP-9/1463	U	L. MAN (M1-M3)
HAL-VP-9/1465 *	–	R. + L. HUM (prox.)
HAL-VP-9/1470 *	–	R. MAX (edent.)
HAL-VP-9/1472 *	–	L. FEM (prox.); L. RAD (dist.); L. partial OCX; OCX frag.; R. CAL; FEM (dist.); PAT; VER frag.; long bone frags.
HAL-VP-9/1476 *	–	R. HUM (dist.)
HAL-VP-9/1477	U	L. MAX (P3-M2)
HAL-VP-9/1478	U	L. MAN (M1-M3)
HAL-VP-9/1524 *	–	R. FEM (prox.)
HAL-VP-9/1527	U	R. + L. MAN (L. P4-M1)
HAL-VP-9/1530	U	L. MAX (C-M1)
HAL-VP-9/1537	–	R. MAX (I1, C-M3); L. MAX (C, P3-M3); L. MAN (P4-M3); R. MAN (P4-M3); L. LI2-C in concretion; MAN (condyle); R. + L. TEM frags; L. RAD; R. RAD (prox.); R. ULN (prox.); R. ULN (dist.); R. + L. HUM; L. FEM; R. FEM (dist.); R. + L. TIB; L. OCX frag.; 2 R. OCX frags.; PAT; L. FIB (prox.); L. SCA frag; R. + L. CAL; R. + L. TAL; NAV; assorted

		podials, MTP, and PHX; RIB frags; partial SAC; 2 VER; multiple partial VER; misc. frags.
HAL-VP-9/1539	U	R. MAX (M1-M3)
HAL-VP-9/1542 *	–	R. MAX
HAL-VP-9/1545 *	–	L. ULN (prox.)
HAL-VP-9/1550	U	MAN + MAX
HAL-VP-9/1551 *	–	FEM (dist.)
HAL-VP-9/1562 *	–	R. FEM (prox., shaft); OCX frag.
HAL-VP-9/1568	U	L. MAN (M1-M2, imm.)
HAL-VP-9/1572	U	CRA (R. I1-I2, P3-P4, partial M1-M2; partial L. C, complete P3-M3); R MAN (w/ condyle and M2-M3); isolated R. LM1; isolated R. LI1-I2; R. HUM; R. ULN; R. RAD; MTP (prox.); RIB frag.; misc. frags.
HAL-VP-9/1575	U	R. MAX (partial P3, complete P4-M3); L. MAX (partial I2, partial P3-M1)
HAL-VP-9/1578	U	R. MAN (P4-M2, M3 in crypt)
HAL-VP-9/1579	U	R. + L. MAX (dC-dM2, M1)
HAL-VP-9/1581	U	L. MAN (P4-M3)
HAL-VP-9/1590 *	–	R. ULN (prox.)
HAL-VP-9/1594 *	–	R. ULN (prox.)
HAL-VP-9/1596 *	–	L. ULN (prox.)
HAL-VP-9/1598 *	–	L. HUM (dist.)
HAL-VP-9/1604 *	–	UM
HAL-VP-9/1610	U	FRO
HAL-VP-9/1611	F	FRO
HAL-VP-9/1615 *	U	R. + L. OCX; R. + L. SCA (glenoid fossa); R. ULN (prox. w/ shaft); L. ULN (partial prox.); L. RAD (prox. w/ shaft); R. HUM (dist.); L. FEM (prox., w/ shaft frags.); TIB (dist.); R. + L. CAL; L. TAL; 2 cuneiforms; CUB; NAV; numerous MTP and PHX; ULN shaft frags.; FEM shaft; HUM (prox.); CRA frags.; VER frags.
HAL-VP-9/1618	U	L. MAX (P3-M1)
HAL-VP-9/1619	–	L. MAN (M2)
HAL-VP-9/1622	–	LM1 or 2
HAL-VP-9/1623	U	L. MAX (P3-M3)
HAL-VP-9/1625 *	–	R. + L. OCX frags.; R. RAD (prox.); R. ULN (prox.); R. FEM (prox.); HUM (dist. w/ shaft); FEM (dist. shaft); shaft frags.
HAL-VP-9/1629 *	–	FRO (w/ glabella)
HAL-VP-9/1631 *	–	FRO (w/ glabella); CRA frags.
HAL-VP-9/1632 *	–	TIB (prox. w/ shaft); HUM (dist.); FEM (dist.); OCX frags.; ULN (prox.); LUN; STE; R. + L. PAT; TIB (dist.); PHX frags.; VER frags.; misc. frags.
HAL-VP-9/1643 *	–	L. HUM (dist.)
HAL-VP-9/1644 *	–	R. HUM (dist.)

HAL-VP-9/1646	–	R. UI1

Note: see Supporting Information Table S2 for anatomical abbreviation key.
*Specific referral to *Colobus* cf. *guereza* rather than a more inclusive taxon is based on association with the broader assemblage and morphological congruence with more complete specimens.
Sex abbreviations: F, female; F?, probable female; M, male; M?, probable male; U, uncertain.

FIGURES

Figure 1 Crania of Faro Daba *Colobus* cf. *guereza* in anterior view. Clockwise from top left: HAL-VP-9/730, HAL-VP-9/319, HAL-VP-9/723, HAL-VP-9/332, HAL-VP-9/5, HAL-VP-9/489, HAL-VP-9/1572, and HAL-VP-9/779. The individuals at the far left and right are a probable female and male, respectively; sex is uncertain for the six individuals in the center. Crania are aesthetically arranged to provide a sense of preservation and variation in the assemblage. See subsequent figures for more traditional views. Scale is approximate.

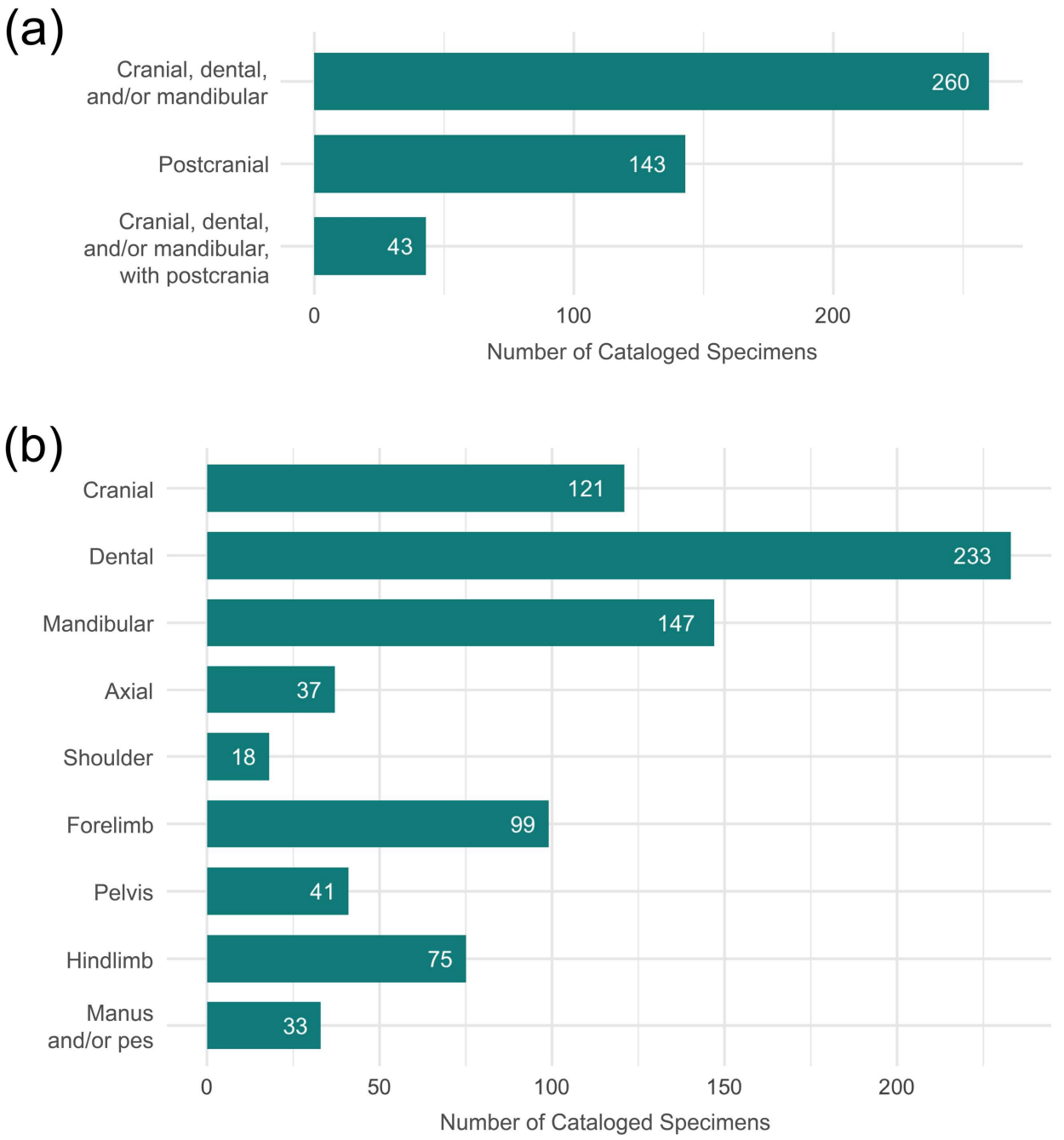

Figure 2 Distribution of anatomical regions represented in the Faro Daba *Colobus* cf. *guereza* sample. (a) Number of cataloged specimens with cranial, dental, and/or mandibular remains, postcranial remains, and both types of remains. (b) Number of cataloged specimens preserving elements from nine anatomical regions. Note that cataloged specimens are counted in multiple categories (e.g., the 43 individuals with both types of remains in (a) are also counted in the two categories above). Elements classified as belonging to the "shoulder" include the clavicle and the scapula; the "pelvis" includes the os coxae and the sacrum. See Appendix 1 for a full list of specimens and element inventory.

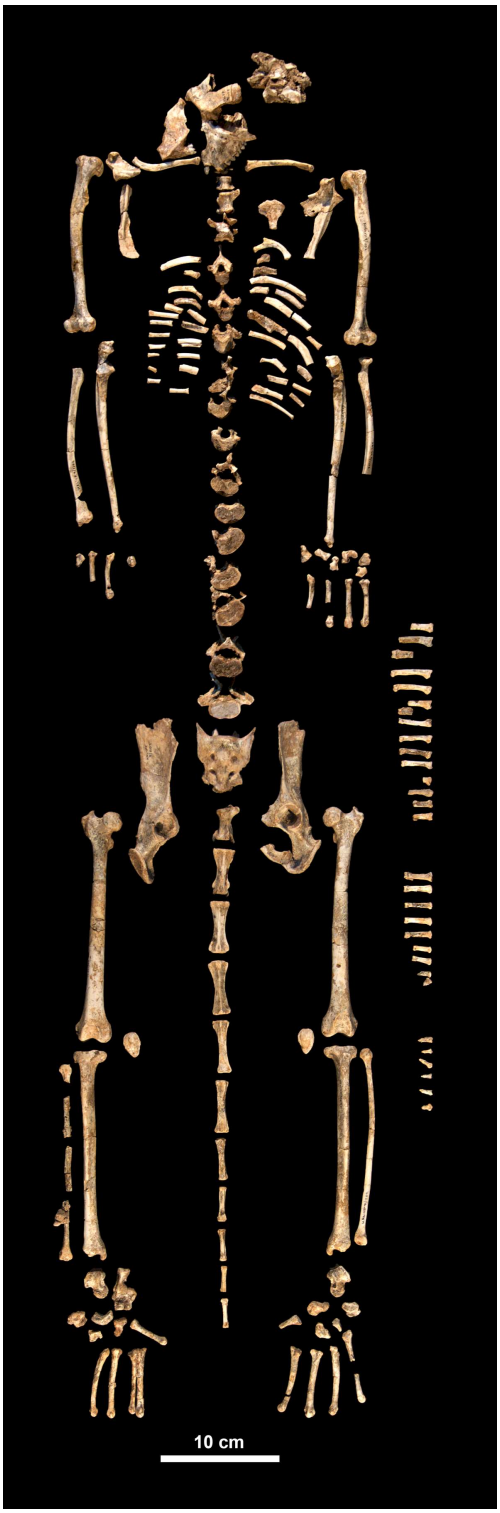

Figure 3 Faro Daba *Colobus* cf. *guereza* skeleton, HAL-VP-9/1102. Sex is uncertain. Phalanges are arranged along the right side from proximal (top group) to intermediate (middle group) to distal (bottom group). This is one of the most complete single individuals recovered, but it should be noted that there are more than a dozen relatively complete partial skeletons in the Faro Daba colobine assemblage (see Appendix 1 for inventory).

Figure 4 Faro Daba *Colobus* cf. *guereza* and extant colobine adult crania. *Top panel*: Faro Daba *Colobus* cf. *guereza* in anterior (top row), superior (center row), and lateral (bottom row) views. Sex is uncertain for all fossil individuals. From left to right: HAL-VP-9/723, HAL-VP-9/779, and HAL-VP-9/1572. HAL-VP-9/723 (left) and HAL-VP-9/1572 (right) are pictured in left lateral view; anterior is to the left. HAL-VP-9/779 (center) is pictured in right lateral view; anterior is to the right. HAL-VP-9/723 includes associated vault fragments, dental remains, and a partial postcranial skeleton that are not pictured here. HAL-VP-9/779 does not preserve any additional associated elements beyond the cranium pictured here. HAL-VP-9/1572 includes mandibular, dental, and postcranial remains that are not pictured here; see Figure 10 for an occlusal view of the maxillary dentition of this individual. *Bottom panel*: Extant colobines in superior (top row) and left lateral (bottom row) views. Anterior is to the left. From left to right: *C. guereza* male (FMNH 31163), *C. angolensis* female (FMNH 27276), and *Pi. badius* female (FMNH 15519). Images of extant specimens by Rebecca A. Banasiak, licensed under a Creative Commons Attribution-Noncommercial 4.0 International License. Scale is the same for both panels.

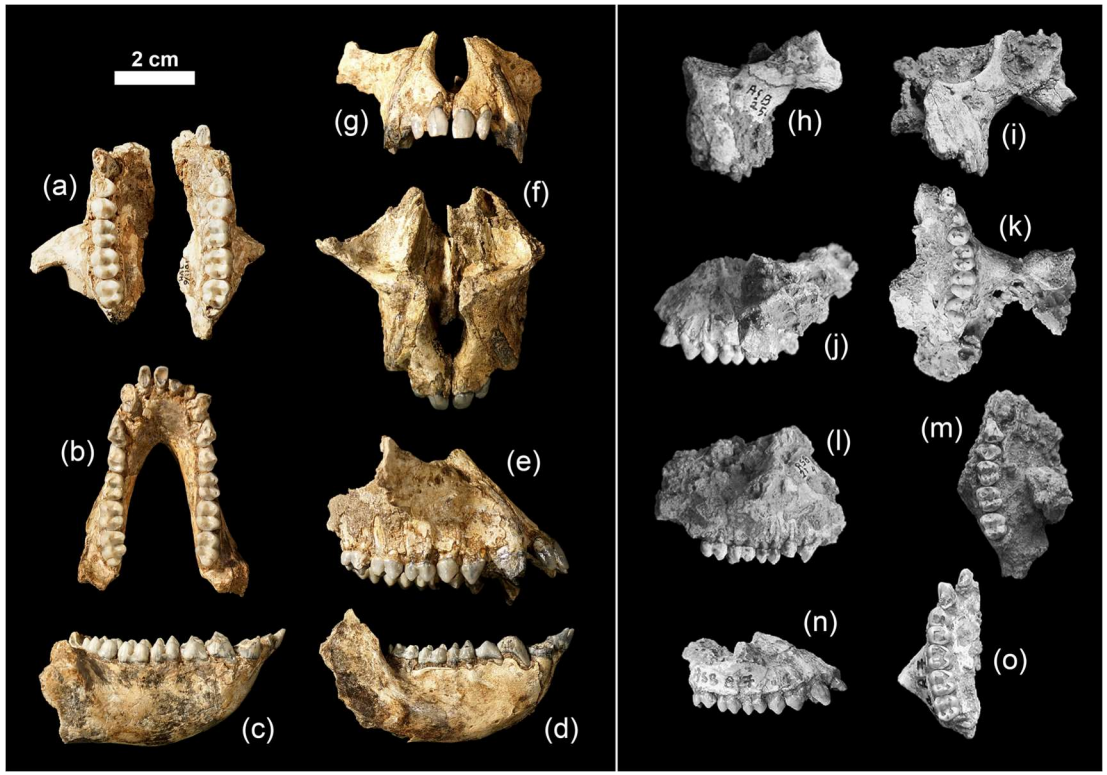

Figure 5 Maxillary and mandibular morphology of Faro Daba *Colobus* cf. *guereza* and maxillary morphology of Asbole *Colobus* sp. specimens prior to matrix cleaning (see Figure 7 for mandibular comparisons). *Left panel*: Two Faro Daba *Colobus* cf. *guereza* adult individuals preserving both maxillary and mandibular anatomy. HAL-VP-9/1101 (female) is pictured on the left and HAL-VP-9/488 (male) on the right. (a) HAL-VP-9/1101 maxilla in inferior view; anterior is up. (b) HAL-VP-9/1101 mandible in superior view; anterior is up. (c) HAL-VP-9/1101 mandible in right lateral view; anterior is to the right. (d) HAL-VP-9/488 mandible in right lateral view; anterior is to the right. (e) HAL-VP-9/488 maxilla in right lateral view; anterior is to the right. (f) HAL-VP-9/488 maxilla in superior view; anterior is down. (g) HAL-VP-9/488 maxilla in anterior view; superior is up. *Right panel*: Four Asbole individuals preserving maxillary anatomy. (h) ASB-254-6, male left maxilla in anterior view. (i) ASB-90, female left maxilla in anterior view. (j) ASB-90, female left maxilla in left lateral view; anterior is to the left. (k) ASB-90, female left maxilla in occlusal view; anterior is up. (l) ASB-214, male right maxilla in right lateral view; anterior is to the right. (m) ASB-214, male right maxilla in occlusal view; anterior is up. (n) ASB-87, female right maxilla in right lateral view; anterior is to the right. (o) ASB-87, female right maxilla in occlusal view; anterior is up. Images of the Asbole fossils are from Frost and Alemseged (2007). Scale is the same for both panels.

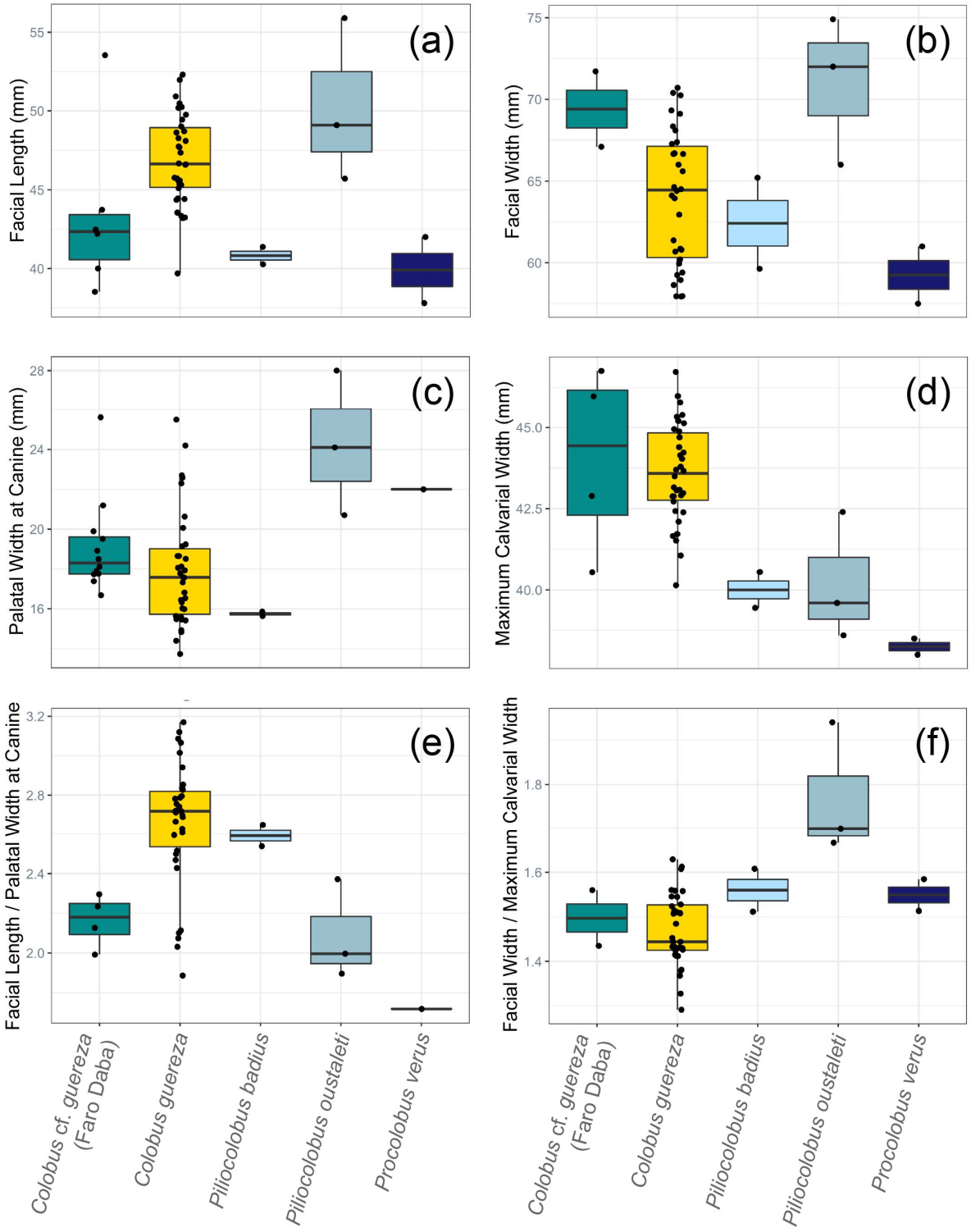

Figure 6 Cranial metrics for the Faro Daba *Colobus* cf. *guereza* fossils and comparative samples. (a) Facial length. (b) Facial width. (c) Palatal width at the level of the maxillary canines. (d) Maximum calvarial width. (e) Ratio of facial length to palatal width at the level of the maxillary canines. (f) Ratio of facial width to maximum calvarial width. Abbreviations: mm, millimeters.

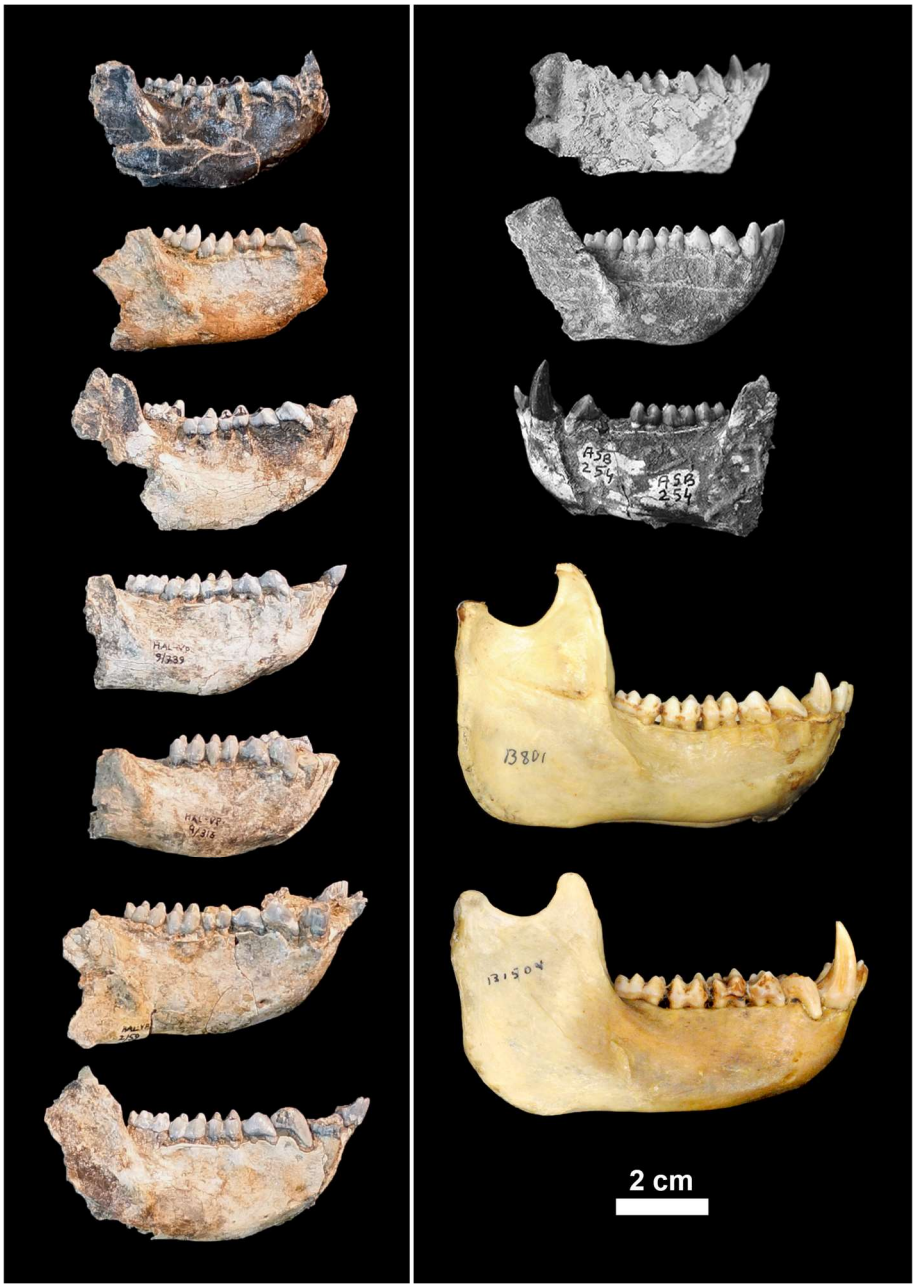

Figure 7 Mandibular morphology of Faro Daba *Colobus* cf. *guereza*, Asbole *Colobus* sp., and extant *C. guereza. Left panel*: Faro Daba *Colobus* cf. *guereza* adult mandibles in right lateral view, demonstrating the preservation and variation in the assemblage. Mandibles are seriated from smallest (top) to largest (bottom) in general size. From top to bottom: HAL-VP-9/627 (probable female), HAL-VP-9/338, HAL-VP-9/590, HAL-VP-9/739 (female), HAL-VP-9/316, HAL-VP-2/59, and HAL-VP-9/488 (male). Sex is uncertain unless otherwise indicated above. *Right panel*: Asbole *Colobus* sp. and extant *C. guereza.* From top to bottom: ASB-215-2 (female), ASB-80 (female), ASB-254-13 (male), and extant *C. guereza* specimens HTB 0801 (female) and HTB 1504 (male). Mandibles are in right lateral view, except for ASB-254-13, which is in left lateral view. Images of the Asbole fossils are from Frost and Alemseged (2007). Scale is the same for both panels.

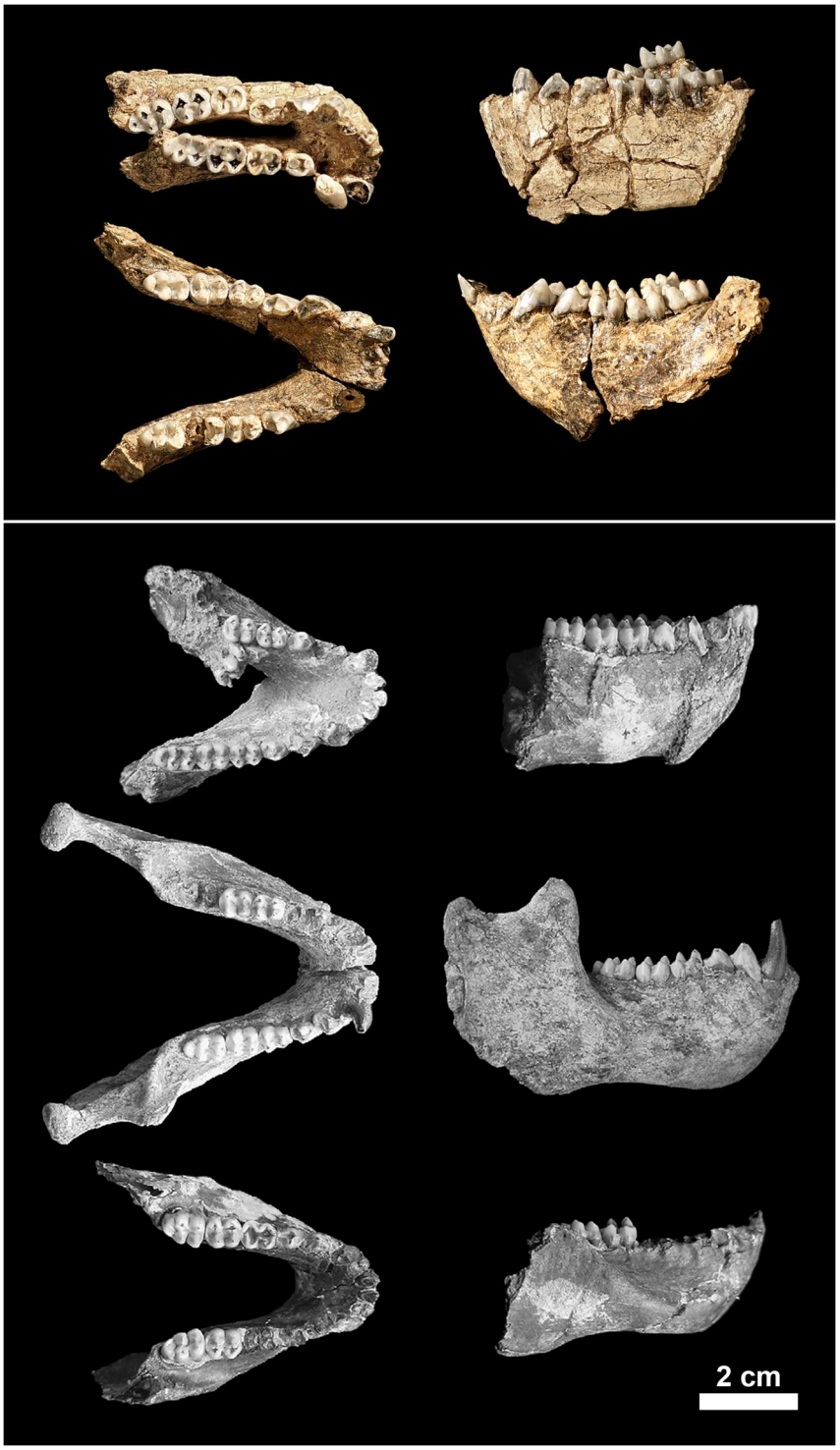

Figure 8 Faro Daba *Colobus* cf. *guereza* and Asbole *Colobus* sp. mandibles. *Top panel*: Faro Daba *Colobus* cf. *guereza* adult mandibles in superior (left) and left lateral (right) views. Top row: HAL-VP-9/733 (probable female). Bottom row: HAL-VP-9/556 (male). *Bottom panel*: Asbole *Colobus* sp. adult mandibles in superior (left) and right lateral (right) views. Top row: ASB-78 (male). Center row: ASB-100 (male). Bottom row: ASB-76 (female). Images of the Asbole fossils are from Frost and Alemseged (2007). Scale is the same for both panels.

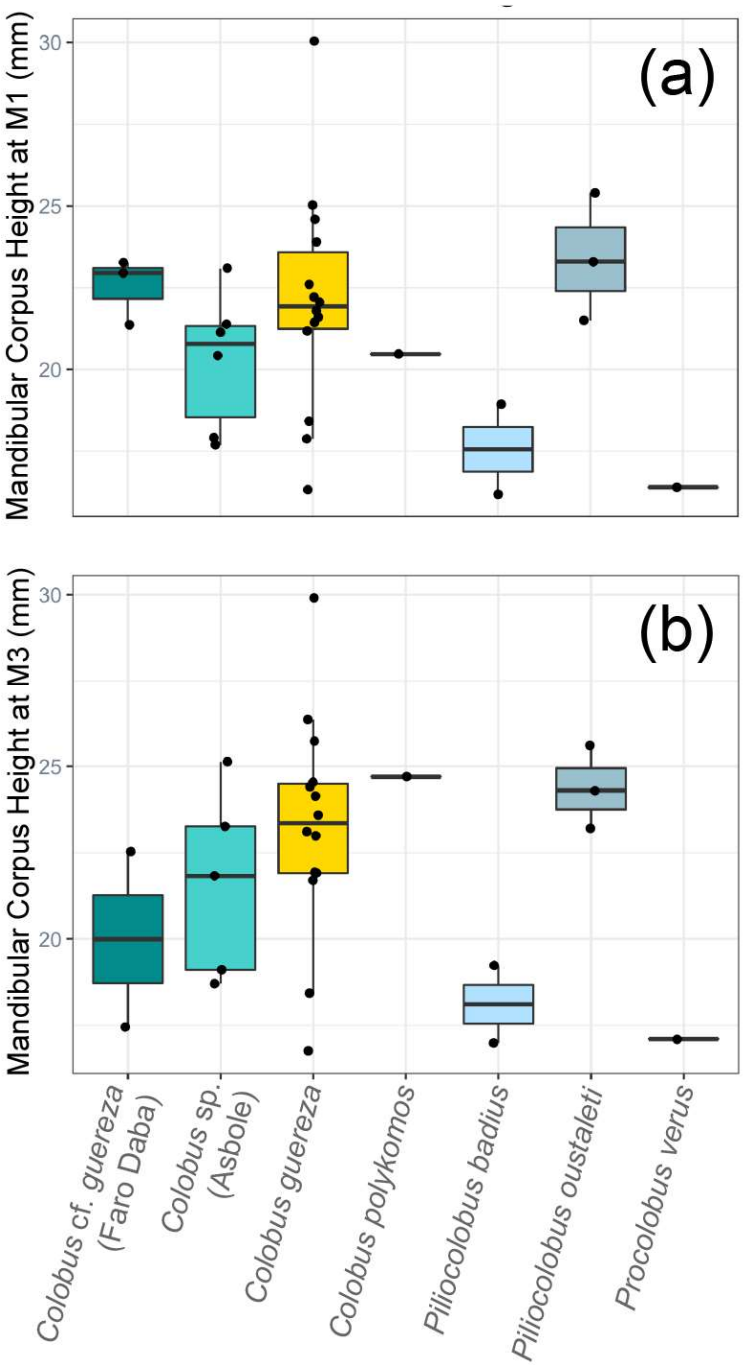

Figure 9 Mandibular metrics for the Faro Daba *Colobus* cf. *guereza* fossils and comparative samples. (a) Height of the mandibular corpus at the midpoint of the mandibular first molar. (b) Height of the mandibular corpus at the midpoint of the mandibular third molar. Abbreviations: mm, millimeters; M1, first molar; M2, second molar.

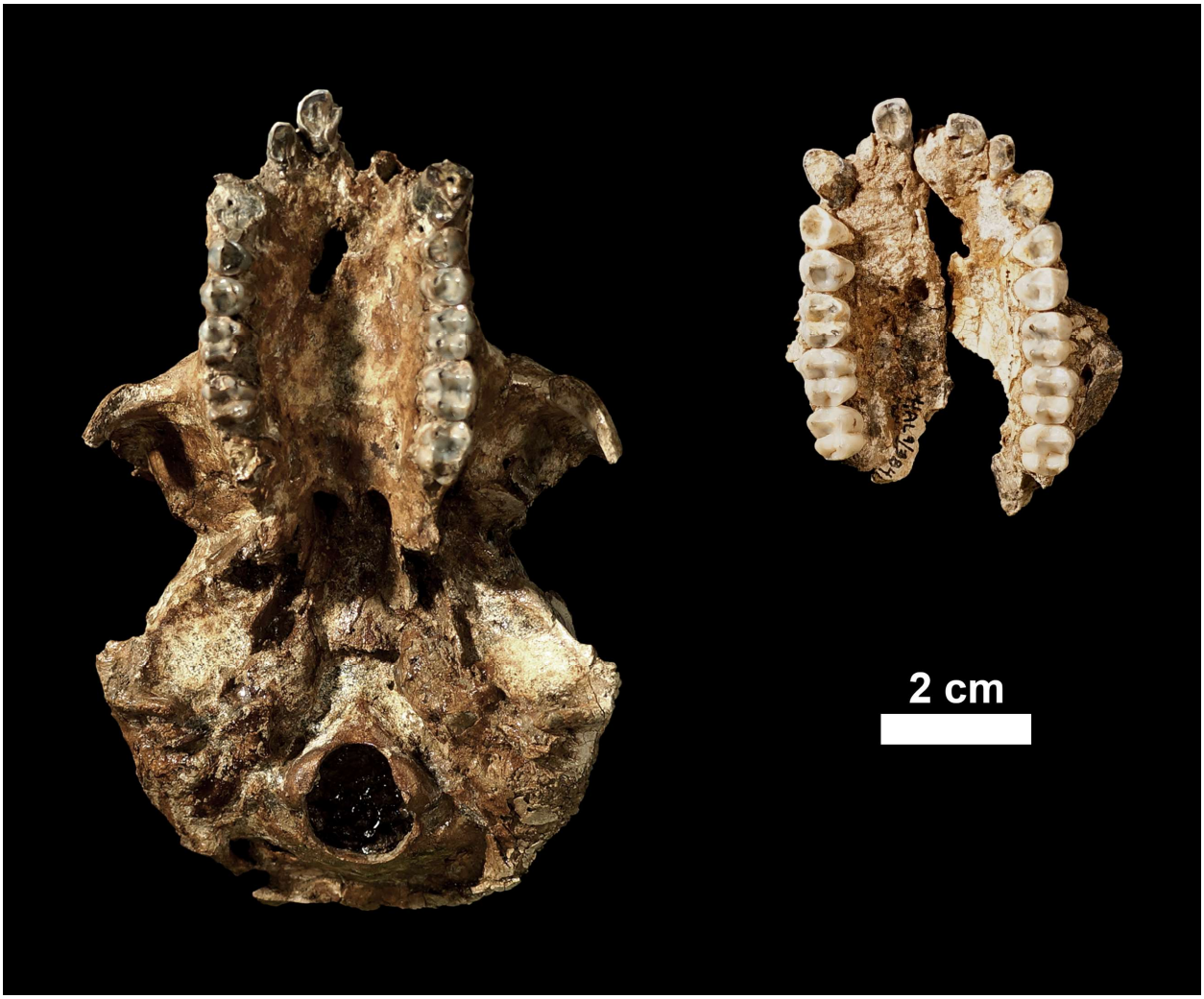

Figure 10 Nearly complete adult maxillary dentitions of *Colobus* cf. *guereza* individuals HAL-VP-9/1572 (left) and HAL-VP-9/384 (right) in inferior view; anterior is up. Sex is uncertain for both individuals. See Figure 4 for additional views of the HAL-VP-9/1572 cranium.

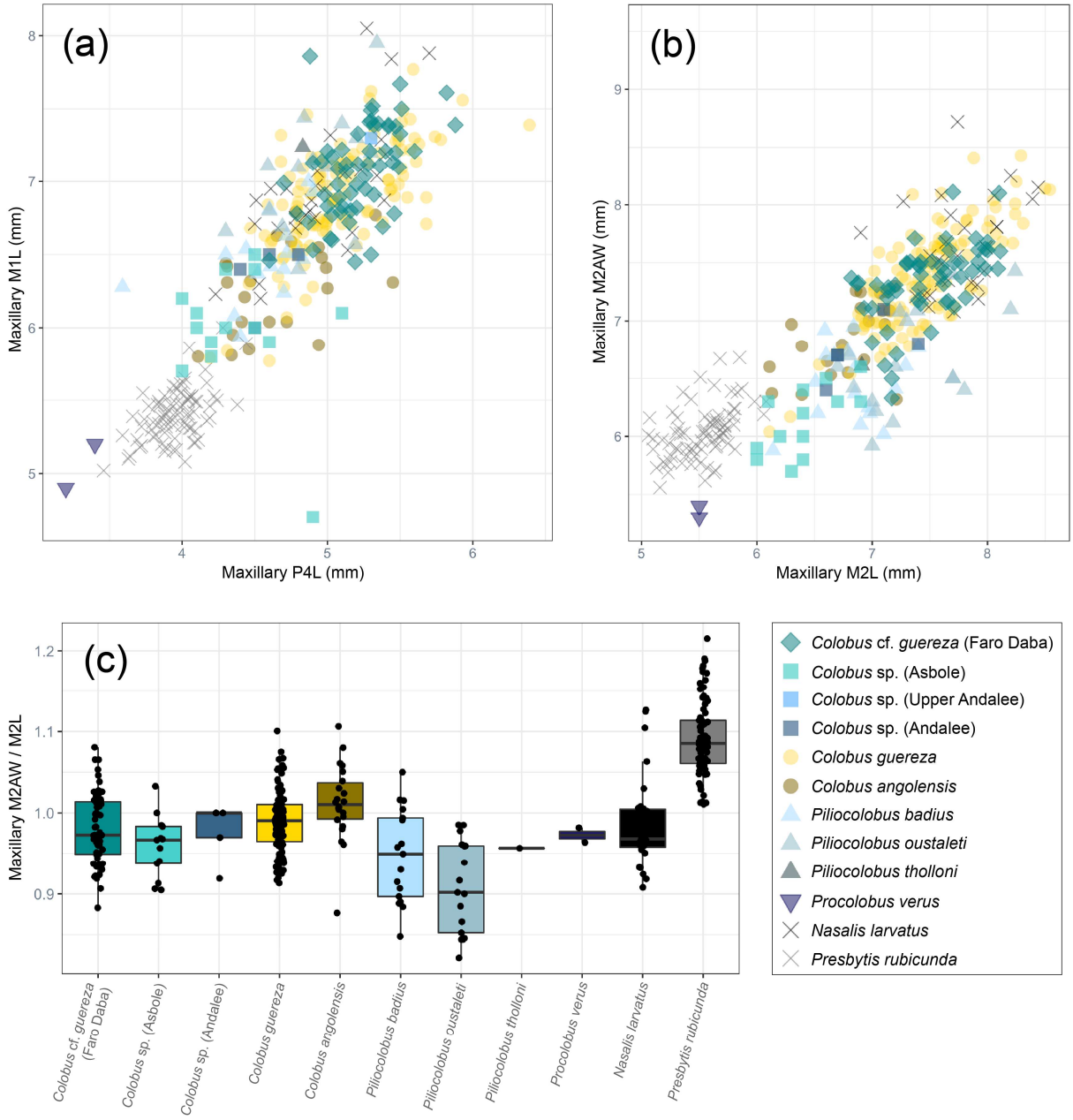

Figure 11 Maxillary dental metrics for the Faro Daba *Colobus* cf. *guereza* fossils and comparative samples. (a) Mesiodistal crown length of the maxillary fourth premolar vs. maxillary first molar. (b) Mesiodistal crown length vs. anterior crown width of the maxillary second molar. (c) Ratio of the maxillary second molar anterior crown width to mesiodistal crown length. Abbreviations: mm, millimeters; L, mesiodistal crown length; AW, buccolingual width of the anterior loph; P4, M1, and M2 refer to the fourth premolar and first and second molars, respectively.

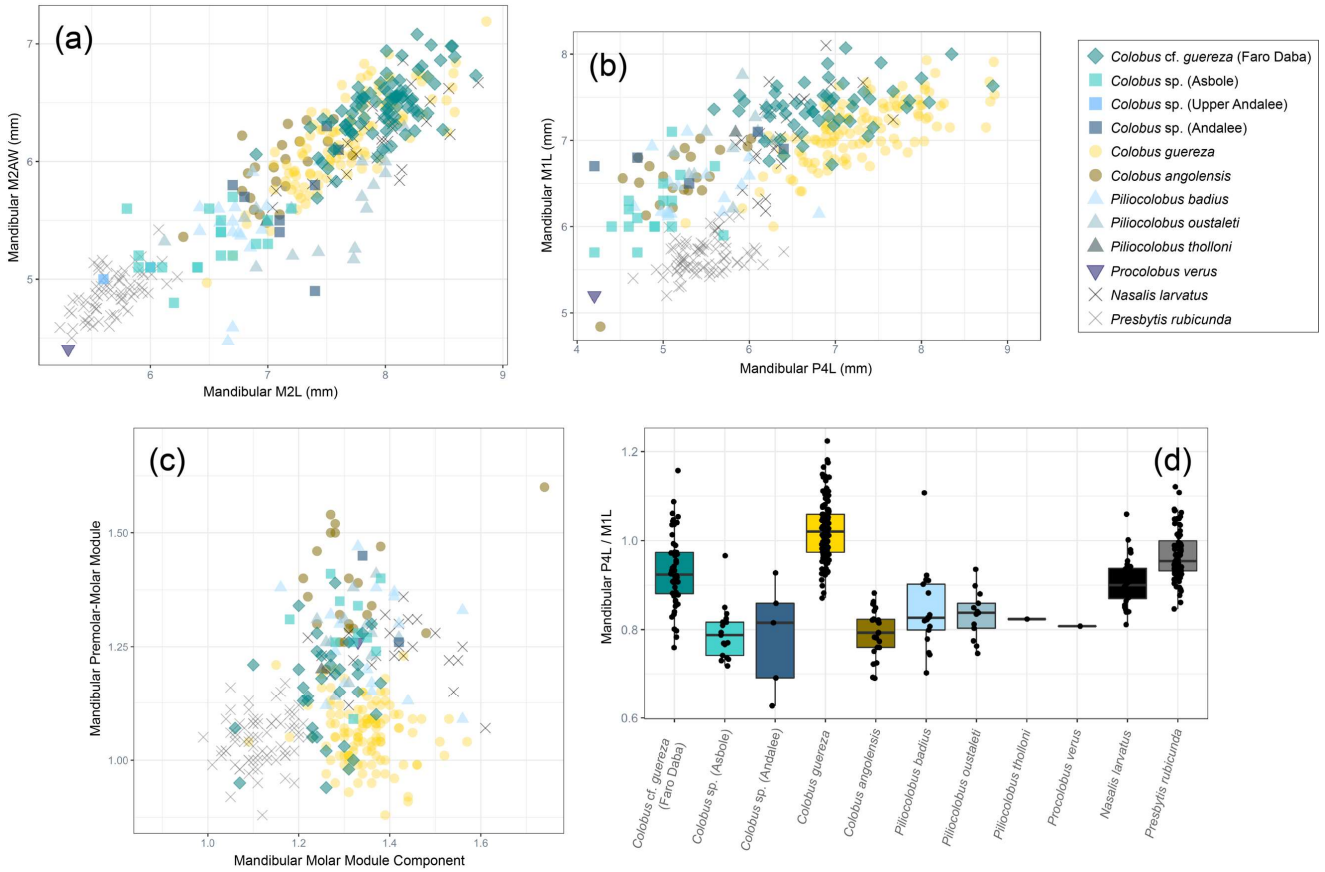

Figure 12 Mandibular dental metrics for the Faro Daba *Colobus* cf. *guereza* fossils and comparative samples. (a) Mesiodistal crown length vs. anterior crown width of the mandibular second molar. (b) Mesiodistal crown length of the mandibular fourth premolar vs. mandibular first molar. (c) Molar module component (MMC) vs. premolar-molar module (PMM); see Methods section for details on these dental ratios. Note that although three *Colobus* cf. *guereza* individuals at the low end of the MMC axis appear here as outliers, there are additional individuals that span the perceived gap in MMC values; they are not included here because they do not preserve the PMM. (d) Ratio of the mandibular fourth premolar mesiodistal crown length to mandibular first molar mesiodistal crown length. Abbreviations: mm, millimeters; L, mesiodistal crown length; AW, buccolingual width of the anterior loph; P4, M1, and M2 refer to the fourth premolar and first and second molars, respectively.

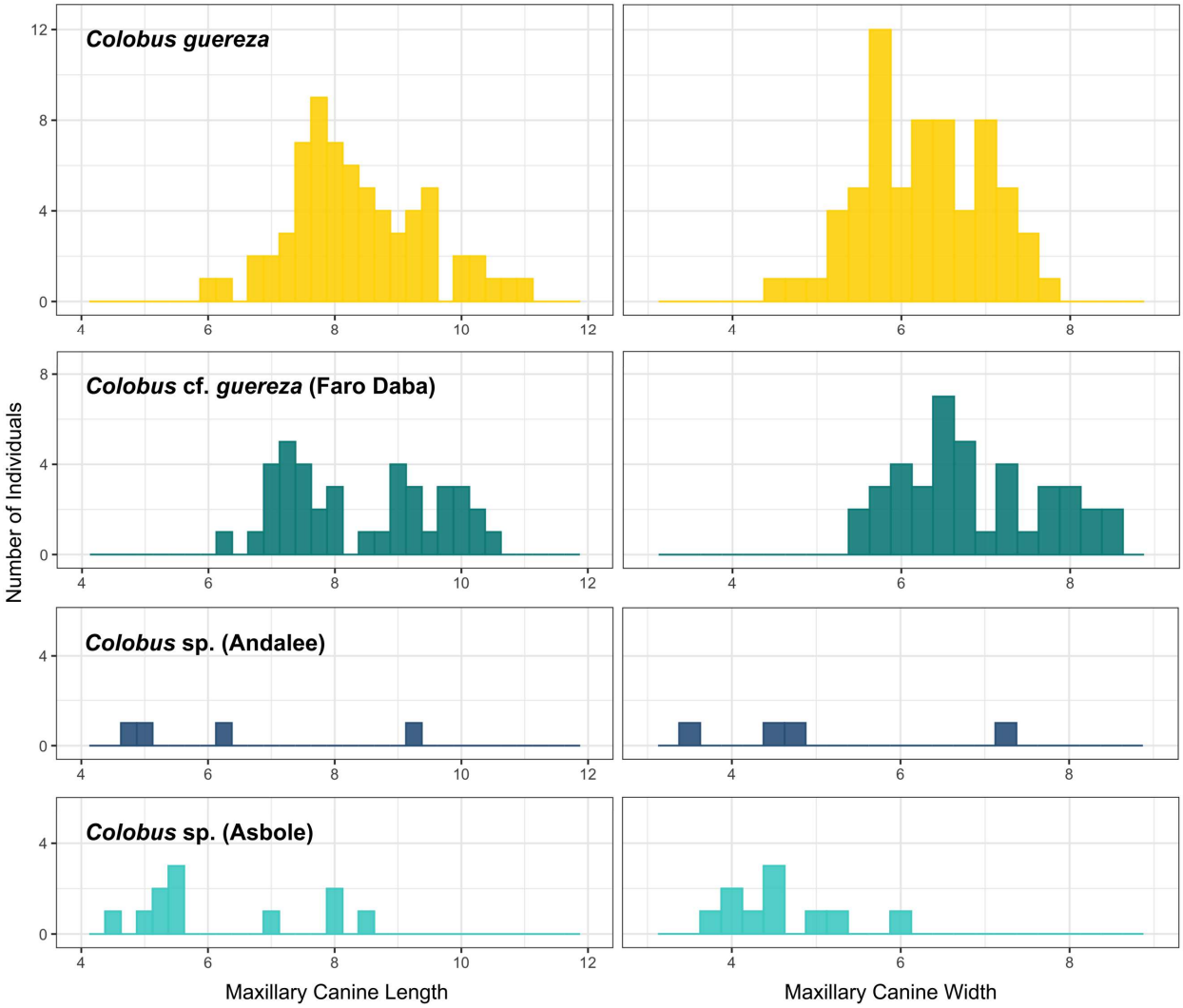

Figure 13 Frequency distributions of maxillary canine crown mesiodistal length (left) and buccolingual width (right) for the Faro Daba *Colobus* cf. *guereza* fossils and comparative *Colobus* samples. Measurements are in millimeters. The Faro Daba *Colobus* cf. *guereza* align closely with the extant *Colobus guereza* sample. The Middle Pleistocene *Colobus* sp. samples from "Andalee" and Asbole, Ethiopia, are smaller on average than both more recent samples. See text for a discussion of the implications of this size difference.

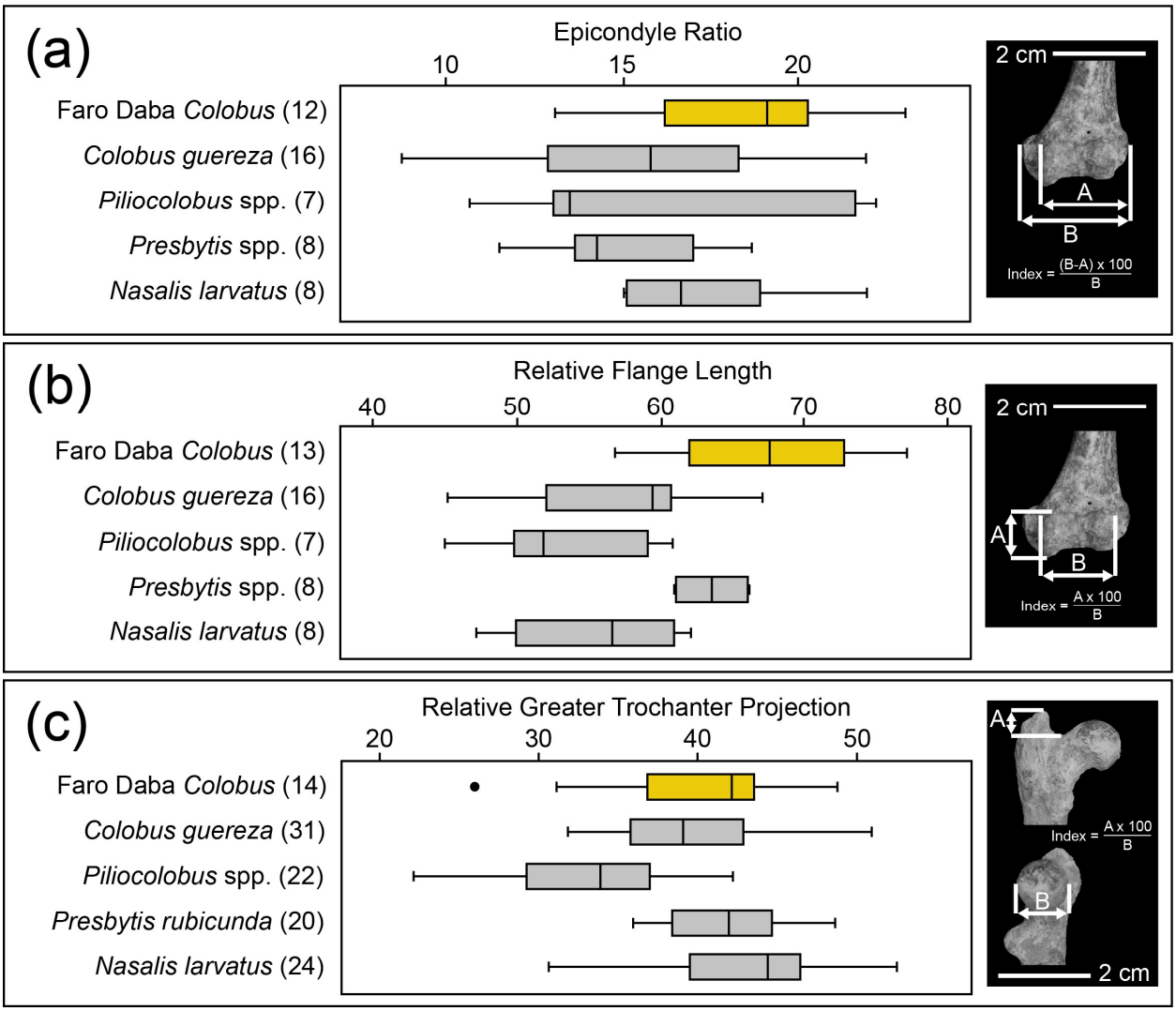

Figure 14 Boxplots of three postcranial metrics for the Faro Daba *Colobus* cf. *guereza* fossils and extant comparative samples. Sample sizes are indicated in parentheses. These metrics have been interpreted to reflect locomotory habitus in cercopithecids (see text for discussion). (a) Epicondyle ratio of the distal humerus. (b) Relative flange length of the distal humerus. (c) Relative greater trochanter projection of the proximal femur. Comparative plots for extant colobines are adapted from Frost et al. (2020).

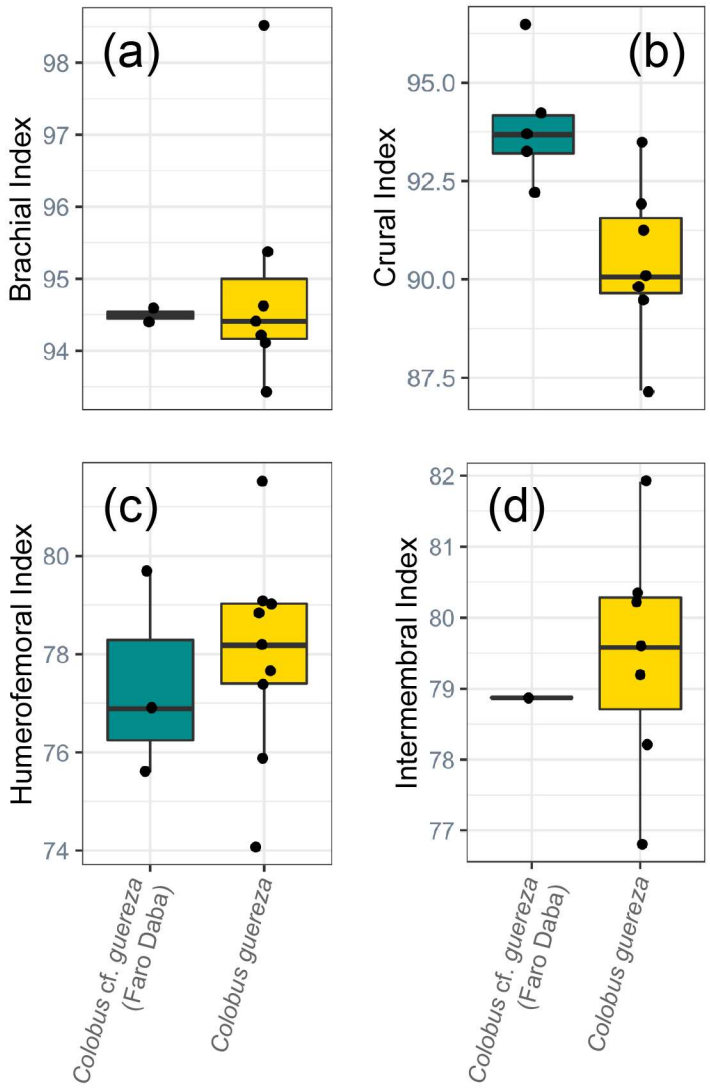

Figure 15 Postcranial indices for the Faro Daba *Colobus* cf. *guereza* fossils and extant *Colobus guereza*. (a) Brachial index: (maximum radial length / maximum humeral length) * 100. (b) Crural index: (maximum tibial length / maximum femoral length) * 100. (c) Humerofemoral index: (maximum humeral length / maximum femoral length) * 100. (d) Intermembral index: (maximum humeral + radial length) / (maximum femoral + tibial length)) * 100.

Figure 16 Faro Daba *Colobus* cf. *guereza* humeri in anterior view, demonstrating size variation in the assemblage. Humeri are seriated by distal end size from largest (left) to smallest (right). From left to right: HAL-VP-9/5, HAL-VP-9/1102, HAL-VP-9/1572, HAL-VP-9/1615, HAL-VP-9/1075, HAL-VP-9/1077, HAL-VP-2/32, HAL-VP-9/284, HAL-VP-9/1537, and HAL-VP-9/1444. See Figure 16 for additional humeral remains; note that some specimens pictured here have associated elements pictured in other figures.

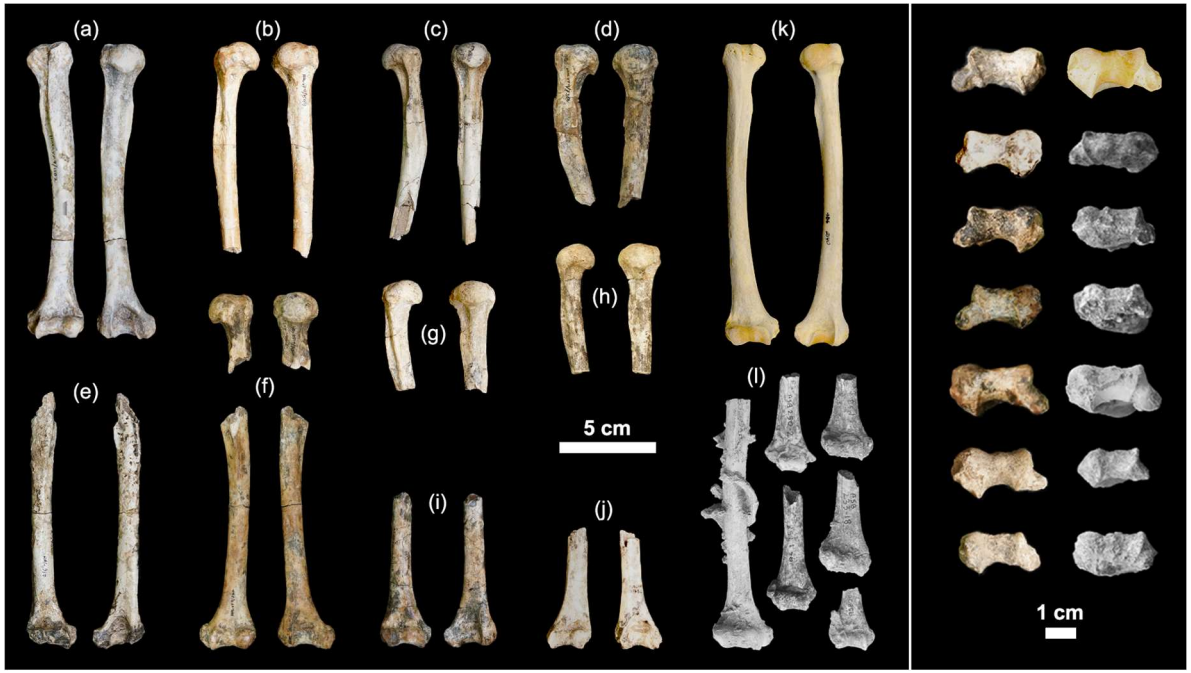

Figure 17 Humeral morphology of Faro Daba *Colobus* cf. *guereza*, Asbole *Colobus* sp., and extant *C. guereza*. *Left panel*: (a) HAL-VP-9/1102 left humerus in anterior (left) and posterior (right) views. (b) HAL-VP-9/594 right proximal humerus in medial (left) and posterior (right) views. (c) HAL-VP-9/640 left proximal humerus in medial (left) and posterior (right) views. (d) HAL-VP-9/730 right proximal humerus in medial (left) and posterior (right) views. (e) HAL-VP-9/7 right distal humerus in anterior (left) and posterior (right) views. (f) HAL-VP-9/730 left proximal and distal humerus. Proximal portion is shown in medial (left) and posterior (right) views. Distal portion in shown in anterior (left) and posterior (right) views. (g) HAL-VP-9/1615 right proximal humerus in medial (left) and posterior (right) views. (h) HAL-VP-9/284 right proximal humerus in medial (left) and posterior (right) views. (i) HAL-VP-9/1077 right distal humerus in anterior (left) and posterior (right) views. (j) HAL-VP-9/632 left distal humerus in anterior (left) and posterior (right) views. (k) Extant *C. guereza* right male humerus (HTB 2140) in anterior (left) and posterior (right) views. (l) Asbole *Colobus* sp. distal humeri in anterior view. All are from the right side. Clockwise from left: ASB-210, ASB-250-2, ASB-91, ASB-233-18, ASB-204, and ASB-158. *Right panel*: Distal humeri in distal view, anterior is up. Scale is approximate. Left column, from top to bottom: HAL-VP-9/284 (left side), HAL-VP-9/632 (left side), HAL-VP-9/1077 (left side), HAL-VP-9/730 (left side), HAL-VP-9/1077 (right side), HAL-VP-9/1615 (right side), HAL-VP-9/1444 (right side). Right column, from top to bottom: HTB 2140 (right side), ASB-254-25 (left side), ASB-91 (right side), ASB-158 (right side), ASB-210 (right side), ASB-204 (right side), and ASB-233-18 (right side). See Figure 15 for additional humeral remains; note that some specimens pictured here have associated elements pictured in other figures. Images of the Asbole fossils are from Frost and Alemseged (2007).

Figure 18 Faro Daba *Colobus* cf. *guereza* ulnae in right lateral view, demonstrating size variation in the assemblage. Ulnae are seriated by proximal end size from largest (left) to smallest (right). From left to right: HAL-VP-9/1615, HAL-VP-2/59, HAL-VP-9/1572, HAL-VP-9/1102, HAL-VP-9/419, HAL-VP-9/284, HAL-VP-9/1048, HAL-VP-9/1537, and HAL-VP-9/989. See Figure 18 for additional ulnar remains; note that some specimens pictured here have associated elements pictured in other figures.

Figure 19 Faro Daba *Colobus* cf. *guereza* ulnae and radii with extant and fossil comparisons. *Top panel, from left to right*: HAL-VP-9/1102 left ulna, HAL-VP-9/640 left partial proximal ulna, extant *C. guereza* male right ulna (HTB 2140), and Asbole *Colobus* sp. left proximal ulna (ASB-42-A). Each ulna is shown in lateral (left) and anterior (right) views, except for ASB-42-A, which is only shown in lateral view. *Bottom panel, from left to right*: HAL-VP-9/284 right radius, HAL-VP-9/284 left partial radius, and extant *C. guereza* male right radius (HTB 2140). Each radius is shown in approximately medial (left) and anterior (right) views. See Figure 17 for additional ulnar remains; note that some specimens pictured here have associated elements pictured in other figures. Images of the Asbole fossils are from Frost and Alemseged (2007). Scale is the same for both panels.

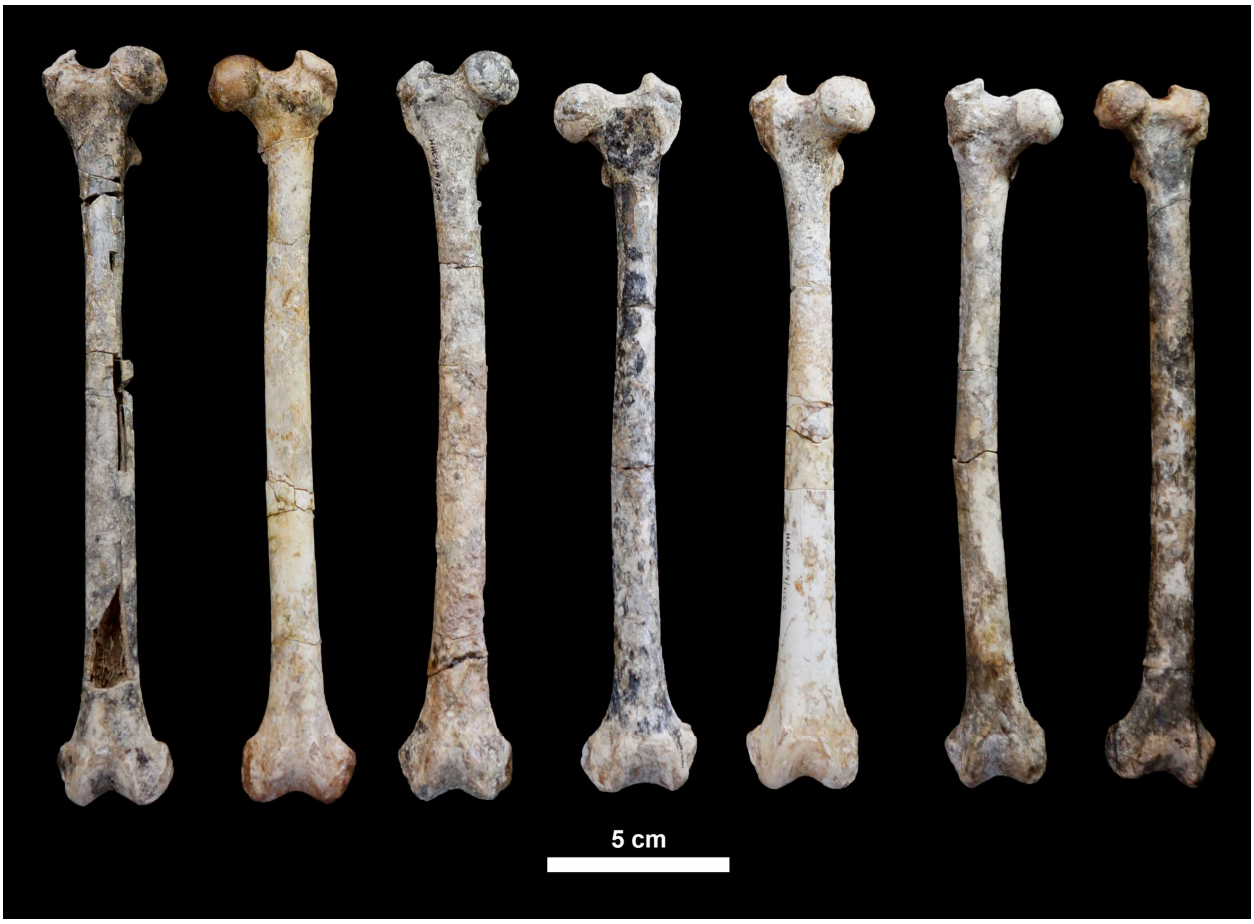

Figure 20 Faro Daba *Colobus* cf. *guereza* femora in anterior view, demonstrating size variation in the assemblage. Femora are seriated from largest (left) to smallest (right). From left to right: HAL-VP-2/88, HAL-VP-9/594, HAL-VP-9/730, HAL-VP-9/5, HAL-VP-9/1102, HAL-VP-9/284, and HAL-VP-9/1537. See Figure 20 for additional femoral remains; note that some specimens pictured here have associated elements pictured in other figures.

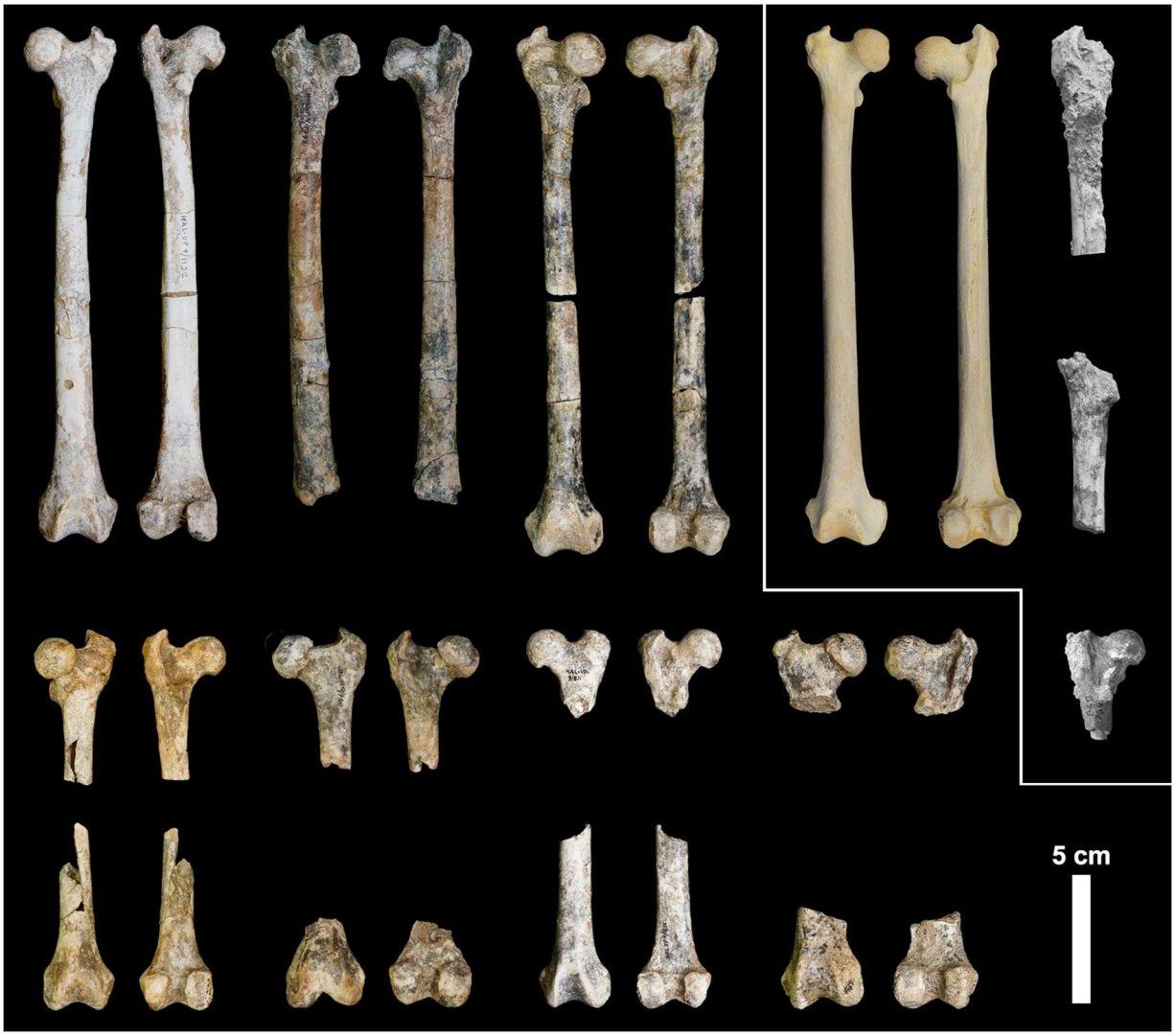

Figure 21 Faro Daba *Colobus* cf. *guereza* femora with extant and fossil comparisons. *Left panel*: Faro Daba *Colobus* cf. *guereza* femora. Each individual is shown in anterior (left) and posterior (right) views. Top row, from left to right: HAL-VP-9/1102 (left side), HAL-VP-9/1077 (right side), and HAL-VP-9/5 (right side, proximal and distal portions). Bottom row, from left to right: HAL-VP-9/284 (left side), HAL-VP-9/730 (left side), HAL-VP-9/811 (left proximal end, right distal end), and HAL-VP-9/732 (right side). *Right panel*: Extant *C. guereza* and Asbole *Colobus* sp. femora. Clockwise, from left: *C. guereza* right femur (HTB 2140) in anterior (left) and posterior (right) views, and three Asbole *Colobus* sp. left proximal femora in posterior view prior to matrix removal (ASB-210, ASB-250-1, and ASB-254-27). See Figure 19 for additional femoral remains; note that some specimens pictured here have associated elements pictured in other figures. Images of the Asbole fossils are from Frost and Alemseged (2007). Scale is the same for both panels.

Supporting Information

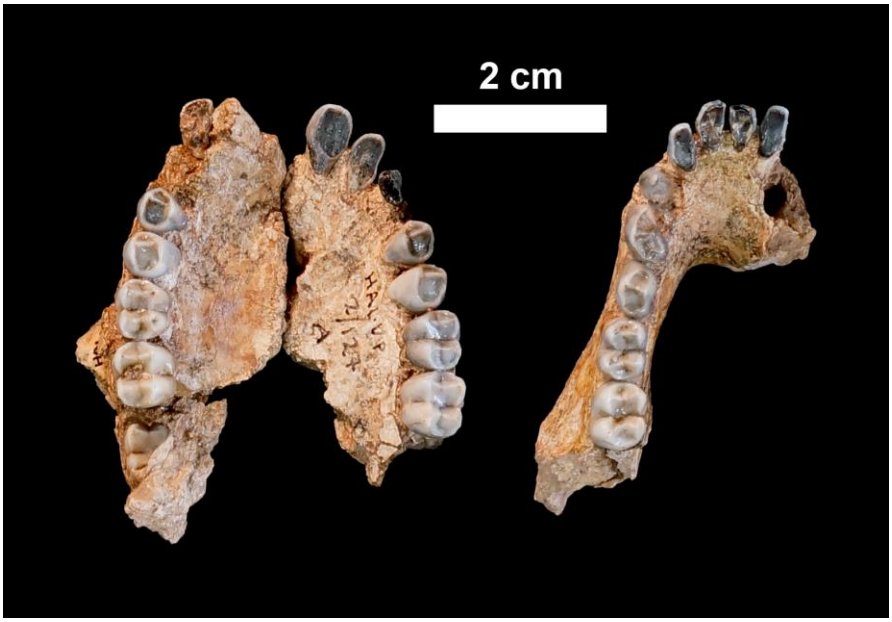

Figure S1 Faro Daba *Colobus* cf. *guereza* juvenile maxilla (left) and mandible (right) of individual HAL-VP-2/127 in occlusal view. Anterior is up. Sex is uncertain. Note that the unerupted right maxillary third molar is visible in the crypt.

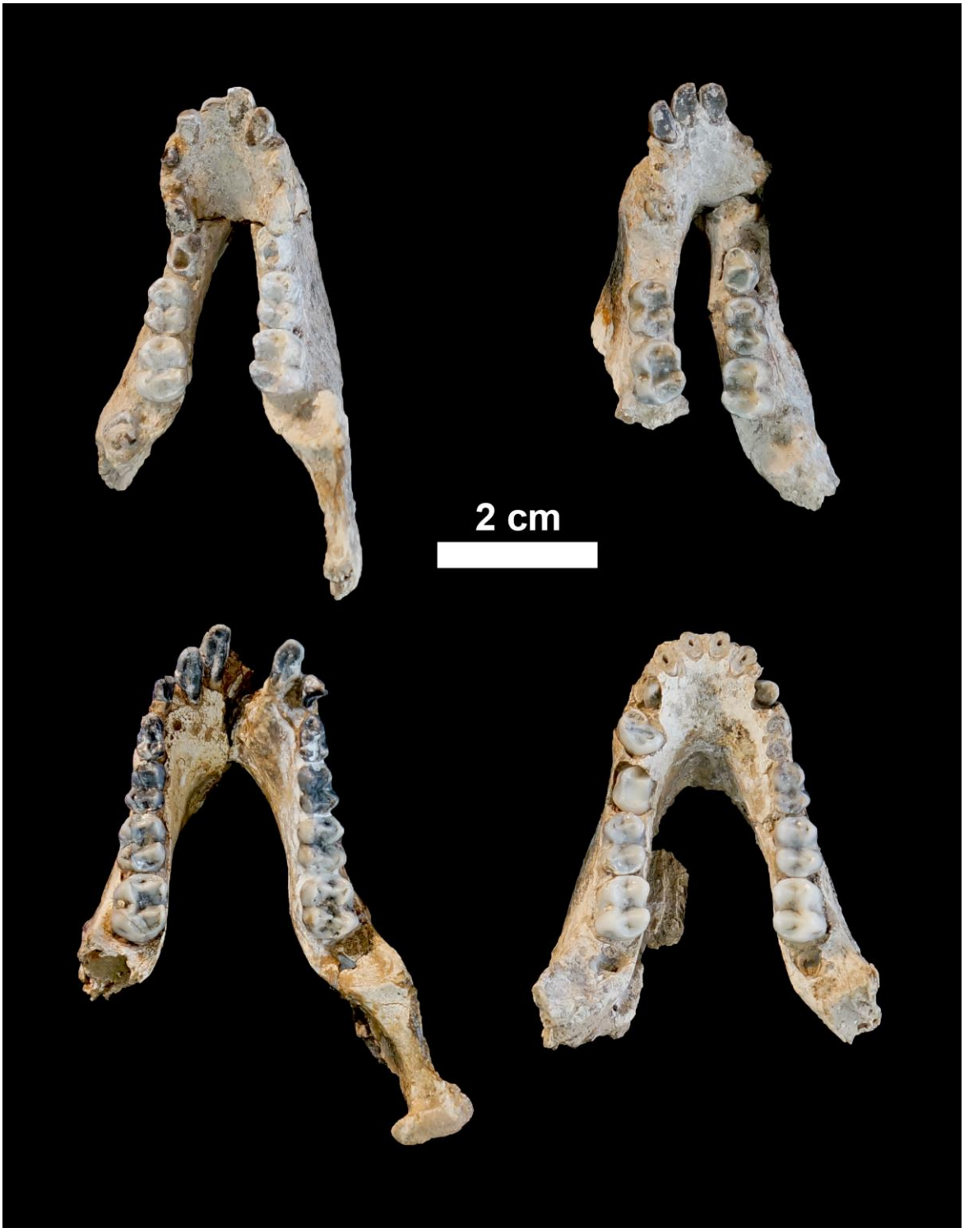

Figure S2 Faro Daba *Colobus* cf. *guereza* juvenile mandibles in occlusal view, demonstrating a small subset of the ontogenetic variation in the assemblage. Anterior is up. Clockwise, from top left: HAL-VP-3/43, HAL-VP-9/1461, HAL-VP-9/303, and HAL-VP-9/778. Sex is uncertain for all individuals. Note that unerupted third molars are visible in HAL-VP-3/43, HAL-VP-9/303, and HAL-VP-9/778.

Table S1 Age scoring criteria

Score	Description
1	Individual only has deciduous dentition
2	Individual has mixed dentition[a]
3	Individual has permanent dentition but the third molar is not fully erupted
4	Individual has permanent dentition with only light wear[b]
5	Individual has permanent dentition with moderate wear[c]
6	Individual has permanent dentition with heavy wear[d]

[a]Instances where the deciduous dentition would have been in function during life but has been lost and only permanent teeth in the crypt remain were scored as mixed.
[b]No dentine exposure that exceeds 1 mm in diameter.
[c]Exposed dentine on the first and second molars does not connect between cusps.
[d]Dentine is exposed on all three molars and the exposures connect between cusps.

Table S2 Anatomical abbreviations used in specimen inventory

Elements	
CRA	Cranium
FRO	Frontal
MAX	Maxilla
ZYG	Zygomatic
TEM	Temporal
OCC	Occipital
NAS	Nasal
MAN	Mandible
I1 – I2	First – second incisor
C	Canine
P3 – P4	Third – fourth premolar
M1 – M3	First – third molar
dI1 – dI2	Deciduous first – second incisor
dC	Deciduous canine
dM1 – dM2	Deciduous first – second molar
CER	Cervical vertebra
THO	Thoracic vertebra
LUM	Lumbar vertebra
VER	Vertebra
SAC	Sacrum
OCX	Os coxae
STE	Sternum
RIB	Rib
SCA	Scapula
CLA	Clavicle
HUM	Humerus
ULN	Ulna
RAD	Radius
FEM	Femur
PAT	Patella
TIB	Tibia
FIB	Fibula
CAR	Carpal

LUN	Lunate
CAP	Capitate
MTP	Metapodial
MTC	Metacarpal
MTC1 to 5	Metacarpal 1 to 5
PHX	Phalanx
CAL	Calcaneus
TAL	Talus
NAV	Navicular
CUB	Cuboid
MTT	Metatarsal
MTT1 to 5	Metatarsal 1 to 5
SES	Sesamoid
Descriptive terms	
Caud.	Caudal
Dist.	Distal
Edent.	Edentulous
Frag.	Fragment
Frags.	Fragments
Imm.	Immature
L.	Left
L	Lower
Misc.	Miscellaneous
Prox.	Proximal
R.	Right
Symph.	Symphysis
U	Upper